SILVER NANOWIRE BASED MULTIFUNCTIONAL FIBERS AND FABRICS

A THESIS SUBMITTED TO
THE GRADUATE SCHOOL OF NATURAL AND APPLIED SCIENCES
OF
MIDDLE EAST TECHNICAL UNIVERSITY

BY

DOĞA DOĞANAY

IN PARTIAL FULFILLMENT OF THE REQUIREMENTS
FOR
THE DEGREE OF DOCTOR OF PHILOSOPHY
IN
METALLURGICAL AND MATERIALS ENGINEERING

NOVEMBER 2022

Approval of the thesis:

SILVER NANOWIRE BASED MULTIFUNCTIONAL FIBERS AND FABRICS

submitted by **DOĞA DOĞANAY** in partial fulfillment of the requirements for the degree of **Doctor of Philosophy** i**n Metallurgical and Materials Engineering, Middle East Technical University** by,

Prof. Dr. Halil Kalıpçılar
Dean, Graduate School of **Natural and Applied Sciences** _____

Prof. Dr. Ali Kalkanlı
Head of the Department, **Metallurgical and Materials Eng.** _____

Prof. Dr. Hüsnü Emrah Ünalan
Supervisor, **Metallurgical and Materials Eng., METU** _____

Assoc. Prof. Dr. Simge Çınar Aygün
Co-Supervisor, **Metallurgical and Materials Eng., METU** _____

Examining Committee Members:

Prof. Dr. Cevdet Kaynak
Metallurgical and Materials Eng., METU _____

Prof. Dr. Hüsnü Emrah Ünalan
Metallurgical and Materials Eng., METU _____

Assoc. Prof. Dr. Hüseyin Avcı
Metallurgical and Materials Eng., ESOGÜ. _____

Assist. Prof. Dr. Hasan Tarık Baytekin
Chemistry, METU _____

Assist. Prof. Dr. Emre Ozan Polat
Mechatronics Eng., Kadir Has University _____

Date: 23.11.2022

I hereby declare that all information in this document has been obtained and presented in accordance with academic rules and ethical conduct. I also declare that, as required by these rules and conduct, I have fully cited and referenced all material and results that are not original to this work.

Name Last name : Doğa Doğanay

Signature :

ABSTRACT

SILVER NANOWIRE MODIFIED MULTIFUNCTIONAL FIBERS AND FABRICS

Doğanay, Doğa
Doctor of Philosophy, Metallurgical and Materials Engineering
Supervisor: Prof. Dr. Hüsnü Emrah Ünalan
Co-Supervisor: Assoc. Prof. Dr. Simge Çınar Aygün

November 2022, 158 pages

The demand for functional textiles has been increasing for the last two decades. In particular, advancements in the internet of things, artificial intelligence and data science have forced scientists and engineers to develop better functional and/or electronic textiles that meet consumer demands. However, due to some deficiencies, functional textiles could not reach their true potential. Some of these deficiencies can be addressed with practice-based approaches. On the other hand, there are also some universal challenges that require urgent solutions with an inclusive approach. First of all, the materials that give functionality must offer high performance and be non-toxic. In addition, functional textiles must function stably for a long period of time. Both the production methods of the materials and their application to textiles must be suitable for mass production. Another shortcoming of electronic textiles is their use with rechargeable batteries. Providing the power requirements of these devices with external batteries is one of the most important factors limiting their daily use.

In this thesis, silver nanowires (Ag NWs) were preferred as the functional materials due to their high conductivity and low toxicity compared to their counterparts. Ag

NW based functional and electronic textiles were developed considering the design criteria mentioned above. The antimicrobial efficacy of the Ag NW modified fabrics against a wide range of bacteria was first investigated. A small amount of Ag NW modification onto conventional fabrics has been shown to provide superior antimicrobial performance against a Gram-positive coccus (*Staphylococcus aureus*), a Gram-negative bacillus (*Escherichia coli*), a Gram-positive and spore-forming bacillus (*Bacillus cereus*), and a yeast-like fungus (*Candida albicans*). Later, Ag NW decorated fabrics were used as high-performance heatable textiles that operate under low voltage suitable for wearable and mobile applications. It has been shown that these fabrics can be heated to 50 ^{o}C under an applied power density of 0.05 W/cm^2. The Ag NW based heatable textiles developed in this part of the thesis possessed superior mechanical stability and have a strong potential for use in winter clothing. Then, thermoplastic polyurethane (TPU) films were laminated onto Ag NW decorated fabrics and it was found that the fabrics gained superior washing resistance. Moreover, the same structure has shown superior potential when used as triboelectric nanogenerators (TENGs) that can harvest energy from body movements. The fabric-based TENGs developed in this thesis have one of the highest power outputs (1.25 W/m^2) compared to the literature. A self-powered human-machine interface device was also developed with these fabric-based TENGs. Finally, Ag NWs were utilized as conductive electrode core fibers in core/shell wet spun fiber-based TENGs. All these different applications revealed the strong potential of Ag NWs for functional and electronic textiles.

Keywords: Silver Nanowires, Antimicrobial Fabrics, Heated Fabrics, Wearable Triboelectric Nanogenerators.

ÖZ

GÜMÜŞ NANOTEL MODİFİYE EDİLMİŞ ÇOK FONKSİYONLU ELYAF VE KUMAŞLAR

Doğanay, Doğa
Doktora, Metalurji ve Malzeme Mühendisliği
Tez Yöneticisi: Prof. Dr. Hüsnü Emrah Ünalan
Ortak Tez Yöneticisi: Doç. Dr. Simge Çınar Aygün

Kasım 2022, 158 sayfa

Fonksiyonel tekstillere olan talep son yirmi yılda artmaktadır. Özellikle nesnelerin interneti, yapay zeka ve veri bilimindeki gelişmeler, bilim insanlarını ve mühendisleri tüketici taleplerini karşılayan daha iyi fonksiyonel ve/veya elektronik tekstiller geliştirmeye zorlamıştır. Ancak fonksiyonel tekstiller bazı eksikliklerden dolayı potansiyellerine ulaşamamışlardır. Bu eksikliklerin bir kısmı uygulamaya dayalı yaklaşımlarla giderilebilir. Ancak, kapsayıcı yaklaşımlarla acil çözümler gerektiren bazı evrensel zorluklar da vardır. Öncelikle işlevsellik kazandıran malzemelerin yüksek performans sunması ve toksik olmaması gerekir. Ek olarak, fonksiyonel tekstiller uzun süreler boyunca kararlı bir şekilde işlev görmelidir. Ayrıca hem malzemelerin üretim yöntemleri hem de tekstil üzerine uygulamaları seri üretim için uygun olmalıdır. Elektronik tekstillerin bir diğer eksikliği ise şarj edilebilir pillerle kullanılmasıdır. Bu cihazların güç gereksinimlerinin harici bataryalarla sağlanması, günlük kullanımlarını sınırlandıran en önemli faktörlerden birisidir.

Bu tez çalışmasında, muadillerine göre yüksek iletkenlikleri ve düşük toksisiteleri nedeniyle fonksiyonel malzeme olarak gümüş nanoteller (Ag NT) tercih edilmiştir.

Ag NT temelli fonksiyonel ve elektronik tekstiller yukarıda belirtilen tasarım kriterleri göz önünde bulundurularak geliştirilmiştir. İlk olarak Ag NT ile modifiye edilmiş kumaşların çeşitli bakterilere karşı antimikrobiyal performansları araştırıldı. Geleneksel kumaşlar üzerinde az miktarda gümüş nanotel modifikasyonunun, Gram pozitif koklara (*Staphylococcus aureus*), Gram negatif basillere (*Escherichia coli*), gram pozitif ve spor oluşturan basillere (*Bacillus cereus*) ve maya benzeri bir mantarlara (*Candida albicans*) karşı üstün antimikrobiyal performans sağladığı gösterilmiştir. Daha sonra Ag NT ile modifiye edilmiş kumaşlar giyilebilir ve mobil uygulamalar için düşük voltaj altında yüksek performanslı ısınabilen tekstiller olarak kullanılmıştır. Bu kumaşların 0.05 W/cm^2 doğru akım altında 50 ^{o}C'ye ısıtılabildiği gösterilmiştir. Tezin bu bölümünde geliştirilen Ag NT bazlı ısınabilen tekstiller üstün mekanik stabiliteye ve kışlık giysilerde kullanım için güçlü bir potansiyele sahiptir. Daha sonra, Ag NT ile modifiye edilmiş kumaşlar üzerine termoplastik poliüretan (TPU) filmler lamine edilmiş ve laminasyon işleminin kumaşlara üstün yıkama direnci kazandırdığı tespit edilmiştir. Ayrıca, aynı yapı, vücut hareketlerinden enerji toplayabilen triboelektrik nanojeneratörler (TENG'ler) olarak kullanım için de üstün potansiyele sahiptir. Bu tezde geliştirilen kumaş temelli TENG'ler, literatüre kıyasla en yüksek güç çıkışlarından birine sahiptir (1.25 W/m^2). Kumaş temelli bu TENG'ler ile kendi kendine çalışan bir insan makine arayüz cihazı da geliştirilmiştir. Son olarak, Ag NT'ler, çekirdek kabuk yapısına sahip ıslak eğrilmiş fiber bazlı TENG'lerde iletken elektrot fiberlerde kullanılmıştır. Sonuç olarak, Ag NT'lerin fonksiyonel ve elektronik tekstil uyularmarı için güçlü potansiyele sahip olduğu farklı uygulamalarla birlikte gösterilmiştir.

Anahtar Kelimeler: Gümüş Nanoteller, Antimikrobiyal Kumaşlar, Isınabilen Kumaşlar, Giyilebilir Triboelektrik Nanojeneratörler

To my wife

ACKNOWLEDGMENTS

This journey, which I started knowing little, ends up learning a lot and still knowing very little. I worked with great pleasure almost every day and benefited from the support and kindness of countless people. Firstly, I would like to express my endless gratitude to my advisor Prof. Dr. Hüsnü Emrah Ünalan. It is a great honor to work under his supervision. He constantly supported me not only with his words but also with his actions. He will always be a role model for me in my future career. I also would like to thank my co-advisor Assoc. Prof. Dr. Simge Çınar Aygün for her support. I would like to thank my thesis progress committee members, Prof. Dr. Cevdet Kaynak and Assoc. Prof. Dr. Hüseyin Avcı for their valuable suggestions, advices and inputs. I learned that for a young researcher it is very important to have a good mentor. As my mentor and one of the most important factors in my love for research, thank you Assist. Prof. Dr. Şahin Çoşkun.

This thesis was partially supported by the Middle East Technical University through the Scientific Research Projects Programme under project number TEZ-D-308-2021-10715.

This thesis, which I tried to bring together different disciplines, would be incomplete without people that I collaborate. First of all, I would like to thank Prof. Dr. Gülçin Akça from Gazi University and Akın Kanıcıoğlu for their help in conducting the antibacterial tests. I would like to thank Prof. Dr. Ayşe Tavukçuoğlu from METU for her help with IR imaging and Sevim Polat Genlik for her circuit design. I also would like to thank Burak Altuntaş and Erdem Ağbahça for their support to established measurement setups for triboelectric nanogenerators. I also appreciate İsmail Eken for his help with illustration of the schematic figure and Zehra Yakar for his help with knitting the fabricated fibers.

We met with Mete Batuhan Durukan when we started our graduate education in 2013. At first, he was just a casual laboratory friend to me, but over time he became

my brother. He was always there for me in my toughest times. He shared my feelings in my happiest times. Also, my research perspective expanded with our discussions. I would like to thank my brother with all my heart for always being there for me. Learning from seniors is the way often experienced. However, I also learned a lot from my junior Melih Ögeday Çiçek. I would like to thank him to be a great colleague and close friend. I also would like to thank Mustafa Caner Görür for being a trustworthy friend. I would like to thank Onuralp Çakır for being a tidy and hardworking teammate.

It was very important to work in a happy and friendly environment. I consider that working in a friendly and supportive working environment is one of the most important factors in increasing productivity. Therefore, I owe my deepest gratitude to Nanolab members, Tufan Bölükbaşı, Onur Demircioğlu, Yusuf Tütel, Loay Madbouly, Serkan Koylan, Murathan Çuğunlular, Ali Deniz Uçar, Öykü Çetin, Deniz Keskin, Dr. Alptekin Aydınlı, Dr. Ümran Ceren Başköse, Dr. Yaqoob Khan, Dr. Aryan Azad. I would also like to express my gratitude to my dear friends Ece Alpugan and Özlem Ünal, whom we lost at a young age. You will always be in my heart. I also would like to thank Nanovatif members, Hüseyin Utkucan Kayacı, Enes Saygı and Gürcan Utku Özdemir.

I would like to thank my father Salim Doğanay, who was also a friend to me, for his support throughout my life. I would also like to express my gratitude to my dear sister Merih Doğan, whose work I admire and who has always been a role model to me. I would like to express my endless thanks to my mother Ayşe Doğanay, who always showed me her trust and love. Last but not the least, I am also thankful to my lovely wife Tuba Doğanay for all the time she spent with me. She was always by my side and encouraged me when I lost the courage to finish the thesis. I love you.

TABLE OF CONTENTS

LIST OF TABLES

TABLES

LIST OF FIGURES

FIGURES

CHAPTER 1

INTRODUCTION

Clothing has been always one of the main concerns of human beings together with sheltering and nutrition. The initial purpose of the garments was mainly for protection against environmental conditions such as cold and hot weather. Natural sources such as animal skin and fur were the only available materials for the first clothes[1,2]. Then, humans discovered the advantages of woven fibers over the animal skin and fur. The timeline of the important advancements in textile industry is provided in

Figure 1.1. The use of wool and cotton in cloth production are two important developments that have begun to change people's lives[3]. Innovations in textile machinery were effective steps for humanity and considered as the beginning of the industrial revolution[4]. Moreover, synthetic fiber production is one of the most significant developments in the textile industry in the early 1900s [5]. As traditional textiles began to fail to meet modern human needs, functional fibers and textiles started to be developed in the 1960s. For example, Dow Chemical Co. patented a finishing method with fluorocarbon resin to provide water and oil repellent features for textiles in 1967[6]. Another function that the industry desired to add to their products has been the antimicrobial effect since 1980s [7]. There were two motivations for this desire. The initial purpose was to protect the user from pathogens and odor-generating microorganisms. The second purpose was to increase durability of textile itself by preventing reproduction of microorganisms on the fibers. It is because some of these microorganisms were known to cause degradation of the chemical structure of the fibers. As a result of these, the antimicrobial agents started to be extensively used in the textile products. Then, the side effects of antimicrobial agents to

environment and health become an important issue[8]. Hence, new antibacterial agents started to be investigated which have less cytotoxicity but still enough antimicrobial efficacy.

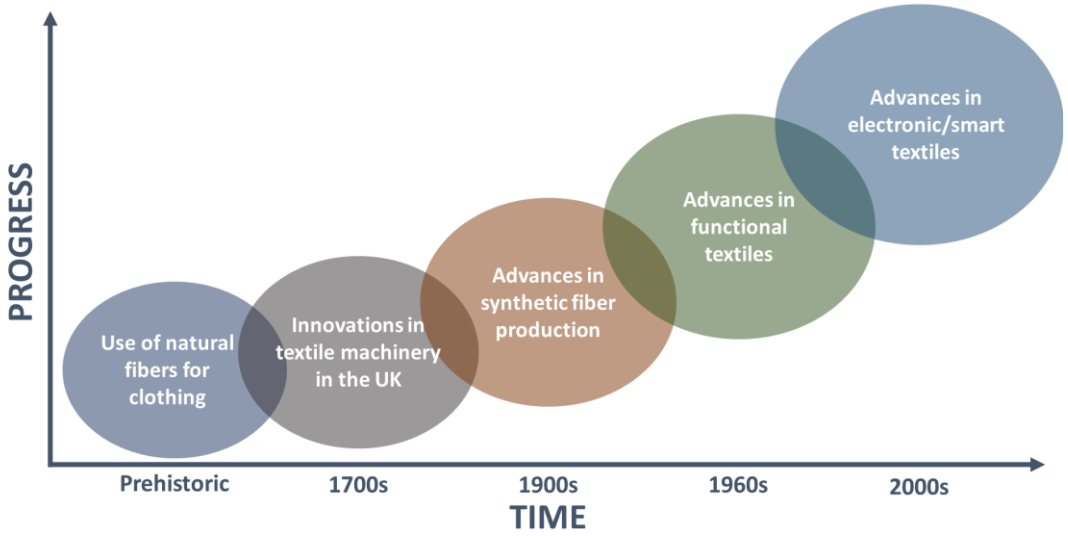

Figure 1.1 Timeline of major developments in the textile industry.

The last century witnessed significant advancement in all aspects of industry like medicine, agriculture, and construction etc. Particularly, the developments in the electronics sector begun to change human life. The rapid integration of computers into our daily lives since the 1980s has had a significant impact on almost every aspect, from the daily routines of individuals to their work lives. The introduction of the internet has remarkably accelerated this change. These developments and changes have also deeply affected the textile industry. As a result of this, electronic textiles have been introduced as a new concept. The first examples of electronic textiles are quite primitive considering the todays products/academic research level. The early examples usually consisted of conventional electronic circuits/devices tailored onto standard textiles [9,10]. While these were highly valuable pioneers, they were not suitable for use in our daily lives. Because they were far from providing comfort and durability that an outfit should offer. Later, conductive fibers were proposed to overcome some of these barriers. Initially, metal fibers such as copper,

nickel and stainless steel were used in electronic textiles [11]. Later, polymeric fibers were coated with metals and used in electronic textile products[12]. These conductive fibers were weaved and knitted together with the conventional insulator fiber to create conductive paths for different applications. Heated textiles were also one of the applications of these conductive fibers. They were proposed as promising building blocks for winter wear since 2000s [13]. These conductive fibers generate heat under an applied voltage according to Joule heating principle. Heated blankets for example have been used in our daily lives. However, they are several problems to overcome for these heated products to extend their use in our daily lives. First of all, they require high input voltages, which prevent their use in mobile applications. Today's portable battery technology can only offer limited voltage ranges (i.e., 3-12 V). Moreover, these fibers are also not stable enough to be used in the textile products. Because they are prone to fatigue failure when repeated forces act on them in daily use and washing conditions. Another shortcoming of fiber based heated fabrics is that, the heated region is only the fibers itself. This limits their applications since overall heating of the fabrics is impossible unless all the fabric is produced with conductive fibers. Provided that the fabric constructed with all conductive fibers, it would become very heavy and its cost will be very high. Moreover, fabric touch will be lost. Therefore, conductive fibers are typically limited in number in heated fabric applications. Because of these reasons, heated apparels remained as prototypes for a long time.

There is another fundamental problem that prevents the use of electronic textiles in our daily lives. All wearable devices fabricated with these electronic textiles require power input to operate. Currently, heavy and bulky rechargeable batteries are used to power up the wearable devices. This is a serious problem that reduces consumer comfort. In other words, making a fiber/fabric-based electronic system often makes non-sense if it requires heavy and bulky external power sources. Reducing the weight

of the batteries cannot be a direct solution. Because the size reduction also reduces the battery capacity, which in return causes them to be charged more often.

The developments in nanotechnology have given scientists hope to solve aforementioned problems. This effect first manifested itself in antimicrobial textiles. Copper (Cu), silver (Ag) nanoparticles (NPs) are decorated onto textiles [7]. The higher surface area to volume ratio of these NPs compared to their bulk form increases their antimicrobial efficacy. The use of small amounts of nanomaterials can provide adequate antimicrobial performance at low cost. However, depending on their sizes, the NPs can be toxic [14]. On the other hand, NWs with lengths of micrometers are known to show low cytotoxicity [15]. In this thesis Ag NWs, were introduced as antimicrobial agents on conventional fabrics against different bacteria and microbes (Chapter 2).

Utilization of conductive nanomaterials for electronic textiles stands out as a promising solution for fatigue failure mentioned above. Carbon nanotubes, graphene, metallic nanowires and transition metal carbides, carbonitrides and nitrides (MXenes) have been utilized to provide electrical conductivity to fibers and fabrics since 2010s [16–19]. Each material has unique advantages over the others. For example, carbon nanotubes and graphene have higher chemical and environmental stability than the others [20,21]. Although chemical vapor deposition (CVD) grown carbon nanotubes and graphene are very conductive, they are very expensive to be used in textile industry [22,23]. On the contrary, the ones produced with economically feasible methods cannot reach sufficient conductivity [24]. MXenes have a price advantage, but are typically very unstable [25]. On the other hand, silver nanowires (Ag NWs) offer the high conductivity with good stability [26]. Therefore, Ag NWs were preferred as the conductive/functional nanomaterials to fabricate electronic textiles in this thesis. First of all, polyol synthesized Ag NWs were dip and dry coated onto cotton fabrics. Joule heating performance and stability of these fabrics were investigated in Chapter 3. It was shown that Ag NW modified fabrics have superior mechanical stability against repeating forces. The use of these Ag NWs to modify

cotton textiles overcomes the mechanical instability problem of conventional electronic textiles. Moreover, Ag NW modified heated textiles presented in this thesis operate at very low applied voltages. This enables them to be used with conventional power banks. In addition, homogeneous coating of Ag NWs onto fabric surface allowed areal heating of fabrics. However, washing stability of Ag NW modified fabrics were remained as a problem that is solved in the following chapter.

Triboelectric nanogenerators (TENGs) were first proposed in 2012 as the one of the alternative solutions for today's energy problems [27]. Combined effect of triboelectrification and electrostatic induction are the main operating principles of TENGs to harvest mechanical energy. Fundamentals of TENGs are discussed in Chapter 4. Theoretically, any wasted mechanical energy, including human movement, can be harvested through TENGs. Therefore, fiber/fabric-based TENGs have strong potential to be used to provide the energy requirement of electronic textiles. The optimum case would be the transfer of converted energy from textile based TENGs to textile-based energy storage devices. However, we are technologically not mature enough to develop such product due to technical difficulties. On the other hand, textile-based TENGs can be directly used as biomotion sensors. In these cases, TENG sensors do not need external power to operate, unlike a resistive, capacitive wearable sensor. As a result of these features, TENG sensors are described as self-powered. In Chapter 5, thermoplastic polyurethane (TPU) films were laminated onto Ag NW modified fabrics to increase the washing stability of the heated fabrics and to use this structure as wearable TENGs. This provides a combined solution for washing instability of Ag NW modified fabrics and power requirements of wearable devices. It was showed that TPU laminations significantly increase the washing stability of the fabrics. Moreover, TPU laminated Ag NW modified fabrics provided one of the highest power outputs for fabric based TENGs in literature at the time of the study. Then these wearable TENGs were used as self-powered wearable human machine interface (HMI) devices. These results were highly encouraging; therefore, the system was studied in more detail. In Chapter 6, core shell TPU fibers are developed

to demonstrate low-cost scalable fiber based TENGs. The fiber structure enables simple integration to wearable systems. These fibers can be weaved and/or knitted into desired shapes. Moreover, they can also be sewn onto conventional fabrics. The core shell structure was fabricated via wet spinning. The conductive core structure was formed using carbon black (CB), Ag NWs added TPU matrix composites. The dielectric shell was bare TPU. The high output performance of TENGs and the superior stability of the wet spun core-shell fiber demonstrated the great potential of this structure to be used as self-powered wearable sensors.

1.1 Dissertation Objectives

Functional textiles have been investigated since 1960s for different purposes [10]. Even though they promise a lot for humanity in different fields, functional textiles did not reach their potential due to certain limitations. Some of these limitations may require application-based solutions. However, there are also universal problems for all functional textiles. Above all, functional materials must be of limited toxicity for both the end user and the environment without compromising their added value. In addition, functional materials must have sufficient stability in all aspects, including environmental, mechanical and washing stability. Moreover, these materials should be produced using low-cost methods that are suitable for mass production. Modification techniques of fabrics with these functional materials must be scalable. In addition, the biggest problem in electronic textiles is that the power requirement of these devices is provided by external batteries.

This thesis is focused to find suitable solutions for the aforementioned problems of functional textiles by using Ag NWs as the functional materials. The seven chapters addressed these questions with the following objectives.

Chapter 1: defines fundamental problems of functional and/or electronic textiles.

Chapter 2: develops Ag NW based antimicrobial fabrics against wide range of bacteria

Chapter 3: develops Ag NW modified heated fabrics performing with low input voltage and having superior mechanical stability

Chapter 4: explains foundations of TENGs,

Chapter 5: develops Ag NW based heated fabrics and wearable TENGs having superior washing stability and power outputs to be used in different electronic textile applications like human machine interface (HMI),

Chapter 6: develops core shell fiber based TENGs via co-wet spinning method,

Chapter 7: concludes and share further recommendation for Ag NW based functional textiles.

CHAPTER 2

SILVER NANOWIRE MODIFIED FABRICS FOR WIDE SPECTRUM ANTIMICROBIAL APPLICATIONS

2.1 Introduction

Increased spreading rate of epidemics as a result of growing number of international and domestic flights as well as the population of countries and in particular cities forced people to use both public and personal antimicrobial products [28]. As pathogenic microorganisms become increasingly resistant to existing products, the improvement of antimicrobial agents is required [29,30]. These antimicrobial agents are being used in different areas such as hygiene gels, surgical devices [31,32]. Due to the large surface area and high moisture sensitivity, microorganisms can easily multiply on fabrics. It is known that especially some bacteria can reach over 1 million cells from a single living cell within 7 hours [33]. These microorganisms not only cause hygiene problems and undesired odors; but also, reduce the mechanical strength of the fabrics. Because of these reasons, antimicrobial textiles are extensively researched and also commercialized [34–36].

Some materials are known for their natural antimicrobial performance. For example, silver (Ag) has been used for its superior antimicrobial activity since ancient times, even before the realization of microbes [37]. In the textile industry, bulk Ag and fibers coated with Ag thin films were used firstly and made into market. However, the use of bulk Ag or fibers that are coated with Ag increase the cost of the final product. Moreover, antimicrobial effect is directly related to the Ag^+ ion release rate and this release rate can be increased with the surface area of Ag. Therefore, nanoparticles of silver (Ag NPs) are started to be investigated in literature and used in the market for

antimicrobial textile applications by early 2000s [38–41]. For example, one of the first study on antibacterial performance of Ag NPs were conducted by Feng and coworkers. They investigated the antibacterial mechanisms of Ag NPs via scanning electron microscopy (SEM) and X-ray microanalysis. It is stated that, DNA lose its replication ability as a result of Ag^+ treatment [42]. In another study, Morones et al. investigated the effect of Ag NP size on the antibacterial properties. They showed that decreasing the Ag NP size increases the antibacterial efficacy because smaller Ag NPs can easily penetrate the bacteria cell membrane [43].

With the synthesis of different Ag nanostructures, investigation of their antimicrobial performances gained momentum. For example, silver nanowires (Ag NWs) can offer several advantages over Ag NPs when they are used in antimicrobial textiles. First of all, one-dimensional structure of NWs result in better interaction (or adhesion) between the coated surface (textile fibers) and the nanomaterials, which increase the durability of NWs against environmental effects, mechanical effects and washing. If a nanomaterial is not durable enough on the host material (i.e., textile fiber) it may easily be released into the wastewater during washing or laundering. This does not only limit the long-term use of that textile product; but also, cause some environmental concerns [44]. Secondly, Ag NWs show lower toxicity compared to Ag NPs; yet, have enough antimicrobial effect [44,45]. Up to now, there are only limited number of studies on the explanation of the antimicrobial performance of Ag NWs. For instance, Lei et al. used Ag NWs to fabricate antibacterial Konjac Galactomannan (KGM) matrix nanocomposite films. Basically, KGM granules and Ag NWs were solved/dispersed into water. Following that, the mixture was poured into a petri dish and vacuum dried. It was shown that small amounts of Ag NW addition (1, 2.5 and 5 wt. %) increase the thermal and mechanical performance of the KGM matrix. Moreover, antibacterial performance of the bare KGM matrix was negligible, whereas Ag NW/KGM nanocomposites showed promising antibacterial performance against Escherichia coli [46]. More recently, Zhao and coworkers investigated antibacterial effects of graphene wrapped Ag NWs deposited onto ethylene vinly acetate/polyethylene terephthalate substrates. It has been showed that

the fabricated antibacterial structures have death rates of 50, 45, and 40 % against gram-negative (*Escherichia coli*), gram-positive bacteria (*Staphylococcus aureus*) and yeast-like fungus (*Candida albicans*), respectively [47]. In another study, Jiang and Teng deposited Ag NWs onto polydimethylsiloxane (PDMS) substrates to examine their antibacterial performance against *E. coli* and *S. aureus*. Moreover, they also investigated the biocompatibility of these samples by the observation of the morphology of cytoskeletal structure of human dermal fibroblast [48]. Biocompatible Ag NW deposited PDMS structures showed promising antibacterial performance against *E. coli* and *S. aureus*. In another study, 100% bacterial reduction against *E. coli* and *S. aureus* was shown by Satoungar and coworkers using 3 wt. % Ag NW/polylactic acid (PLA) electrospun fibers. Moreover, considerable decrease in the nanofiber surface resistance was obtained, which showed the potential of Ag NWs/PLA nanocomposites also in the field of electronics[49]. Modification of conventional textiles with Ag NWs were previously conducted in literature for different purposes. For example, Cui et al. used Ag NWs to fabricate stretchable textile-based conductors. In this study, stretchability of Ag NW decorated conductive cupro fabrics demonstrated in the strain range of 0-190% [50]. In another study, Hsu and coworkers used Ag NW coated textiles for personal thermal management. This study showed that, Ag NW modified fabrics offer better thermal insulation than conventional textiles [24].

Almost all previous studies focused on the antibacterial performance of Ag NWs against *S. aureus* (ATCC#25923) and *E. coli* (ATCC#25922). However, to explore the potential of Ag NWs in antimicrobial applications, an extensive study was required against not only Gram positive and negative bacteria but also spore forming bacteria and fungal agents. In this study, a facile dip and dry method was used to fabricate Ag NW modified cotton fabrics. As the most extensive study conducted so far, the antimicrobial performance of Ag NW decorated cotton fabrics was investigated against a wide range of bacteria test strains including Gram positive coccus (*S. aureus*), Gram negative bacilli (*E. coli*), Gram positive bacilli and spore

forming bacteria (*B. cereus* ATCC#14603) and yeast like fungus (*C. albicans* ATCC# 90028). Effective antimicrobial duration of the fabrics was also investigated.

2.2 Experimental Details

2.2.1 Synthesis and Purification of Silver Nanowires

All chemicals were purchased from Sigma Aldrich and used without further purification. Undyed 100% organic woven cotton fabrics and all glassware were cleaned using acetone (99.8%), isopropyl alcohol (99.8%) and finally deionized water (18.3 MΩ). Ag NWs were synthesized according to a previous study [51]. In a typical synthesis, a 10 ml and 0.45 M ethylene glycol (EG) solution of poly(vinylpyrrolidone) (PVP) (monomer-based calculation MW = 55000) was prepared; into which 7 mg of sodium chloride (NaCl) was added. Following that, the solution was heated at 170 °C in a round flask within a silicon bath. In the meantime, a 0.12 M silver nitrate ($AgNO_3$) solution in 5 ml EG was prepared and added drop-wise into the PVP solution by an injection pump (Top-5300 Model Syringe Pump) at a rate of 5 ml/hr. The solution was stirred at a rate of 1000 rpm through a magnetic stirrer during the whole process. Upon the completion of drop-wise addition, the NW solution was annealed for 30 minutes at 170 °C and finally air cooled to room temperature. Then, in order to separate polymer from the Ag NWs, the solution was diluted with acetone (at a ratio 1:5) and centrifuged two times at 8000 rpm for 20 minutes. After that, the NWs were dispersed in ethanol and again centrifuged at 8000 rpm for 20 minutes. The final product was dispersed in ethanol for further characterization and processing. A final decantation process was applied to get rid of side products, such as micron and nano sized Ag NPs.

2.3 Silver Nanowire Modification onto Fabrics

Schematic representation of fabrication steps used in this work together with the antibacterial effect of Ag NW coated fabrics is presented in Figure 2.1. Dip and dry method is one of the most convenient ways to modify fabrics with nanomaterials, which is also scalable for large scale production.

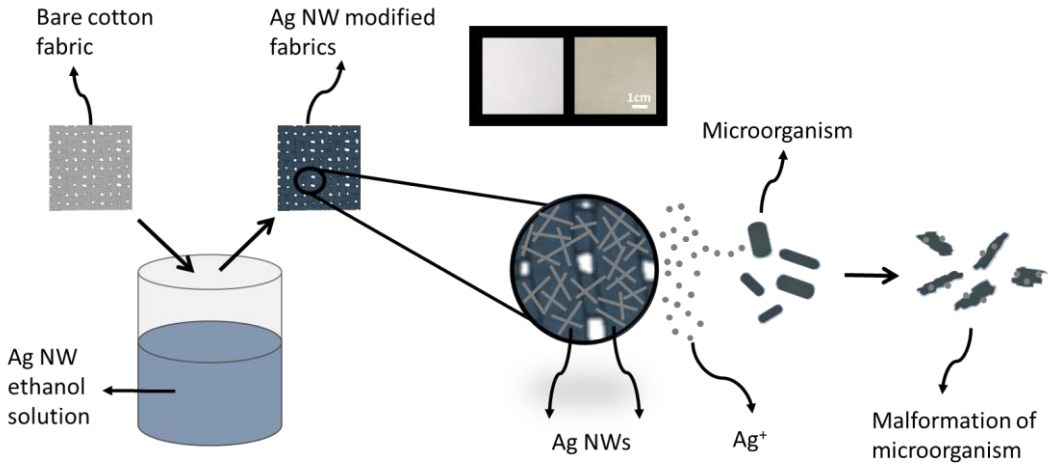

Figure 2.1 Schematic illustration of the Ag NW modification of fabrics and antibacterial mechanism of the modified fabrics. Inset shows a photo of the bare and NW decorated fabrics.

Simply, 1 cm^2 cleaned cotton fabrics were immersed into 20 ml of 0.2 mg/ml ethanolic Ag NW dispersions for 5 minutes then dried at 80 °C for 10 minutes. This procedure was repeated until four different sets of samples in terms of Ag NW amount were obtained. Sheet resistance were measured with two probes along the side of the 1 cm^2 square fabrics via Keithley 2400 Source Meter (Keithley Instruments, INC.) A bare and nonconductive sample was used as reference. Resistance was measured from 4 different points and an average value is reported. Resistance measurements allowed reproducible deposition of Ag NWs onto cotton fabrics. Following decoration of Ag NWs onto fabrics, the exact Ag NW loading on cotton fabrics was determined via inductively coupled plasma mass spectrometry (ICP-MS). For this purpose, NW coated fabrics were immersed into 20 ml of 10%

nitric acid/deionized water mixture until a homogenous and clear solution was observed.

2.3.1 Antimicrobial Analyses

For antimicrobial activities of 1 cm^2 square fabrics against standard test strains of *Staphylococcus aureus* (*S. aureus*,) ATCC#25923 as a Gram-positive coccus, *Escherichia coli* (*E. coli*), ATCC#25922 as a Gram-negative bacillus, *Bacillus cereus* (*B. cereus*) ATCC#14603 as a Gram-positive bacilli and spore forming bacteria, *Candida albicans* (*C. albicans*) ATCC#90028 as a yeast like fungus were investigated via agar disc diffusion technique. After freshly culturing bacterial strains on Mueller Hinton agar (MHA, Merck, Germany), *C. albicans* on Sabourraud Dextrose agar (SDA, Merck, Germany) at 37 °C for 48 - 72 hours, the grown colonies of the strains were harvested. The bacterial and fungal suspensions were prepared in sterilized test tubes containing 5 ml Mueller Hinton Broth (MHB, Merck, Germany) and the final inoculums were adjusted to 1.5 x 10^8 and 2 x 10^8 CFU (colony forming unit)/mL respectively according to 0.5 McFarland test standard, turbidometrically. Additionally, the inoculums were adjusted according to their optical density (OD 450 nm: 0.600) spectrophotometrically. Then, 100 µl of each suspension was inoculated on the MHA for bacterial strains, SDA for *C. albicans*. The fabrics were placed into these agar plates (at least ten samples each). They were incubated at 37 °C for 24 - 48 hours, and after the incubation, the diameters (mm) of the inhibition zones of the samples were measured and calculated as CFU/mL. Fabrics were tested for their time dependent killing capacity for 2, 4, 6, 8, 24 hours' time intervals against the microorganisms. The same concentrations of the bacterial and fungal agents' suspensions were placed in their specific broth media as mentioned before. Then, at least two samples of each fabric were put in the test tubes and incubated for the chosen time intervals at 37 °C. Afterwards, the fabrics were taken out, washed twice with phosphate buffered solution (PBS, pH: 7.0), then, put into another test tube containing sterilized 1 ml distilled water, diluted 10^{-2} and 10^{-3} times and 100 µl of

samples from each test tube were cultured on specific agar plates as mentioned before. Following incubation, the grown colonies were counted and calculated as CFU/mL.

2.3.2 Scanning Electron Microscopy (SEM) Analyses

The homogeneity of the NW modification was monitored through scanning electron microscopy (SEM) analysis using FEI NOVA NANO SEM 430 microscope with secondary image mode and EDX mapping techniques under an operating voltage of 5 kV. A thin gold layer (5-10 nm) was deposited onto the fabrics prior to SEM analysis. To understand the antibacterial mechanism, morphologies of both living and dead bacteria were investigated via SEM. Prior to SEM imaging, both living and dead bacteria were fixed onto fabrics to prevent deformation due to vacuum and voltage according to a procedure described in literature [43]. Each sample was immersed into a 2.5 % glutaraldehyde solution in phosphate buffered saline (PBS) for 30 minutes, which is followed by 60, 70, 80, 90 and 100% ethanol/ PBS for 10 minutes for each solution, respectively.

2.4 Results and Discussion

Frequency distributions of length and diameter and SEM image of Ag NWs are provided in Figure 2.2 (a)-(c), respectively. The average length and diameter of the NWs utilized in this work were 8 μm and 50 nm, respectively.

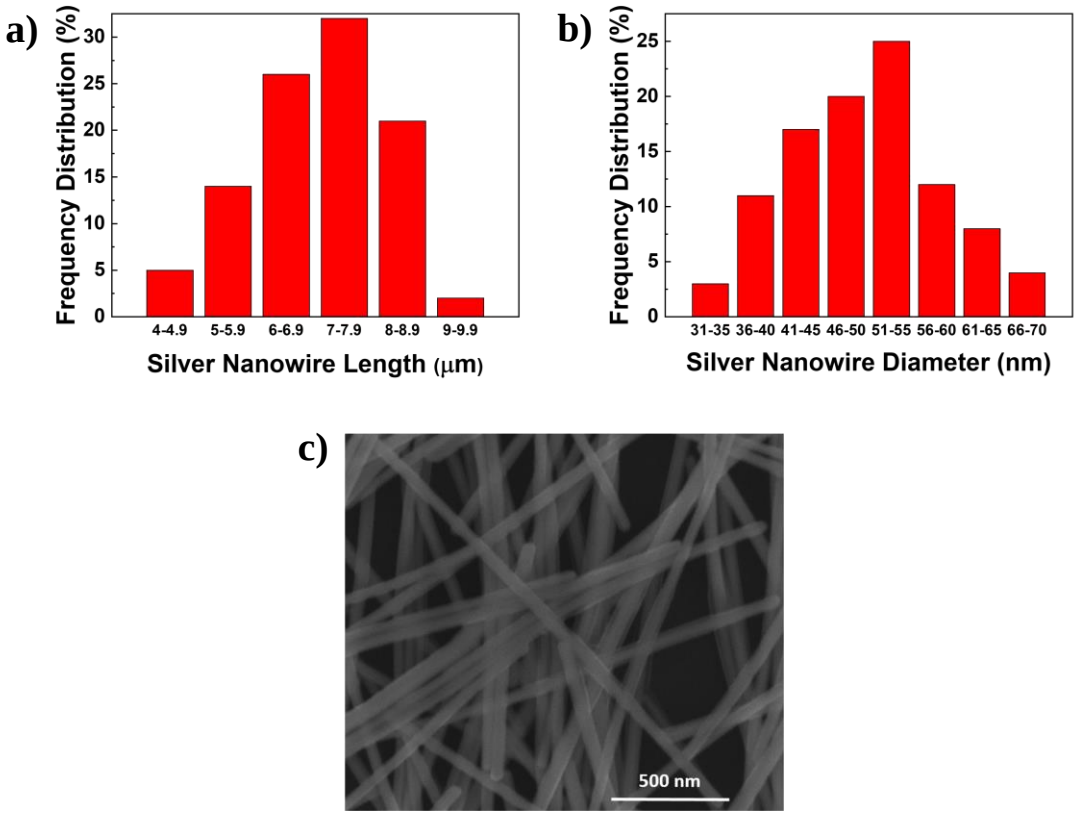

Figure 2.2 Frequency distributions of (a) length, (b) diameter of Ag NWs. (c) SEM image of Ag NWs.

SEM images of Ag NW modified cotton fabrics for each sample set with corresponding NW loadings of 0.095, 0.105, 0.125 and 0.375 mg/cm^2 are provided in Figure 2.3 (a)-(d), respectively. Fabrics having Ag NW loading of 0.095 mg/cm^2 were non-conductive. Sheet resistances of the fabrics were measured as 1000, 100 and 10 ohm/sq for the fabrics having NW loadings of 0.105, 0.125 and 0.375 mg/cm^2, respectively. SEM image of bare cotton fabric is also provided as an inset in Figure 2.3 (a). It is clear that individual fibers can be easily coated with Ag NWs. Moreover, the Ag NW loading can be simply controlled through the number of dip and dry cycles. Homogeneity of Ag NW modified fabrics was observed via energy dispersive X-ray spectroscopy (EDS) mapping technique, results of which are provided in Figure 2.3 (e) and (f). Dots in Figure 2.3 (e) belong to Ag atoms, which revealed that the NWs were homogenously decorated onto the fabrics (inset image in the same

figure). Dots in Figure 2.3 (f) belong to carbon atoms, which is the main element forming the molecular structure of cotton.

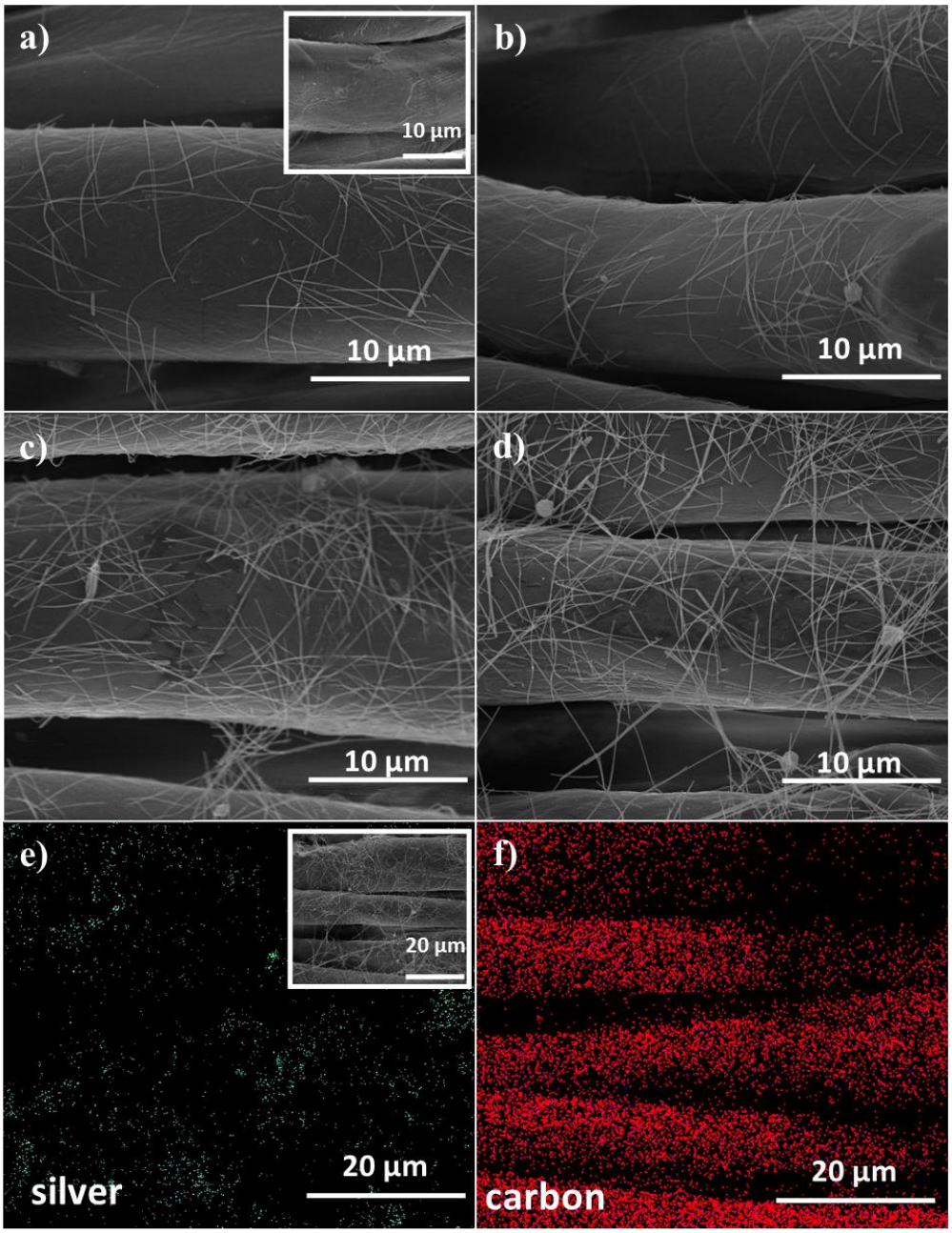

Figure 2.3 SEM images of Ag NW modified fabrics with Ag NW loadings of (a) 0.095 (inset shows an SEM image for bare cotton fabric), (b) 0.105, (c) 0.125, and (d) 0.375 mg/cm^2. EDS mapping of Ag NW modified fabric at a NW loading of 0.375 mg/cm^2 for (e) silver (inset shows the SEM image of EDS spot) and (f) carbon.

Photos of bare cotton and Ag NW decorated cotton fabrics following disk diffusion tests against *Staphylococcus aureus* (Gram positive coccus), *Escherichia coli* (Gram negative bacilli), *Bacillus cereus* (Gram positive bacilli and spore forming bacteria), *Candida albicans* (a yeast like fungus) are provided in Figure 2.4 (a)-(d), respectively. Ag NW decorated fabrics showed promising antibacterial performance against all bacteria, whereas bare cotton fabric had no influence against any of the bacterium strain that were tested in this work.

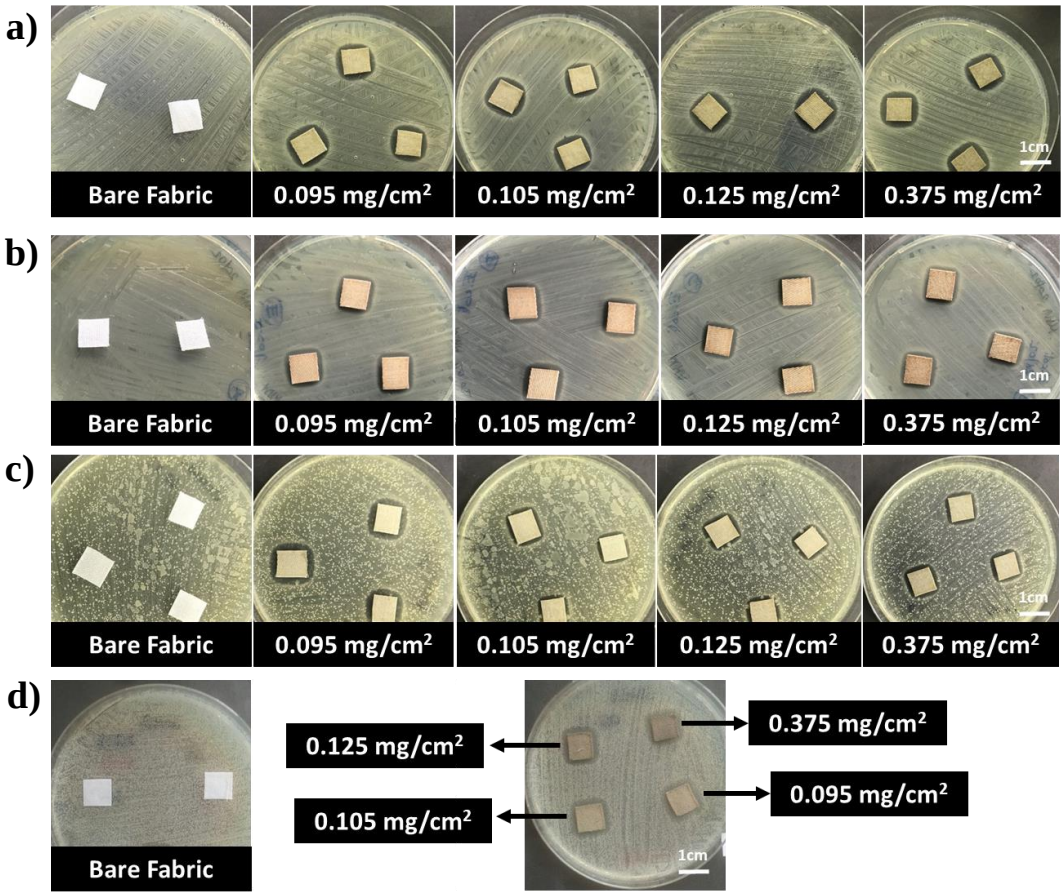

Figure 2.4 Photos of bare cotton and Ag NW modified fabrics following disk diffusion test against (a) *Staphylococcus aureus*, (b) *Escherichia coli*, (c) *Bacillus cereus*, (d) *Candida albicans*.

The size of the inhibition zones against all bacteria test strains are provided in Figure 2.5 (a). The inhibition zones can be described as the clear zones around the Ag NW coated fabrics on the petri plates, which contains bacterial suspensions cultured on suggested specific agar medium. While Ag^+ ions are diffusing into the bacterial agar media, it inhibits the bacteria and fungi grown on the agar at the meeting point, and there will be no bacterial growth until the concentration Ag^+ ions were enough to kill the bacterial and fungal cells. The size of the inhibition zones was measured for square samples, therefore; the inhibition zones are slightly lower at the edges of the samples. Size of the inhibition zones of Ag NW modified fabrics against *S. aureus* with NW loadings of 0.095, 0.105, 0.125 and 0.375 mg/cm^2 were 15, 14, 15 and 15 mm, respectively. This result implied that NW loading has no particular influence on the inhibition zones. A similar behavior was reported by Hebeish et al. for Ag NP decorated cotton textiles [52] . Size of the inhibition zones of Ag NW modified fabrics against *E. coli* with NW loadings of 0.095, 0.105, 0.125 and 0.375 mg/cm^2 were 14, 14, 15 and 14 mm, respectively. Similar to, *S. aureus* strains NW loading did not show any particular effect on the size of the inhibition zone, which was also observed for Ag NP and Ag NW decorated textiles in literature [49,53]. It is expected that Ag NWs would show wider inhibition zone against Gram negative bacteria since Ag^+ ions are positively charged. However, inhibition zones for *S. aureus* and *E. coli* were found to be more or less the same. Size of the inhibition zones of Ag NW modified fabrics against *B. cereus* with NW loading of 0.095, 0.105, 0.125 and 0.375 mg/cm^2 were 15, 13, 16 and 15 mm, respectively. The size of the inhibition zone was found to be independent of the NW loading, similar to *S. aureus* and *E. coli* strains, especially when standard deviations were taken into consideration. Sizes of the inhibition zones of Ag NW modified fabrics against *C. albicans* with NW loading of 0.095, 0.105, 0.125 and 0.375 mg/cm^2 were 13, 14, 14 and 14 mm, respectively. Similar to previous strains, NW loading had no influence on the size of the inhibition zones. Therefore, smaller amounts of Ag NW loading can also be investigated to determine the limits of Ag NW modified fabrics for antimicrobial applications.

Effective antimicrobial duration is an important feature for antimicrobial fabrics. The fabrics should have enough efficacy for a long-term use. Therefore, antimicrobial effect of 0.375 mg/cm^2 Ag NW modified fabrics were tested with respect to time for all tests strains and the results are compared in Figure 2.5 (b). Against *S. aureus*, the Ag NW modified cotton fabrics reached their maximum efficacy within two hours and killed 99.9 % of the bacteria and kept their performance for 8 hours. Then the antimicrobial activity started to decrease, and the bacterial concentration was found to catch its initial level after 24 hours. The death rate of Ag NW modified cotton fabrics against *E. coli* reached maximum (99.9%) within 2 hours and fabrics kept their performance for 24 hours. The fabrics reached maximum efficiency within 4 hours, and the death rate reached to 99.9% against *B. cereus*. Moreover, the fabrics kept their performance for 24 hours. The time required to reach maximum efficiency was longer for *B. cereus* than that for both *S. aureus* and *E. coli*. This can be attributed to the spore forming character of *B. cereus*. The bacteria colonies might protect themselves up to 4 hours. On the other hand, death rate reached a maximum of 99.9% within 2 hours and remained unchanged for 24 hours against *C. albicans*.

The discussion whether the antibacterial effect is caused by the nanostructure itself or Ag^+ ions released from the nanostructure has been recently concluded. Xui and coworkers showed that the nanostructure effect can be neglected, and the antibacterial effect is mainly due to the released Ag^+ ions [54]. However, the exact mechanism of the antibacterial effect of Ag^+ ions is unclear. Two possible mechanisms are discussed in the literature [43]. The first suggested mechanism is the direct membrane damage as a result of the interaction between Ag^+ ions and sulfur containing proteins of the cell membrane [55]. The second mechanism is the Ag^+ ions uptake through the cell. In this case, Ag^+ ions interact with respiratory chain proteins and prevent the deoxyribonucleic acid (DNA) replication [56]. Even though it is not clear which mechanism dominates for specific cases, these mechanisms are accepted as consecutively taking place.

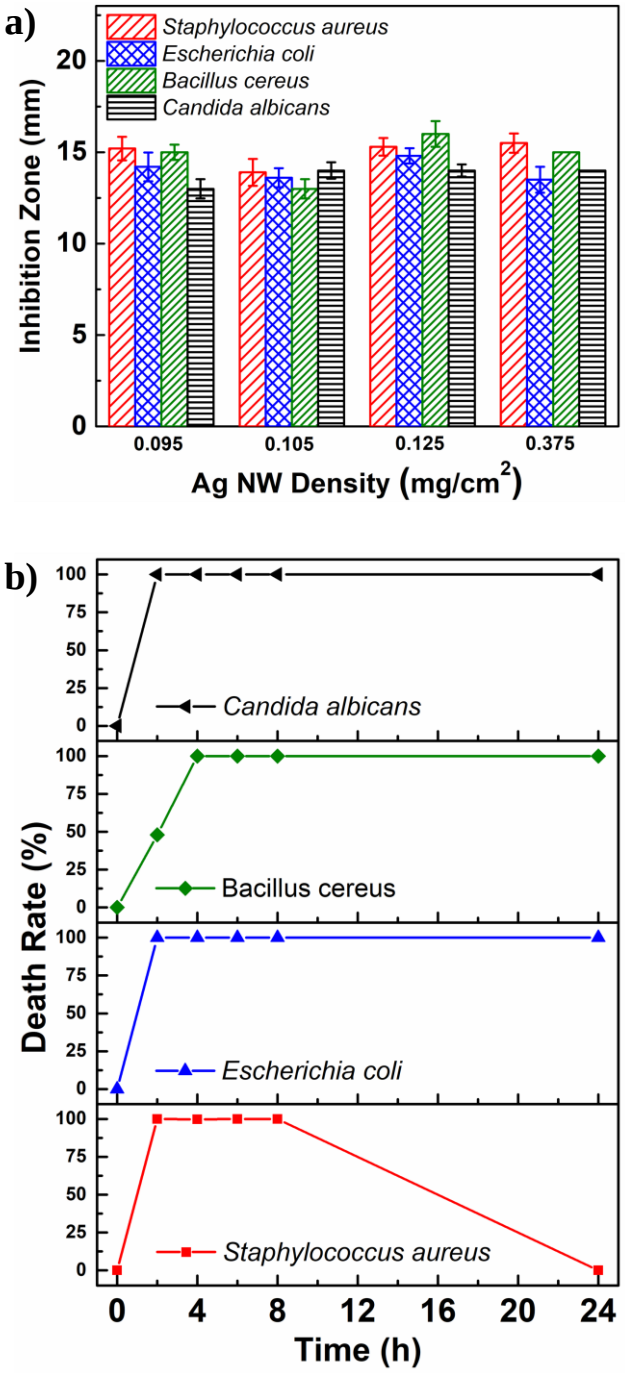

Figure 2.5 (a) Size of inhibition zones for Ag NW modified 1 cm^2 cotton fabrics measured by disk diffusion method with respect to Ag NW loading. (b) Bacterial death rate with respect to contact time against *S. aureus*, *E. coli*, *B. cereus* and *C. albicans* for 0.375 mg/cm^2 Ag NWs modified fabrics.

Morphologies of both living and dead bacteria were investigated via SEM to understand the antibacterial mechanism. SEM images of the bacteria on bare cotton and Ag NW decorated cotton fabrics are provided in Figure 2.6 (a)-(h). Perfect shapes of *S. aureus*, *E. coli*, *B. cereus* and *C. albicans* (indicated with arrows in Figure 2.6 (a), (c), (e) and (g) respectively) were observed implying that all tested bacteria can easily survive and multiply on bare cotton fabric. On the other hand, cellular malformation of the bacteria was occurred when the bacteria met the NW decorated fabrics. The final shapes of the dead *S. aureus*, *E. coli*, *B. cereus* and *C. albicans* bacteria are pointed with arrows in Figure 2.6 (b), (d), (f) and (h), respectively. Especially, due to the greater size of *C. albicans*, pit formations on the bacteria membrane are clearly observed (Figure 2.6 (h)). These pit formations are consistent with the antibacterial mechanisms of the Ag NW as mentioned before.

The results obtained in this chapter and next chapters clearly shows that deposition of Ag NWs makes fabrics multifunctional. Multifunctionality of the fabrics should not be limited only to antimicrobial textiles, but should be extended further with applications such as heated textiles and wearable self-powered sensors that will be discussed in the following chapters.

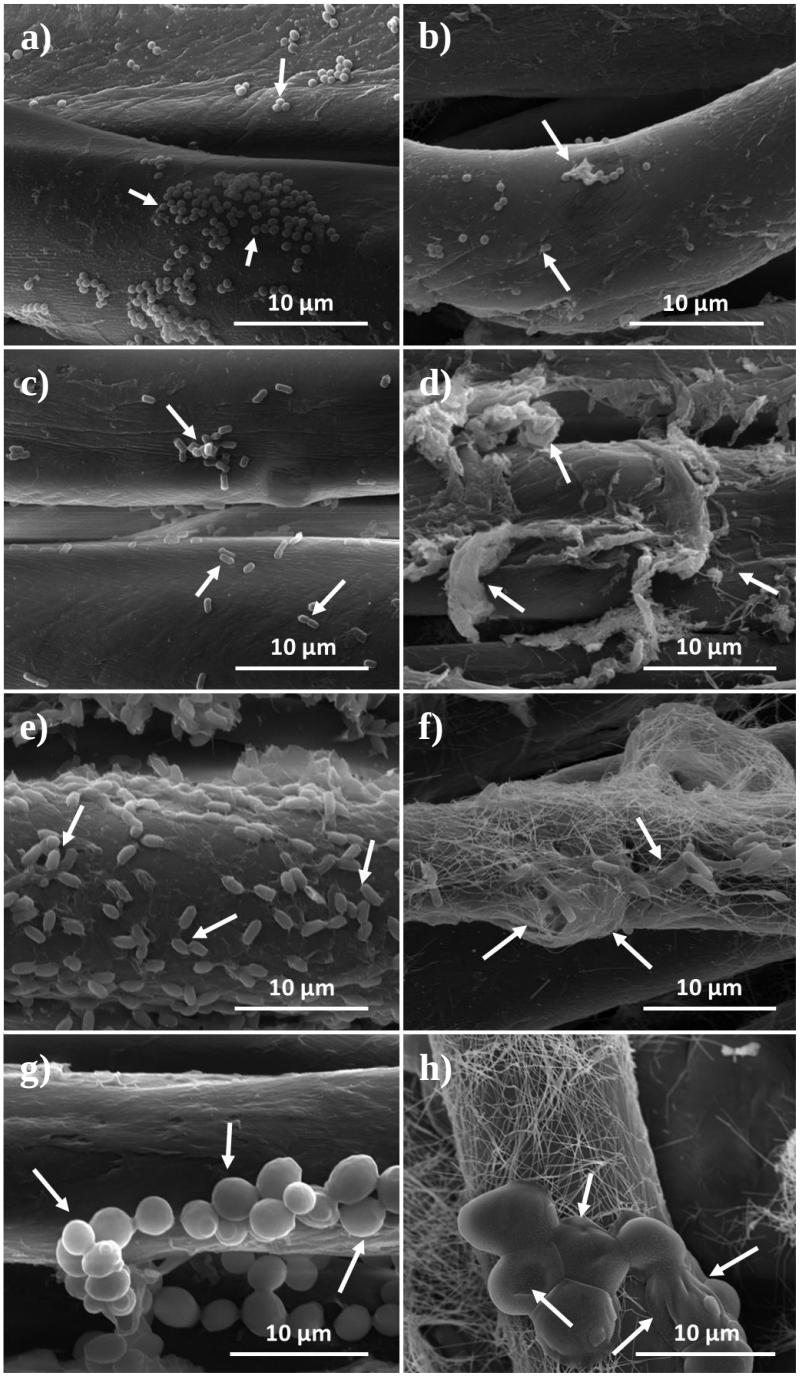

Figure 2.6 SEM images of (a) living and (b) dead *S. aureus*, (c) living and (d) dead *E. coli*, (e) living and (f) dead *B. cereus*, (g) living and (h) dead *C. albicans*. living arrows show the actual shape of the living bacteria and the cellular mal-formation of the bacteria. Living bacteria are on the bare cotton fabrics and dead bacteria are on the Ag NW modified fabrics.

2.5 Conclusions

Antimicrobial performance of Ag NW modified cotton fabrics was investigated in this study. Dip and dry method was utilized as a facile, scalable and reproducible way to modify cotton fabrics with Ag NWs. Moreover, the Ag NW loading on the fabrics can be easily controlled with this method. Ag NW modified fabrics showed promising antibacterial performance against a wide range of bacteria strains. The inhibition zones of the 1 cm^2 modified fabrics were found to be around 15 mm for each bacterium strain (*S. aureus*, *E. coli*, *B. cereus* and *C. albicans*). Moreover, measured Ag NW loading was found to have no influence on the size of the inhibition zone for all bacterium strains. In addition, effective antibacterial duration was also investigated for all of the test strains. It was observed that the modified fabrics reach their maximum antimicrobial efficacy within the first 2 hours against *S. aureus*, *E. coli*, *C. albicans*. On the other hand, maximum efficacy was found as 4 hours against *B. cereus*, which was attributed to the spore forming nature of *B. cereus*. Moreover, the modified fabrics kept their performance up to 24 hours against *E. coli*, *C. albicans*, *B. cereus* and 8 hours against *S. aureus*. All in all, Ag NW decorated cotton fabrics demonstrated herein showed promising antibacterial performance and this revealed the potential of the use of Ag NWs as antibacterial modifiers in the textile industry due to their wide range, relatively long-term antimicrobial effect and scalable production route. As shown, the small amount of Ag NW decoration enabled promising antimicrobial performance with a cost-effective way compared to conventional antimicrobial textiles.

CHAPTER 3

SILVER NANOWIRE MODIFIED HEATED TEXTILES

3.1 Introduction

Classical fabrics started to be evolved into so called “electronic textiles”. Most prominent examples of smart textiles include but not limited to outdoor wear, foldable displays, portable power supplies, sensors, healthcare, military equipment and work wears [57]. Nanomaterials provide enhanced properties and impart new functionalities to the textiles. Various nanomaterials have been introduced for the formation of antibacterial, water repellent, soil resistant, antistatic, anti-infrared and flame-retardant textile materials [58,59]. One direction in this vastly developing field is the fabrication of electrically conductive textiles with application areas such as electromagnetic interference (EMI) shielding and wearable antennas. They can also function as interconnects for built-on electronic devices just as health monitoring sensors, supercapacitors and batteries [60–63]. There are several methods to modify conventional textiles. Casting, depositing, spinning, printing, solution growth and dipping and drying methods have been widely used to fabricate electrically conductive textiles [64–71]. Among all, dipping and drying methods seems to be the most economic and easy way in laboratory scale.

Another intriguing application area of electrically conductive textiles is a heating unit that operates by the Joule heating mechanism. Carbon nanotubes (CNTs), a well-known 1-D nanomaterial, have been used as a conductive material in heated textiles [72,73]. One of the recent studies has shown that the increasing fiber length of the conductive fabrics decreases the heating performance [72]. For instance, under an applied voltage of 40V, the fabrics were observed to be heated up to 90°C. Although individual carbon nanotubes are highly conductive, the junction resistance between two carbon nanotubes is found to be very high [74]. For instance, the maximum

temperature has been determined as 70°C under an applied voltage of 60V. Although the temperature is enough for heating purposes, 60 V is too high to be used for electronic textiles. Moreover, low operating voltage is compulsory not only for heating applications but also for other applications such as memory and sensors [75,76]. Such a high contact resistance in these aforementioned works increases the overall resistance of the fabrics resulting in an extensively high applied voltage. That is a problem for mobile heating applications. As opposed to CNTs, Ag NWs seem to be a promising candidate. Silver among all metals, have the highest electrical and thermal conductivity. It is cheaper than gold and platinum, and is more stable in air than its biggest competitor, copper. Due to these superior properties of bulk Ag, its nanostructures, especially Ag NWs attracted much interest. So far, Ag NWs have been used as transparent and conducting thin films in light emitting diodes, solar cells and photodetectors [77–79]. Moreover, Ag NWs were demonstrated as heating elements on transparent substrates [80–82]. For instance, Ag NWs deposited on polyethylene terephthalate (PET) surface has shown such a performance that the transparent heater reaches to 55°C under an applied voltage of 7 V [80]. Another study, utilizing polydimethylsiloxane (PDMS) as a stretchable substrate, investigated the effect of stretching amount on warming up performance of the heaters [81]. Furthermore, oxidation resistant hybrid materials in conjunction with the Ag NWs were used in these transparent heaters to increase lifetime of the NWs [82]. UV-blocking performance of Ag NW decorated functional fabrics were also demonstrated [83]. Different fabrics coated with Ag NWs via dip and dry method were also investigated in terms of their electrical conductivity performance under various mechanical treatments [84]. Furthermore, highly Ag NW loaded cotton fabrics have been determined to be promising candidates for heating applications by taking into consideration their infrared reflection properties [24]. Moreover, Ag is famous as its high antibacterial activities; therefore, its nano forms are widely investigated to utilize for antibacterial purposes [51]. Therefore, antibacterial activity of Ag NW decorated textiles have also been investigated by Cui and co-workers [24]. In none of these prior arts, the true potential and limits of Ag NW decorated cotton fabrics as

heating elements are demonstrated in terms of the thermal response and stability under different conditions.

In this work, heating performance of Ag NW decorated cotton fabrics are reported. Dip and dry method, allowing the control on the thermal performance of the cotton fabrics, is used for the decoration of Ag NWs onto the fabrics. In addition, a simple heating circuit, which is operated with a 3V battery, is also demonstrated to clearly show the potential of the heated fabrics for mobile heating applications.

3.2 Experimental Procedure

3.2.1 Materials

The 100 % cotton textiles were used for the experiments. All glassware and textiles used in the experiments were cleaned using acetone (99.8%), isopropyl alcohol (99.8%) and finally with deionized water (18.3 MΩ). All chemicals were purchased from Sigma-Aldrich and used without further purification. Ethylene glycol (anhydrous, 99.8%), polyvinylpyrrolidone (PVP) (monomer-based calculation MW = 55000), sodium chloride (NaCl, 99.5%) and silver nitrate (AgNO3, ACS reagent, ≥99.0%) were used for the polyol synthesis of Ag NWs.

3.2.2 Synthesis of Silver Nanowires

Ag NWs were synthesized according to our previous study [51]. Following synthesis nanowires were purified. Purification involved washing for several times with ethanol and centrifuging for the recovery of the nanowires. The final product was then dispersed in ethanol for further characterization and processing.

3.2.3 Ag NW Decoration onto Cotton Fabrics

Simple dip and dry method was used to fabricate the conductive fabrics. Basically 20 ml of 0.2 mg/ml ethanolic solutions of Ag NWs were prepared. Afterwards, pre-cleaned bare cotton fabrics were immersed into this solution for 5 minutes and dried at 80 °C for 10 minutes. This procedure was repeated until a resistance of 2.5 ohm/cm was measured from the samples. Silver paste and copper tape were used to ease the connection between copper wires and Ag NW decorated cotton fabric heaters.

3.2.4 Characterization

The presence and homogeneity of the Ag NWs on the fabrics were monitored using a Scanning Electron Microscope (SEM). The SEM studies were performed on a FEI NOVA NANO SEM 430 microscope operated under low voltage to prevent burning. Sheet resistance measurements are performed using a Keithley 2400 source meter. Thermal response of the textiles was measured using an Agilent 34910A data acquisition unit using 4 thermocouples. Thermal monitoring of textiles was also done by InfRared Thrmography (IRT) and changes in surface temperature during heating period were recorded versus time by taking sequential images with FLIR (ThermoCam SC640) thermal camera. Bending tests were performed via a custom-made bending setup. To simulate washing conditions, Ag NW decorated fabrics were stirred on a hot plate at 500 rpm for 30 minutes in deionized water at 40°C.

3.3 Results and Discussions

A simple schematic presentation of the coating procedure is given in Figure 3.1 (a). The SEM image of the Ag NW decorated textile fabricated through the dip-dry process is shown in Figure 3.1 (b). Individual fibers covered with Ag NWs were visible in the SEM image that ensured the formation of a homogenous and conductive network via dip and dry process over large areas. Each dip and dry cycle

increased the amount of deposited Ag NWs on the cotton fabrics. This resulted in a decrease in the electrical resistance of the fabric in certain extent as given in Figure 3.1 (c), showing the change in electrical resistance versus the number of dipping-drying cycles. A sheet resistance value of 2.5 ohm/cm was achieved after 25 dipping-drying cycles. That simple method allowed successful formation of a homogeneous and three-dimensionally (3D) conductive network within the fabrics with controlled resistance.

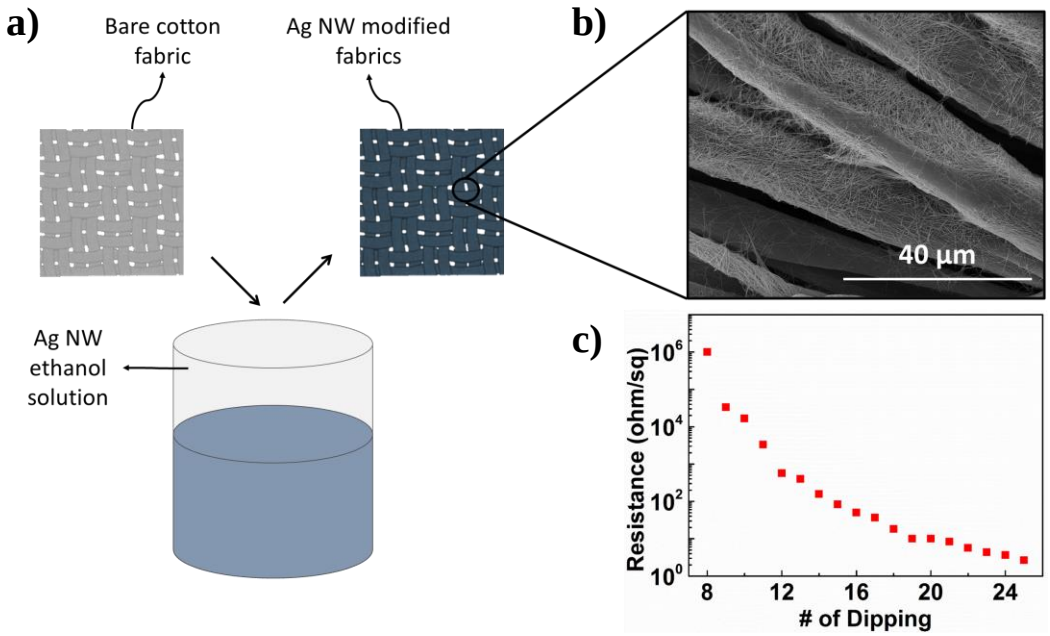

Figure 3.1 (a) Schematic illustration for the decoration of Ag NWs onto the fabrics. (b) SEM image of the individual fibers of the cotton fabric. (c) Plot showing the change in sheet resistance of the fabrics with respect to number of dipping-drying cycles.

Time dependent temperature response of fabrics was monitored by thermocouples under various applied voltages, results of which are provided in Figure 3.2 (a). Following the warming up period of the heaters, they reached a steady state condition where the surface temperature was the highest and constant. A sharp drop in surface temperature was observed immediately after the end of the heating process. This heating and cooling profile is a typical behaviour of Joule heating (electrothermal

heating). According to energy conservation principle, the input power (q_{input}) is equal to total output power which is the summation of energy absorbed by the heating element and substrates (q_1 and q_2), thermal convection ($q_{convection}$) and thermal radiation ($q_{radiation}$), given by:

$$q_{input} = q_1 + q_2 + q_{convection} + q_{radiation} \quad 3.1$$

This can be written by:

$$V^2/_R = C_1 m_1 \frac{dT}{dt} + C_2 m_2 \frac{dT}{dt} + h_c A(T - T_0) + \varepsilon\sigma A(T^4 - T_o^4) \quad 3.2$$

where, m_1, m_2, are mass of heating element (Ag NWs in our case) and substrates (fabrics in our case), respectively. C_1, C_2 are the specific heat capacity of heating element and substrates, respectively. A, T and T_0 are the surface area, initial and final surface temperatures, respectively. h_c, ε, and σ are convection heat transfer coefficient, emissivity and Stephen-Boltzman constant (5.67 x 10^{-8} Wm^2K^{-4}), respectively. V is applied voltage and R is the resistance of the heating element (conductive fabrics in our case).

When temperature reach a steady state, temperature change is zero and $dT/dt = 0$ then Equation 3.2 becomes:

$$q_{input} = hA(T - T_0) + \varepsilon\sigma A(T^4 - T_o^4) \quad 3.3$$

Steady state temperatures were recorded between 30 and 125°C corresponding to applied voltages in between 1 and 6 V. Each recorded temperature value can be used in various fields of applications. A setup that increases temperature up to 50°C can be useful for everyday applications. For instance, it can be adapted in undercoating for conventional products like jackets and shoes. On the other hand, a setup that increases temperature above 50°C can be suitable for extremely cold outdoor conditions. Time required to reach the steady state condition can be described as the

response time. The response time of the textiles was 100 s, which was consistent with the recent studies [24,85] and a response time around 100 s was quite suitable for mobile heating applications under critical conditions. Moreover, cooling period showed that the heat releasing ability of the fabrics was quite high so that the heated textiles can reach to room temperature in several minutes upon shut down. The change in steady state temperatures with respect to the applied voltage in Figure 3.2 (b). Due to applied electric field, charge carriers (electrons) are accelerated and collide with phonons or other defects. As a result of this inelastic collision the observed heat is released. In current case, the junction point between two nanowires is the major defect. Therefore, the heat released from the junction point is higher than that from a nanowire [86]. The plot showing steady state temperature variations with respect to the applied power density is given in Figure 3.2 (c). The power required to heat 1 cm^2 fabric from room temperature to 50 °C was recorded as 0.05 W. This ultra-low power density confirmed that Ag NW decorated textiles are very suitable for mobile heating applications. Upon increasing the applied voltage to 6 V, a surface temperature of 125 °C was achieved, which was followed by a sudden decrease. Only for that case where the surface temperature reached to 125°C, a burned region on the fabric was observed, even by a naked eye. SEM image of this burned region is provided in Figure 3.2 (d). It was clear that Ag NW network was somehow damaged and lost connectivity. That resulted in an increase in fabric resistance to megaohm level. It was assumed that some of the Ag NWs were damaged due to ignition of cotton fibres and this caused to the interruption of the 3D network. It was clearly the cotton fabric not the Ag NWs, which limited the attainable temperatures. It is known that these nanowires can operate at higher temperatures on heat resistant substrates [82]. However, such a high temperature (125°C) is probably not needed for heated cotton fabric applications.

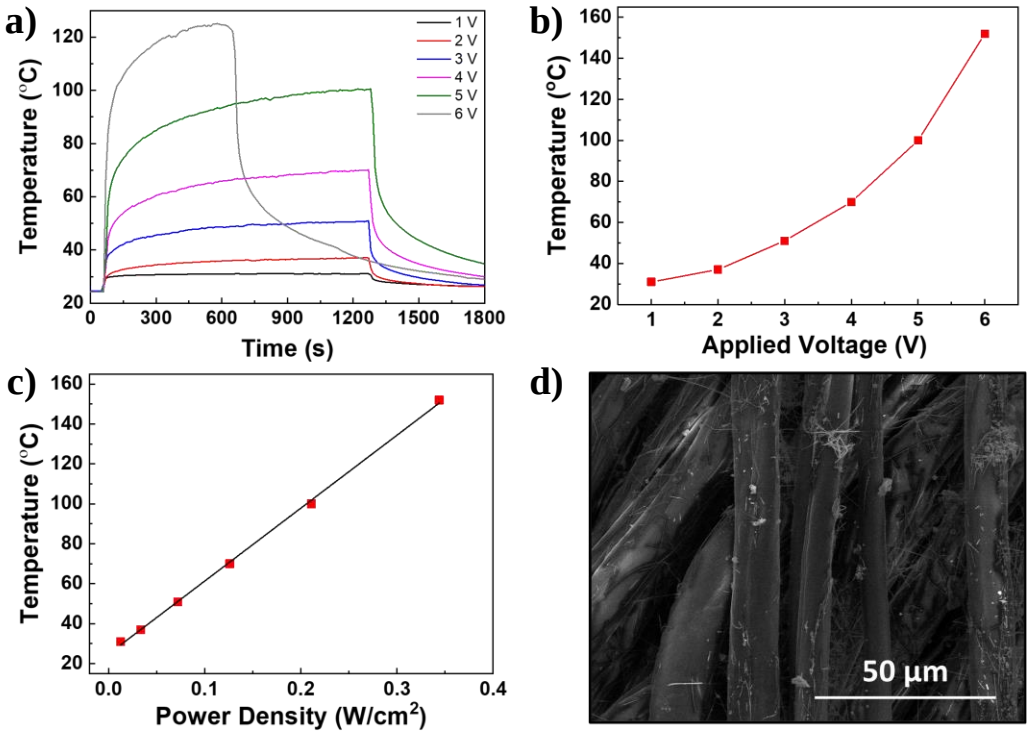

Figure 3.2 (a) Temperature profiles of the fabrics under different applied voltages. (b) Steady state temperature values of the heated fabrics with respect to the applied voltage and (c) power density (lines are for visual aid). (d) SEM image of the burned region following the application of 6V.

The case where 3.5 V was applied on Ag NW decorated cotton textile was monitored by infrared thermography. The IR images of the fabric for on and off states and the plot showing the evolution of its surface temperature are presented in Figure 3.3. Temperature distribution of the fabrics under applied voltage was quite uniform (Figure 3.3 (a), (b)) revealing the homogeneity of the Ag NW coating. The three stages of temperature changes namely, warming up period, the period when the surface temperature is highest and constant and cooling down period, were also observed in the plot showing the evolution of surface temperature obtained from IR thermography (Figure 3.3 (c)). The thermal response time was measured as 100 s for this particular case and the fabric surface reached 70°C with the application of 3.5 V. Those results were also consistent with the thermocouple measurements. The

results obtained so far clearly showed that the dip-dry method offers an easy, effective and homogenous deposition route for Ag NWs onto cotton textiles.

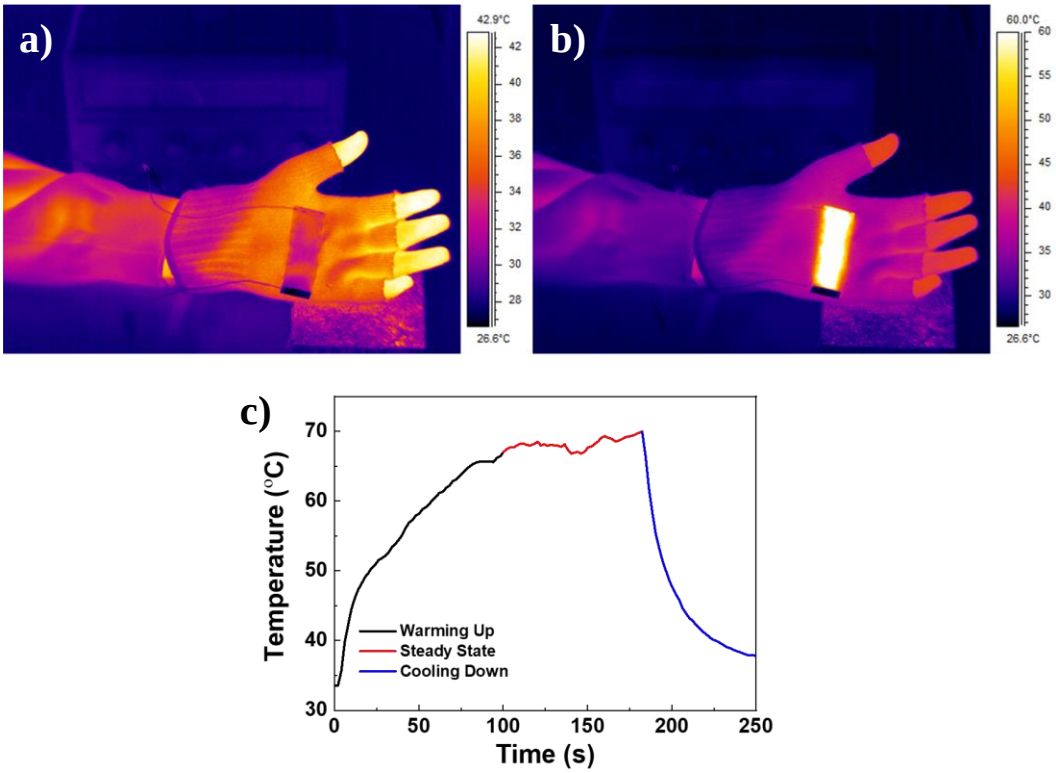

Figure 3.3 (a) Initial IR image (IR448) before starting to heat the fabric (off state). (b) IR image of the fabric when its surface temperature is highest and constant during the heating period under an applied voltage of 3.5V (on state). (c) Temperature profile of the fabrics obtained from IR thermography.

This kind of smart textiles must be stable and reliable under different conditions to fulfil daily operations. One issue is the reproducible performance. Heating profile of the Ag NW decorated textiles under 3V for 10 repeated on/off cycles (20 minutes at on state and 10 minutes at off state) is provided in Figure 3.4 (a). Response times and steady state temperatures were found to be stable during voltage cycles. Heating profiles of the same textile sample was recorded for two months and it is provided in Figure 3.4 (b). Profile for the as-fabricated sample is also provided for comparison. These fabrics were stored under ambient conditions without an extra protective coating on them. A sharp performance drop was observed after two months. The

recorded temperature dropped from 52 ºC to 38 ºC for the same fabric after two months of storage. This phenomenon can be attributed to the oxidation of Ag NWs under ambient conditions [86]. However, a suitable protective layer might easily increase the lifetime of Ag NWs and thus the heated textiles, which is investigated in following chapter. The heated textile should also maintain its performance for curved body parts, such as arms, legs or ankles, provided that the heating performance is stable under various bending angles. To simulate this situation, Ag NW decorated textiles were bent to different bending angles and temperature profiles were recorded under an applied voltage of 3 V. The steady state temperatures of these bent textiles under different bending angles are provided in Figure 3.4 (c). The heating performance under different bending angles remained unchanged even at a bending angle of 180º. Commercially available heated fabrics generally consist of either a woven solid metal wire or coated metal films. Solid wire is usually copper or stainless steel and metal thin film is silver. Nevertheless, these kinds of conductive threads are not truly suitable for wearable applications since they are stiff and brittle. Therefore, they can break and cause problems after repeated bending cycles [84]. The heating performance of Ag NW decorated textiles upon repeated bending cycles were also measured and is provided in Figure 3.4 (d). The performance remained unchanged after 5000 bending cycles. It is clear that Ag NW decorated cotton fabric heaters offer high mechanical durability.

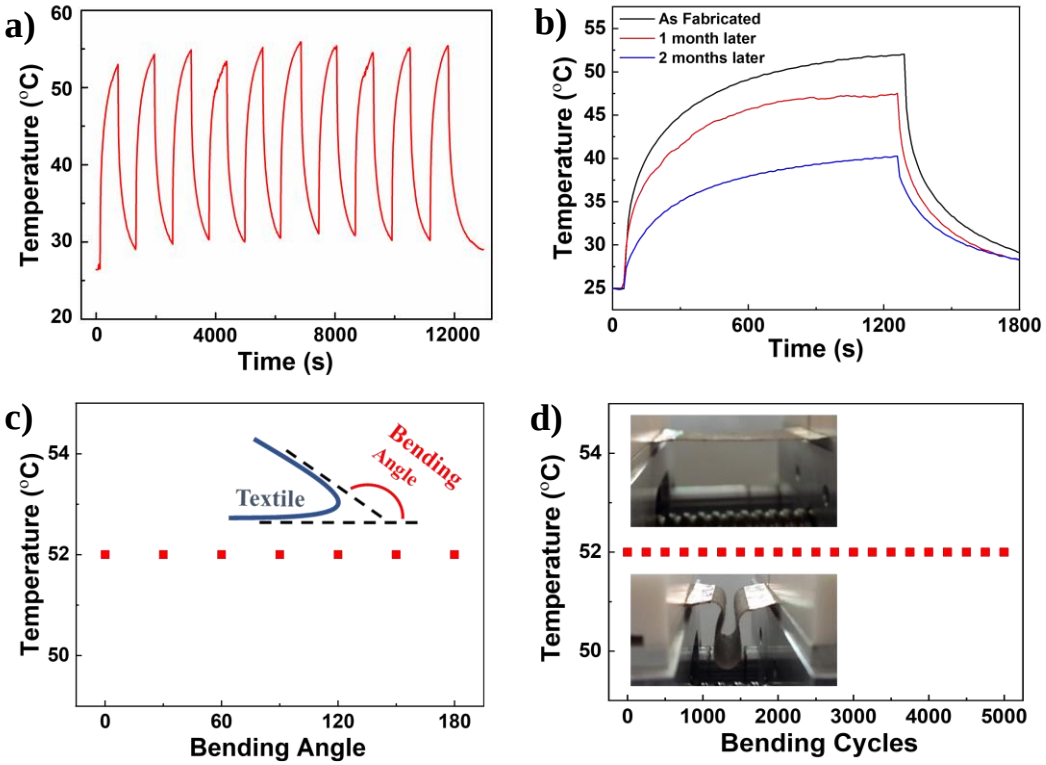

Figure 3.4 Stability of Ag NW decorated textiles under an applied voltage of 3 V. Temperature profile (a) under repeated on and off cycles, (b) after 1 and 2 months of storage period under ambient conditions, (c) change in heating performance upon bending at different angles and (d) after 5000 bending cycles down to a bending angle of 180°. Inset shows the photograph of custom-made bending setup.

Washing stability of the smart textiles is another important parameter that should be addressed. For this reason, the heating performance of the Ag NW decorated textiles under an applied voltage of 3 V with corresponding sheet resistance values following washing tests were monitored and provided in Figure 3.5 (a) and (b), respectively. After the first washing test, the temperature of the fabrics increased from 57 °C to 86 °C accompanied with a decrease in sheet resistance from 2.4 to 1.6 ohm/cm. As the number of washing cycles was increased, attained temperatures by the textiles were decreased while the sheet resistance was increased. The reason behind this intriguing behaviour can be explained by the presence of PVP on the lateral surfaces of the nanowires. During the first washing, insulating PVP gets dissolved in water

decreasing the sheet resistance of the fabrics [87]. As a consequence, a high level of current passes through the fabric increasing the attained steady state temperature (from the Joule's law). Detecting the effect of water on the PVP layer is quite challenging with spectroscopic techniques such as Raman of FTIR. Cellulose is the building block of the cotton fabrics and it suppresses the Raman and FTIR spectra of PVP. Moreover, in case of operating SEM under low voltages, resolution levels required to detect the PVP layer cannot be attained. Therefore, in order to control PVP layer thickness after the first washing step, Ag NWs were deposited onto a polished silicon wafer. Thickness of the PVP layer for the as-deposited samples without washing was measured as 10 nm (Figure 3.5 (c)). This PVP layer got almost completely dissolved by water after the first washing cycle as evidenced by the SEM image provided in Figure 3.5 (d). An SEM image of the Ag NW decorated textiles after five washing cycles is provided in Figure 3.5 (e). Following several washing cycles, it was observed that the 3D network of the Ag NWs got damaged. Ag NW layer on the outermost fibers seemed to get lost; but the fabrics still possessed conductivity provided through the Ag NWs on the inner fibers.

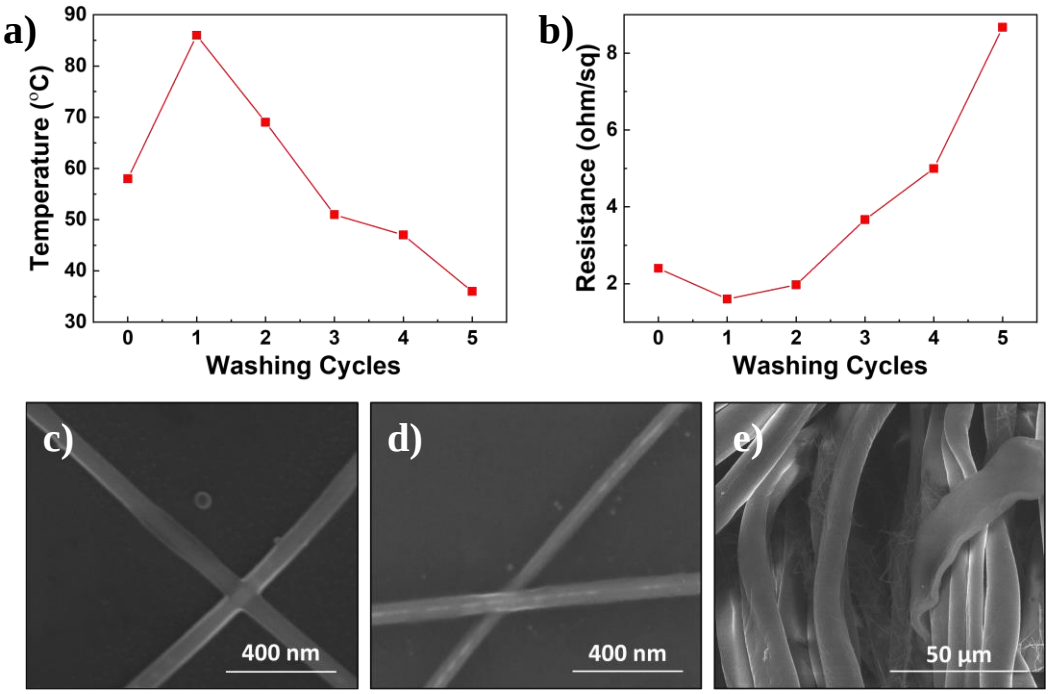

Figure 3.5 Effect of washing cycles on the (a) heating performance and (b) sheet resistance of the Ag NW decorated fabrics. Lines are for visual aid. SEM images of (c) as-deposited Ag NWs onto silicon wafer, (d) washed Ag NWs on wafer and (d) five times washed Ag NW decorated fabric.

In order to make these fabrics truly mobile and to precisely control their temperature, a simple control circuit with hysteresis (bang bang) control was designed. Designed circuit that operates between two states was drawn with LTSpice IV circuit simulator program, as shown in Figure 3.6 (a). A photograph of the heated fabric with the designed circuit is provided in Figure 3.6 (b). The fabric and NTC thermistor are shown isolated for simplicity in the schematic. Switching was provided via an operational amplifier (LM358P), which provided output signal by comparing the voltage values between its non-inverting (+) and inverting (-) input terminals. When the fabric was cold, the input voltage at the non-inverting terminal, due to the high resistance of the NTC thermistor was high. This means that the operational amplifier went into positive saturation and provided the output voltage as +Vcc (in this case +Vcc was equal to the voltage of the source/battery). When the temperature of the

fabric reached the desired temperature (which can be adjusted using the potentiometer), the resistance of the thermistor dropped, so that the operational amplifier provided the output voltage as –Vcc (in this case –Vcc is equal to 0 V) by changing its saturation region.

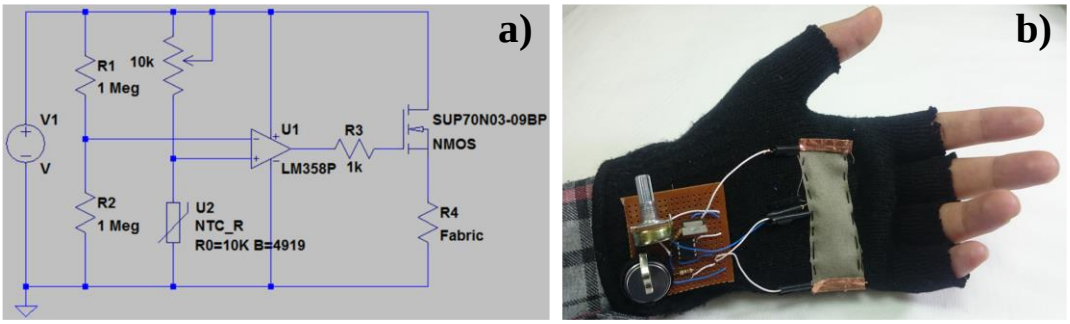

Figure 3.6 (a) Schematic representation of the designed circuit for mobile heating applications. (b) A photograph of the Ag NW decorated fabric sewed on a glove with the control circuit.

Finally, effect of the fabric density on the heating homogeneity of the Ag NW modified fabrics were investigated. Ag NWs were dip coated on 10 x10 cm fabrics having the densities of 54 and 160 g/m^2. Heating homogeneities of the fabrics under same applied power were investigated via thermal camera. Average temperature of heated fabrics was recorded as 53.0 and 51.2 ^{o}C, for the fabrics having the density of 54 and 160 g/m^2, respectively (Figure 3.7 (a) and (c)). Percentage of the pixels within the corresponding temperature intervals indicates heating homogeneity. The fabric having the density of 54 g/m^2 has broader temperature distribution than the fabrics having the density of 160 g/m^2 (Figure 3.7 (b) and (d)). This result implies that Ag NWs were modified onto fabrics more homogenous for the fabrics having higher densities.

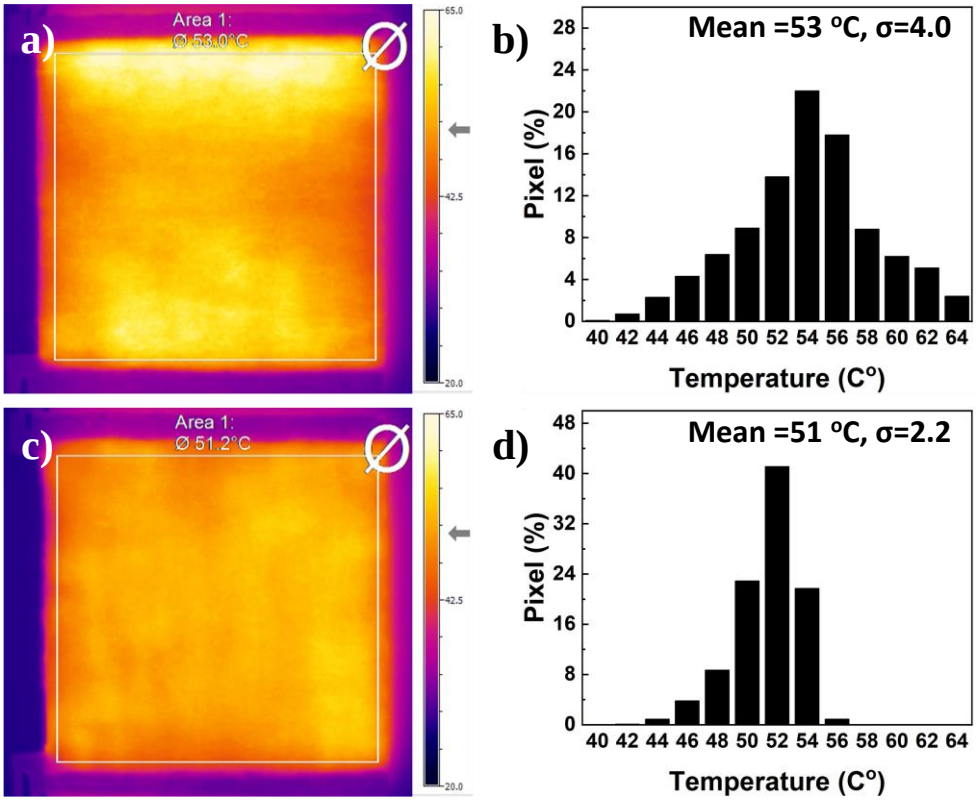

Figure 3.7 (a) IR image and (b) temperature distribution of fabric having fabric density of 54 g/m^2. (c) IR image and (d) temperature distribution of fabric having fabric density of 160 g/m^2.

Heated fabrics demonstrated herein showed great potential for mobile heating applications particularly due to their low power consumption. This was provided through Joule heating and enabled by the Ag NWs with small diameters. In addition, high aspect ratio of the nanowires allowed their uniform and homogeneous decoration onto the textile fibers providing 3D interconnected network. Nanowire morphology was also important in determining the mechanical performance of the heated textiles combined with the ductile nature of the Ag NWs.

3.4 Conclusions

The heating performance and stability of the Ag NW decorated cotton fabrics were investigated in this study. It was found that the facile dip and dry method can be used to reproducibly fabricate Ag NW decorated conductive fabrics. Time dependent heating profiles of the fabrics under different applied voltages revealed that the operating temperatures can be easily set by the applied voltages. In addition, Ag NW decorated fabrics showed high stability under different bending angles. The heating performance of the fabrics remained unchanged after 5000 bending cycles. However, due to relatively low environmental stability of Ag NWs, the heated fabrics lose their performance after two months of ambient storage. Washing stability of the Ag NW decorated fabrics was examined in detail. Heating performance of the fabrics got dramatically increased after the first washing cycle. This is attributed to the dissolution of PVP layer in water resulting in the reduction of the overall resistance of the system. In the following washing cycles, the 3D conductive network of the Ag NWs got damaged and the heating performance dropped. It is evident that a proper coating should be developed to improve the environmental and washing stability of the fabrics.

CHAPTER 4

FUNDAMENTALS OF TRIBOELECTRIC NANOGENERATORS

4.1 Background

Triboelectrification has been known since Thales of Miletus from Anatolia for more than 2600 years. This physical phenomenon occurs between all matters that are solid, liquid and gas. Avoiding from the negative effects of triboelectrification was the main concern for both the industry and scientific fields. Since triboelectrification may cause serious problems such as explosions and electronic equipment damage. However, it was first purposed by Wang in 2012 that, triboelectrification is a promising solution for some of today's technology/energy problems [27] [REF]. This work shifted the main focus of triboelectrification research to faulting/utilization, rather than inhibition/prevention. In their early studies, Wang and coworkers, showed that triboelectrification phenomenon can be successfully implemented as a power source through converting harvested mechanical energy into electrical energy. These devices stated to be called as triboelectric nanogenerators (TENGs). Following these early studies, an exponential growth has been observed in the number of studies for the use of TENGs in different applications. Contact electrification (triboelectrification) and electrostatic induction are the two successive effects which are the fundamental phenomena of TENGs. Although there have been many important studies on the precise mechanisms of contact electrification over the past two decades, it is still debated. Electron, ion and material transfers are the proposed mechanisms as the origin of contact electrification. These mechanisms will be discussed in the following sections. Then, the foundations of TENGs will be covered.

4.2 Contact Electrification

4.2.1 Electron Transfer Model

The origin of the contact electrification between metal-metal and metal-dielectric surfaces certainly involves electron transfer [88]. Electron transfer between these surfaces has a strong correlation between work function of metals and valence/conduction bands of insulators [89–91]. Dominance of electron transfer mechanism over other mechanisms for metal-dielectric contact were also experimentally shown using atomic force microscopy in 1989 [92]. On the other hand, electron transfer between dielectric-dielectric surfaces upon contact is more difficult. Since transferring an electron from valance band of one dielectric to conduction band of the other dielectric requires much higher energy than the thermal energy at room temperature ($kT \approx 0.0026$ eV) [93]. However, electrons located in intermediate states (surface or defect) within the band gap are often referred as the electron source to overcome these high energy barriers. There are several studies conducted to demonstrate electron transfer mechanism for dielectric-dielectric contacts in late 2000s and early 2010s. In one of these studies, Lui and Bard show that some electrochemical reactions like metal deposition, chemiluminescence, hydrogen formation, pH variations can be conducted by the tribocharged polymer surfaces [94–96]. These chemical reactions occur under presence of electrons. Therefore, they concluded that electron transfer is the charging mechanism for contact electrification. However, observed charge densities of contact electrification as the result of their experiments were higher than the theoretical calculations. They explain this difference by describing the term cryptoelectrons. Then, Baytekin et al. showed that mechanoradicals produced by the mechanical stress during contact electrification carry out these redox reactions but not the cryptoelectrons[97]. Recently, Wang et al. stated that electron transfer is the dominant mechanism for contact electrification for all solid-solid pairs [98]. An interatomic interaction model was developed to explain foundations of electron transfer for contact electrification.

Figure 4.1 (a) shows interatomic interactions between two atoms of contact surfaces. An equilibrium distance called bond length is established when two atoms bond. When the interatomic distance is shorter than the bond length, the atoms tend to repel each other. On the other hand, the atoms tend to attract each other when the distance is greater than the bond length. According to interatomic interaction model for contact electrification, electron transfer occurs between two materials when the interatomic distance between the materials is shorter than the bond length (repulsive force regime). In this regime electron clouds of the atoms overlap. As a result of this overlap, separate potential well of the atoms becomes asymmetric double wells. Potential barrier between two atoms is lowered resulting in electron transition from one atom/molecule to the other atom/molecule as schematically shown in Figure 4.1 (b). The transferred electrons retain their new positions as the atoms are separated. If there is an electron transfer occurred as the result of contact electrification, thermionic or photoelectron emissions are needed to be observed. Experimental observations of thermionic and photoelectron emissions also support electron transfer model between metal and dielectric surfaces [99,100].

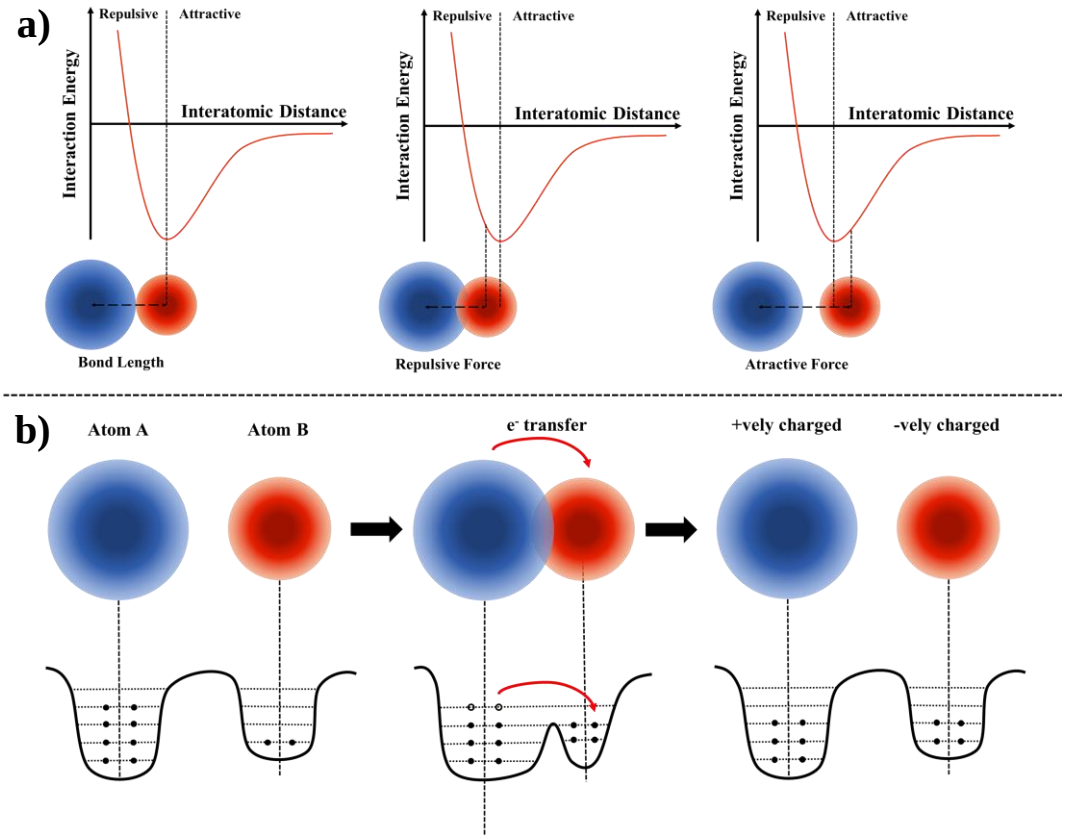

Figure 4.1 Schematic representation of (a) interatomic interactions of two atoms at equilibrium position, repulsive and attractive regions, (b) electron-cloud-potential-well model of electron transfer mechanisms for contact electrification [98,101]. Adapted with permission of Elsevier.

4.2.2 Ion Transfer Model

Ion transfer model is also proposed as the origin of the contact electrification [88,93]. There are basically two approaches that exist in this model depending on the type of the contacted polymer. If contact materials contain mobile ions, contact electrification occurs as a result of mobile ion transfer. A schematic representation of this model is provided in Figure 4.2 (a). In the schematic, cations are covalently bound to the polymer and anions are mobile. The same mechanism is valid if the anions are covalently bound and the cations are mobile. When, two surfaces come

into contact, mobile ions (anions or cations) transfer from ionic polymer to the other surface. Medley used ion exchange resins as one of the contact surfaces to validate the proposed mechanism. Medley showed that after contact electrification, ion exchange resins are charged with the same sign as their covalently bonded ion [102]. These results indicate that, mobile ions were transferred to the other contact surface. Later, Diaz and coworkers extend this work with different ionic polymers and observed that ion-containing polymers are always charged with the same sign of covalently bound ions [103,104]. They also showed that increasing the concentration of mobile ions increases the surface charge. However, mobile ion transfer mechanism is not sufficient to explain contact electrification of non-ionic polymers. Therefore, ion transfer model was improved for non-ionic polymers. Diaz and coworkers suggest a water bridge model to explain ion transfer mechanism for non-ionic polymers, which is schematically represented in Figure 4.2 (b). For non-ionic polymers, the absorbed water on the polymer surfaces is the source of the ion transfer. Typically, 1-2 nm thick water film is absorbed on the polymer surfaces. In this film, OH^- ions accumulate in the Stern layer and H^+ ions are solved in the water bridge. Once two polymers are in contact, the OH^- ions are redistributed onto the surfaces of the polymers depending on the OH^- accumulation affinities of the surfaces. The surface having more OH^- ions is negatively charged and the surface having less OH^- ions is positively charged. Whitesides and coworkers showed that contact charging of polystyrene increases in basic environment and decrease in acidic environment [105]. Their results support the OH^- absorption model for the contact electrification. The difference in OH^- absorption affinities of the polymers is still controversial. However, OH^- absorption magnitudes of the surfaces can be characterized by zeta-potential analyses [93]. A positive correlation between zeta potential and contact electrification for several polymers were also reported. However, there are also some contradictory cases reported in literature [106]. Water bridge model was challenged in several studies at different relative humidity levels. Whitesides et al. observed that surface charge increases in high relative humidity levels [105]. Diaz and coworkers reported the same trend in contact charge at different

relative humidity [107]. However, poly(tetrafluoroethylene) (PTFE) was similarly charged under vacuum and air in Homewood's experiment [108]. More recently, at their zero-humidity experiment Baytekin et al. showed that water is not necessary for contact electrification yet it effects the amount of charge [109].

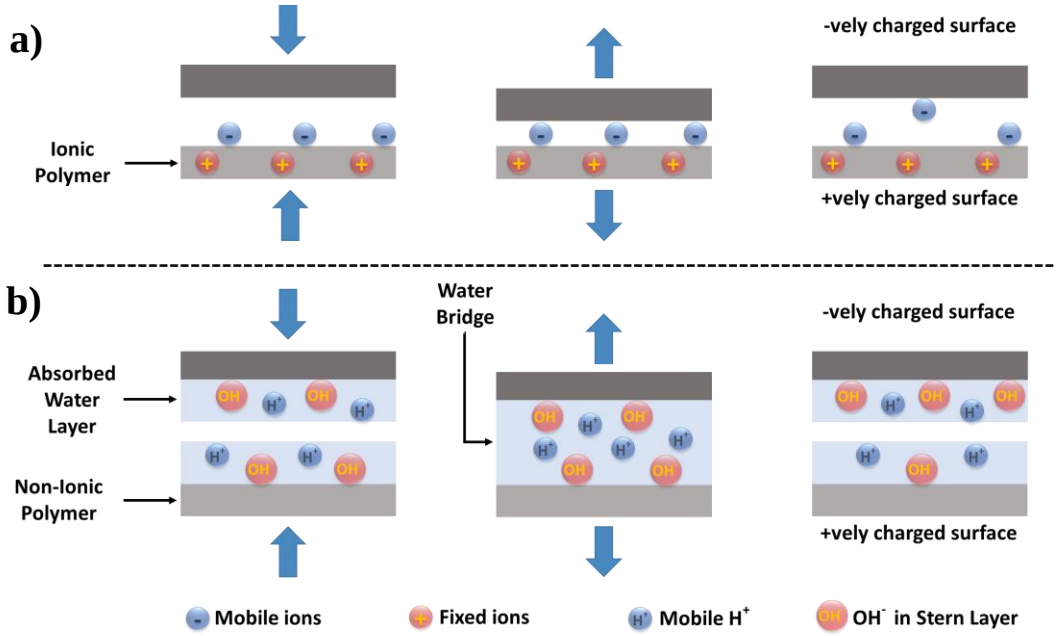

Figure 4.2 Schematic representation of (a) ion transfer model of contact electrification for ionic polymer, (b) water bridge model to explain ion transfer mechanism of contact electrification [93]. Adapted with permission of John Wiley and Sons.

4.2.3 Material Transfer Model

Material transfer model is the third proposed mechanism for contact electrification. Mechanochemistry was considered as an effect of contact electrification since 1960s. For example, in 1962 Henniker stated that free radicals produced by mechanical stress can generate high-energy electrons [110]. Soon after, Salaneck and coworkers observed mass transfers between metal-polymer and polymer-polymer surfaces via X-ray photoemission spectroscopy [111]. In 1990, Sakaguchi et. al showed that

mechanoradicals and mechanoions can be formed during contact electrification [112]. Magnetic force microscopy (MFM) reveals that polymer chains fracture and these machanoradicals and mechanoions are generated by bond cleavage when two polymer surfaces are in contact [97]. Due to instrumental limitations, relation between charge transfer and nanoscale material transfer cannot be observed directly until 2011. Baytekin et al. reported that polymer surfaces are charged with nanoscopic mosaic charge patterns [113]. Their Kelvin probe force microscopy (KPFM), Raman spectroscopy and XPS analyses showed that, the mosaic charge patterns arise as the result of material transfer. It was previously considered that polymer surfaces uniformly charged positively or negatively. However, the mosaic charge patterns include positively and negatively charged regions on the same polymer surface (schematically shown in Figure 4.3). Later on, contact electrification of microdome patterned PDMS and flat gold surface was investigated [114]. The flat gold surface was charged with the same microdome pattern measured via KPFM. This result implies that contact electrification on the gold surface was due to material transfer. Mechanical properties of the polymers are also important aspect of the material transfer model. There are several important studies reported in literature which investigate the relationship between mechanical properties of surfaces and contact electrification. In one of these studies, PTFE beads were rolled onto a PMMA dish for certain time. Initially, PMMA dish was positively charged but after certain time the polarity of the charged reversed. This was attributed to the accumulation of transferred material on the surfaces [115]. In another studies, PVC and PDMS triboelectric pair was used investigating the use of different PDMS curing ratios [116]. This difference in PDMS curing ratio resulted in different mechanical properties for PDMS. It was observed that, softer PDMS had higher surface charge. XPS analyses showed that the amount of material transfer was higher when PDMS was softer. This result implied that material transfer can be controlled by changing mechanical properties of the contact materials.

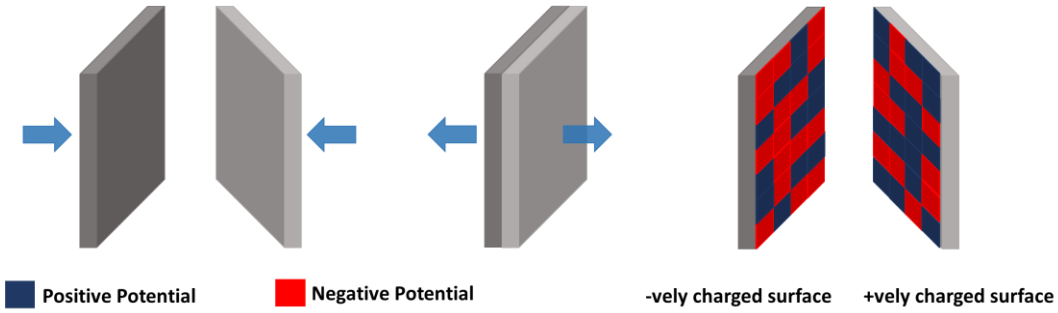

Figure 4.3 Schematic representation of mosaic charge pattern of two surfaces after contact electrification [113]. Adapted with permission of The American Association for the Advancement of Science

4.3 Foundations of Triboelectric Nanogenerator

Energy harvesters received considerable attention in the last decades due to environmental concerns, increasing energy demands, and political reasons. In the last decade, many research and development activities have been carried out on the harvesting of different forms of energy including mechanical energy, solar energy and thermal energy. Each of them has advantages, limitations, different working principles and potentials. The difference in their features plays an important role in determining the potential applications of the utilized energy harvesters. The important aspects of these harvesters are summarized in Table 4-1.

TENGs as a mechanical energy harvester stands out as a potential candidate to be used in wearable applications. Firstly, TENGs provide high power outputs with high conversion efficiency at low working frequencies. Secondly, polymers which are the most used materials in the textile industry, are also the best triboelectric materials. Moreover, TENGs have simple structures which can be produced via existing textile manufacturing techniques. Therefore, implementation of TENGs to wearable applications will be a lot easier than the other energy harvesters.

Table 4-1 Comparison of commonly used energy harvesting techniques [117,118].

Energy Source	Harvesting Type	Advantages	Disadvantages	Power Output
Mechanical Energy	Triboelectric Nanogenerators	-High efficiency, -Low cost, -Simple structure, -High voltage	-AC output, -Low current, -Limited lifetime -Moisture sensitive	0.1μW/cm^2-1mW/cm^2
	Piezoelectric	-Simple structure, -Can be integrated into MEMS, -Insensitive to surface features	-AC output -Limited material selection, -Complex material fabrication techniques, -Low power output	0.1μW/cm^2-10μW/cm^2
	Electromagnetic Induction	-High efficiency, -High current, -High technology readiness level	-Low voltage, -Difficult to use for wearable electronics	0.1μW-1MW
Solar Energy	Photovoltaic	-DC output, -Unlimited energy source, -High conversion efficiency, -High technology readiness level	-Dependent on environmental conditions, -Performance drop without sunlight	1μW-1MW
Thermal Energy	Thermoelectric	-DC output, -Durable, reliable, -Low cost	-Low conversion efficiency, -Low power output	0.1μW/cm^2-1μW/cm^2
	Pyroelectric	-Wide range of operating temperatures,	-AC output, -Limited materials selection	0.1μW/cm^2-1μW/cm^2

As it was also mentioned in previous section that contact electrification (triboelectrification) and electrostatic induction are the two successive effects which are the fundamentals of TENGs. The proposed mechanisms for the contact electrification are summarized in the previous sections. This part of the thesis will cover the foundations of TENGs including the working modes and their theoretical models.

4.3.1 Working Modes of Triboelectric Nanogenerators

Energy harvesting process starts with induced charges on the surface of the materials as the result of contact electrification. (The charged materials will be named as "triboelectric materials/layers" from now on). Then, the change in relative positions of these triboelectric materials will create a potential difference between them. If these materials are connected with each other through an electrical load, free electrons (induced electrons) of conductive electrodes will flow from one electrode to other. (It should be noted that all TENG structures generally consist of a triboelectric layer and a conductive layer). There are four fundamental types of TENGs with working modes that depend on configurations of triboelectric and conductive layers, relative movement of them and the charge polarization direction. Schematic representations of TENGs modes are provided in Figure 4.4.

The most basic mode of TENGs is the vertical contact separation mode. In this mode, the two electrodes physically come into contact and are separated by a certain distance. Triboelectric layers are oppositely charged as a result of contact. In the schematic, each TENG electrodes consist of a triboelectric and a conductive layer. However, one electrode may be composed of a triboelectric and a conductive layer, while the other may simply be made of only conductive layer. A potential difference occurs when the charged electrodes are separated from each other by external forces. When the electrodes are connected with an external charge, electrons flow from one electrode to the other to balance the potential difference. When the gap between the electrodes decreases, electrons flow in the opposite direction from the external

charge. As a result of this periodic motion, an alternating current is produced. The vertical contact separation mode offers some advantages over other modes due to its simple structure for design and manufacture. Also, electrode life in this mode is higher than that in lateral sliding and freestanding modes. This is because in vertical contact separation mode there is very low wear acting on the electrodes.

In the lateral sliding mode, a potential difference occurs between two electrodes due to lateral sliding of the electrodes. Electron flow occurs between the electrodes from the external load to balance the potential difference. Periodic sliding from one direction to the other results in an alternating current. The lateral sliding mode offers higher conversion efficiency than the vertical contact separation mode. However, the life of electrodes is limited due to high wear acting on the electrodes.

Vertical contact separation and lateral sliding modes consist of two electrodes connected with each other with an external load. This structure limits their potential applications when energy is converted from freely moving objects. On the other hand, the single electrode mode consists of one electrode connected to the ground with an external load. Electrons flow between the fixed electrode and the ground as the moving triboelectric layer approaches and moves away. The second triboelectric layer can freely move without an electrical connection to the system. This mode offers design advantages, but its power output is less than the other modes.

In freestanding mode, the two conductive layers are interconnected by an external load. A triboelectric layer is placed on top of these conductive layers. An asymmetric charge distribution is observed when the second triboelectric layer is brought in contact with the electrode. Electron flows is observed between the conductive layers which reduce the potential difference. In this mode, the power conversion efficiency is quite high. However, again the electrode life of electrodes is limited due to high wear acting on the electrodes.

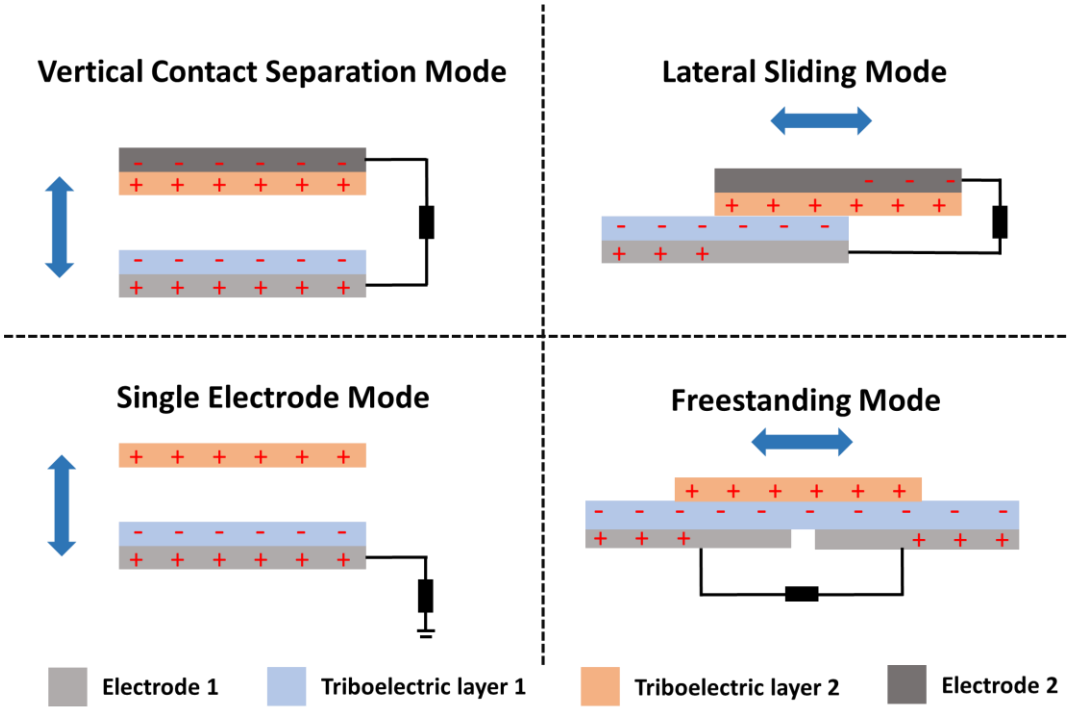

Figure 4.4 Schematic representation of working mode of TENGs.

4.3.2 Theoretical Models of Triboelectric Nanogenerators

Working modes of TENGs have been discussed in the previous section as an overview. Theoretical models should be discussed for better understanding of the TENGs working principles. In this part of the thesis, general concepts of theoretical models will be explained without going into too much detail and mathematical derivations. Theoretical models will be discussed for vertical contact separation mode for the sake of simplicity. In addition, all of the results reported in this thesis are obtained in vertical contact separation mode. Before discussing the types of the model, it is appropriate to hereby revise TENG energy harvester system. Overall TENG harvester systems consist of three components. Mechanical input, TENG transducer and power management circuit, all of which are schematically shown in Figure 4.5. Mechanical energy is first converted to electrostatic energy in TENG transducer and extracted as electrical energy by the power management circuit.

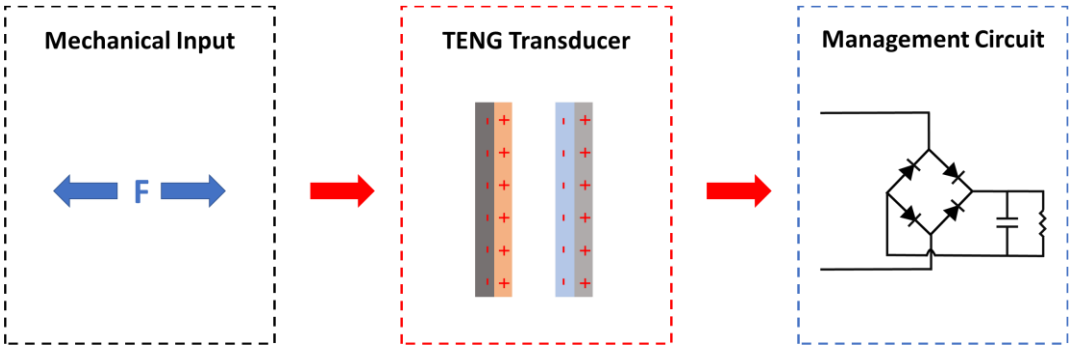

Figure 4.5 Overall energy harvesting system via TENGs. Mechanical energy transformed into electrostatic energy within the TENG transducer then to electrical energy with the management circuit [117]. Adapted with permission of AIP Publishing.

The types of models discussed here originated from these components of the TENG harvester systems. The types of models can be linked with each other by using proper transport equations. There are two main approaches to theoretically describe the working principles of TENGs. Those are equivalent circuit models and formal physical models (Quasi-electrostatic model). Equivalent circuit models derived from lumped parameter circuit theory and consider TENGs as the circuit element as voltage/current source and/or inherent capacitance/impedance. Formal physical models are based on classical electromagnetic theory (Maxwell equations) mainly focused inside the TENG transducer.

4.3.2.1 Equivalent Circuit Models

4.3.2.1.1 Parallel Plate Capacitive Model

Capacitive model is the first theoretical model proposed to explain working principles of TENGs and predict their outputs [118,119]. TENG device is represented as a serially connected voltage source and a capacitor as schematically shown in Figure 4.6 (a). A typical dielectric-dielectric TENGs in vertical contact separation mode consists of two triboelectric layers and two electrode materials. The potential difference between the two electrodes can be represented by,

$$V = -Q/C(x) + Voc(x) \qquad 4.1$$

,where Q is the transferred charged between the two electrodes, $C(x)$ is the capacitance of the TENG system and $Voc(x)$ is the voltage generated by the separated triboelectric charges. Note that $C(x)$ and $Voc(x)$ are separation distance dependent. The Equation 4.1 is the relationship between V-Q-X and the governing equation of the capacitive model.

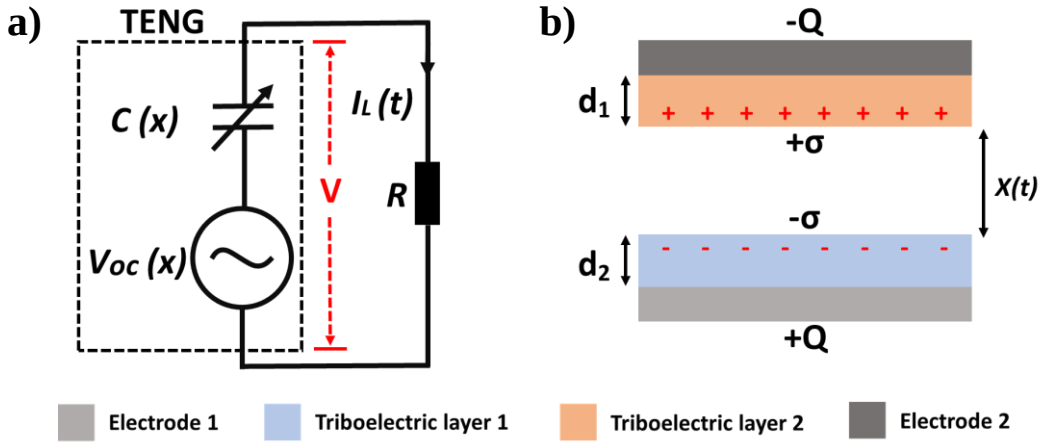

Figure 4.6 (a) Circuit representation of TENG device as a voltage source and inherent capacitance [118]. Adapted with permission of Elsevier. (b) A model of dielectric-dielectric TENG working in contact separation mode [119]. Adapted with permission of RSC Publishing.

The schematic model of a typical dielectric-dielectric TENG in vertical contact separation is provided in Figure 4.6 (b). Two dielectric layers have thicknesses of d_1 and d_2 and relative dielectric constants of ε_{r1} and ε_{r2}, respectively. The dielectrics are positioned face to face with a distance of $X(t)$. Two conductive electrodes are deposited or attached to the outer surface of the dielectrics. The inner surfaces of the dielectrics are oppositely charged with a charge density of σ upon contact. Potential difference between two conductive electrodes is V, that develops upon separation of the dielectric layers. The area of the electrodes is A, which is larger than the total distance ($d_1 + d_2 + x$) between the electrodes. Therefore, the electrodes are assumed

infinitely large. *Q* is induced charge at the electrodes. The voltage between the two electrodes can be represented by:

$$V = E_1 d_1 + E_2 d_2 + E_{air} x \tag{4.2}$$

,where E_1, E_2 and E_{air} are electric field strengths inside dielectric 1, dielectric 2 and air, respectively. Electric field strength for each can be calculated from the Gauss theorem.

$$E_1 = -\frac{Q}{A\varepsilon_0\varepsilon_{r1}} \tag{4.3}$$

$$E_2 = -\frac{Q}{A\varepsilon_0\varepsilon_{r2}} \tag{4.4}$$

$$E_{air} = \frac{-\frac{Q}{A} + \sigma(t)}{\varepsilon_0} \tag{4.5}$$

When equation 4.2, 4.3, 4.4 and 4.5 are combined, voltage becomes:

$$V = -\frac{Q}{A\varepsilon_0}\left(\frac{d_1}{\varepsilon_{r1}} + \frac{d_2}{\varepsilon_{r2}} + x\right) + \frac{\sigma\, x(t)}{\varepsilon_0} \tag{4.6}$$

If effective field strength d_0 is defined as $d_1/\varepsilon_{r1} + d_2/\varepsilon_{r2}$, then *V-Q-X* relation becomes:

$$V = -\frac{Q}{A\varepsilon_0}(d_0 + x(t)) + \frac{\sigma\, x(t)}{\varepsilon_0} \tag{4.7}$$

The equation 4.7 can be used to calculate output performance of TENGs. Under open circuit condition, Q is 0. Thus, open circuit voltage (*Voc*) becomes;

$$Voc = \frac{\sigma\, x(t)}{\varepsilon_0} \tag{4.8}$$

Under short circuit condition, V is 0. Thus, short circuit charge and current are;

$$Qsc = -\frac{Q}{A\varepsilon_0}(d_0 + x(t)) \tag{4.9}$$

$$Isc = \frac{dQsc}{dt} = \frac{A\sigma d_0}{(d_0 + x(t))^2}\frac{dx}{dt} = \frac{A\sigma d_0 v(t)}{(d_0 + x(t))^2} \tag{4.10}$$

The output properties can be predicted when a resistor load is connected to TENGs (shown in Figure 4.6 (a)) by combining governing *V-Q-X* equation 4.7 and Ohm's law;

$$R\frac{dQ}{dt} = -\frac{Q}{A\varepsilon_0}(d_0 + x(t)) + \frac{\sigma\, x(t)}{\varepsilon_0} \tag{4.11}$$

The equation is a first order differential equation and can be solved by defining boundary conditions [117–119]. The initial boundary condition is $Q = 0$ when $(t = 0)$. If the device is under a periodic motion with a period of T, we have a periodic output. The final boundary condition of this periodic motion is $Q\ (t) = Q$. With the help of these boundary conditions, output voltage, charge and current of the device can be predicted provided that different resistor loads are connected. Theoretically calculated output performance of a metal-dielectric TENG system working in

vertical contact separation mode are provided in Figure 4.7 (a)-(f) [119]. Structure and the parameters of the theoretically calculated TENG is provided in Figure 4.7 (a). When a small load resistance is connected to the electrodes, induced charges are transfer from one electrode to the other one and get easily saturated (t = 10 ms). On the other hand, high load resistance limits the charge transfer rate as provided in Figure 4.7 (b). Differences in charge transfer rates cause the difference for output current as can be deduced from equation 4.10. That is, when the resistance load is high, output current is low and vice versa (Figure 4.7 (c)). Unlike current and charge, the output voltage is high when the load resistance is high, as provided in Figure 4.7 (d). This is because the high resistive load limits the charge transfer. The peak values of output current and voltage under different load resistances are provided in Figure 4.7 (e). This graph can be divided into three different regions. Resistance load is low in Region I and current is approximately equal to short circuit conditions. The TENG device works as a current source. On the other hand, the device works similar to open circuit condition when load is high (Region III). Therefore, output voltage is approximately equal to *Voc*. Current starts to decrease while voltage increases in Region II, when the load resistance is in the medium range. Therefore, output power is maximum in Region II, which can be seen in the Figure 4.7 (f).

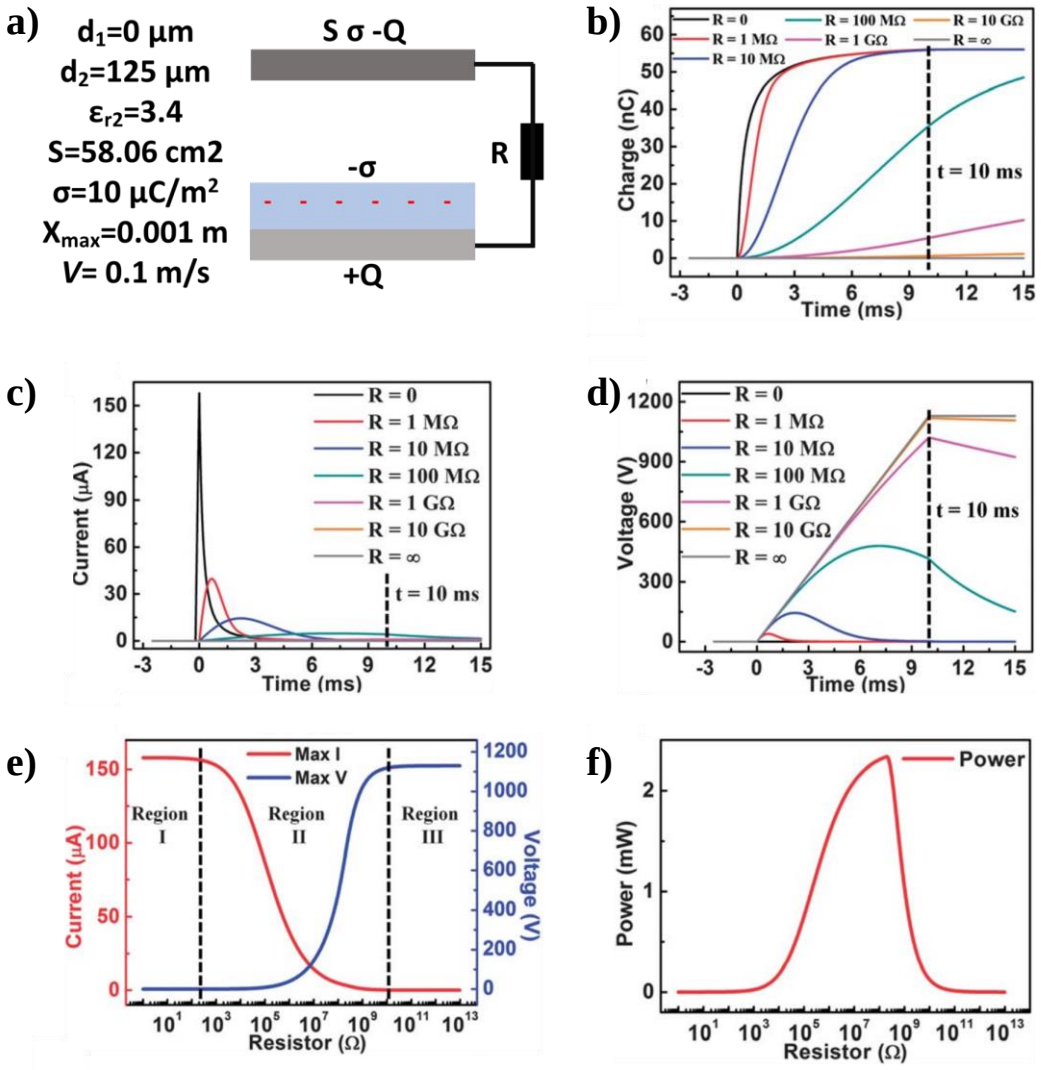

Figure 4.7 (a) Structure and the parameters of the theoretically calculated metal-dielectric TENG response. Calculated output (b) charge, (c) current, (d) voltage of the TENG with respect to time under different resistance loads. (e) Peak current and voltages under different resistance loads. (f) Calculated power output of the TENG under different resistance loads [119]. Adapted with permission of RSC Publishing.

4.3.2.1.2 Thevenin's and Norton's Models

The parallel plate capacitor model represents TENGs as an ideal voltage source and capacitor both of which varies with time as discussed in the previous section. In this

model inherent impedance of the TENG system is modeled without a resistor and include only a capacitive element (Figure 4.6 (a)). On the other hand, inherent impedance of TENGs is considered as the circuit element in Thevenin's and Norton's models which have been used since 1880s to simplify complex circuits. In Thevenin's equivalent circuit model, TENG system is represented by a serially connected voltage source and an inherent impedance element (provided in Figure 4.8 (a)). Basically, capacitor element is replaced with impedance element. In Norton's equivalent circuit model, on the other hand, TENG system is represented by time-varying current source and parallel connected inherent impedance element as schematically shown in Figure 4.8 (b).

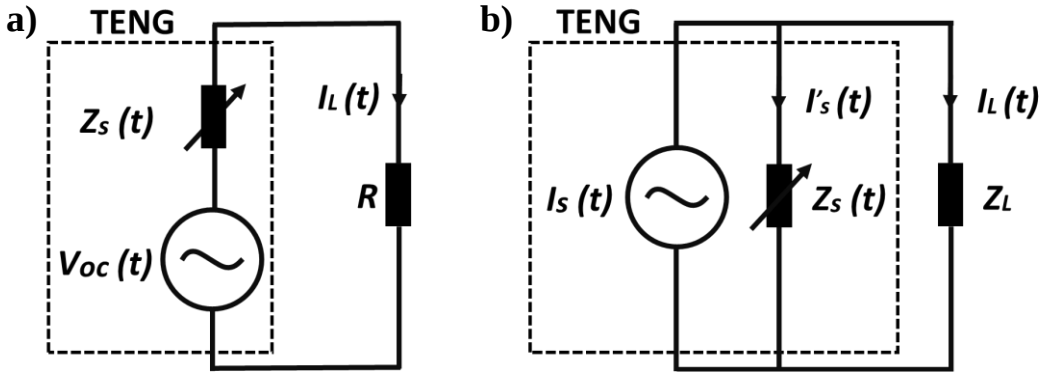

Figure 4.8 Circuit representation of a TENG device using (a) Thevenin's model consisting of a voltage source and inherent impedance, (b) Norton's model consisting of a current source and inherent impedance [120]. Adapted with permission of John Wiley and Sons.

Modeling TENG system with Norton's equivalent circuit is important when the TENG devices have high inherent impedance. Since reliable measurement of open circuit voltage may be difficult when inherent impedance of TENG system is too high. Voltage measurement units have limited impedance. The generated current is divided between *Zs(t)* and load impedance when external load is connected in parallel to the TENGs. The current passing through the load at time *t* can be calculated by Equation 4.12:

$$I_L(t) = I_{SC}(t)\frac{Z_s(t)}{Z_S(t) + Z_L} \quad 4.12$$

The power output of TENG can then be calculated by:

$$P_{out}(t) = I_L(t)^2 Z_L \quad 4.13$$

The maximum power form TENGs is attained when the load impedance is close to inherent impedance of the TENG system. Dharmasena and coworkers theoretically predicted output performance of TENGs by combining distance dependent electric field concept (will be mentioned in the next part) and Norton equivalent circuit model [35].

4.3.2.2 Formal Physical (Quasi-electrostatic) Models

Parallel plate capacitor model discussed in previous section is very useful to predict TENG outputs. However, this model is limited to explain TENG transducer represented in Figure 4.9. New models that rely on classical electromagnetics were proposed to overcome the limitations. The overall TENGs consist of two components in these models which is schematically represented in Figure 4.9. The internal circuit and the external circuit connected with each other at the two conducive electrodes. The fundamental physical mechanisms for current generation and the driving force are the displacement current within the internal circuit. The conduction current in the external circuit on the other hand is the manifestation of the displacement current.

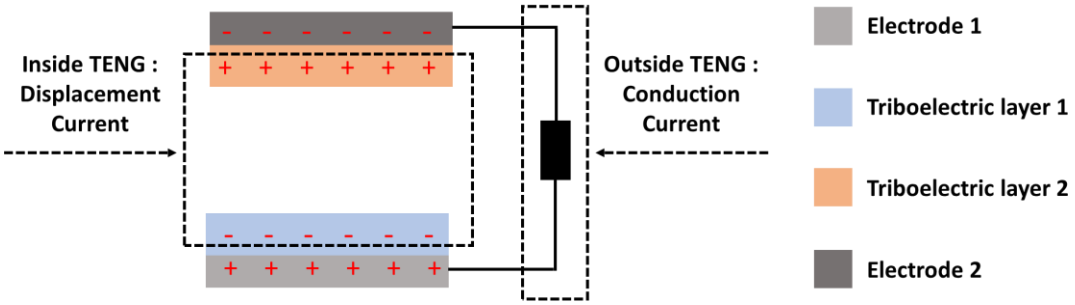

Figure 4.9 Schematic representation of TENGs showing the connection between the displacement current inside the TENG and the conduction current outside the TENG [121]. Adapted with permission of Elsevier.

The first model based on classical electromagnetics was proposed by Dharmasena et al. named as the distance dependent electrical field (DDEF) model [120,122,123]. Later, Shao and coworkers developed 3D mathematical (finite-sized charged plane (FSCP)) model [117,124,125]. In the following sections, these models will be briefly discussed

4.3.2.2.1 Distance Dependent Electrical Field (DDEF) Model

In TENG systems dielectric layers are charged as a result of contact electrification. These charges are static (tribo-charge) and cause induced charges in the electrodes, which are attached/deposited onto the back side of the dielectrics. Electric field inside the dielectric and at the dielectric-electrode interface only results from induced charge in parallel plate capacitor model. On the other hand, the situation is slightly different for TENGs in the real case. That is, the propagation of electric field inside the dielectrics is not only due to induced charge but also due to static charge (tribo-charge) until it is shielded by the electrode. Charge distribution of a typical dielectric-dielectric TENG working in contact separation mode is schematically provided in Figure 4.10 (a).

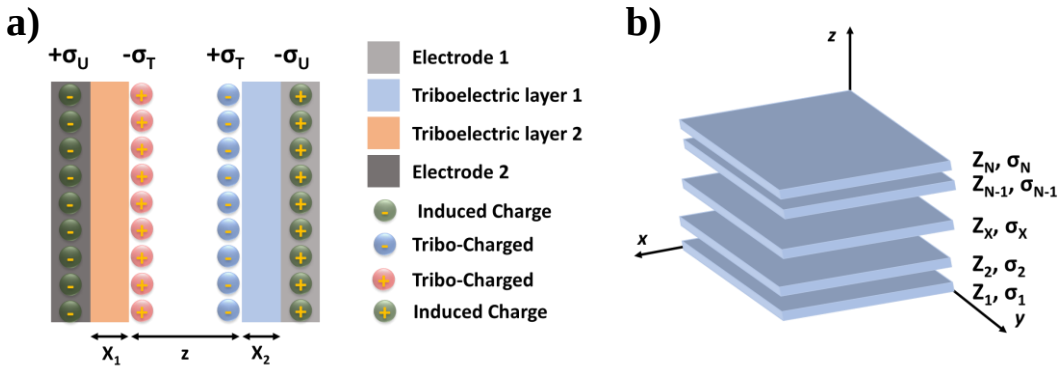

Figure 4.10 (a) Schematic showing the charge distribution of a dielectric-dielectric TENG working in contact separation mode [122]. Adapted with permission of RSC Publishing. (b) N number of finite sized charged planes.

Electric field variation along z-axis for a charged surface placed x-y plane (having charge density of σ) can be derived from Gauss's law;

$$E_z = \frac{\sigma}{\pi\varepsilon_0} tan^{-1}\left(\frac{{}^{L}/_{W}}{2({}^{z}/_{W})\sqrt{4({}^{z}/_{W})^2 + ({}^{L}/_{W})^2 + 1}}\right) = \frac{\sigma}{\pi\varepsilon_0} f(z) \qquad 4.14$$

,where L and W are length and width of the charged plane, respectively. Permittivity of free space is ε_o and z is the distance of the plane. (Derivation of the Equation 4.14 can be found elsewhere [122]). The electric potential (as the result of the electric field) at the interfaces of electrodes can be represented by:

$$\phi_1 = \frac{-\sigma_U}{\pi\varepsilon_1}\left[\int_0^{x_1+x_2+z} f(x)dx\right] + \frac{\sigma_T}{\pi\varepsilon_1}\left[\int_{x_1}^{x_1+z} f(x)dx\right] \qquad 4.15$$

$$\phi_2 = \frac{\sigma_U}{\pi\varepsilon_2}\left[\int_0^{x_1+x_2+z} f(x)dx\right] - \frac{\sigma_T}{\pi\varepsilon_2}\left[\int_{x_1}^{x_1+z} f(x)dx\right] \qquad 4.16$$

where, σ_T is tribo-charge at the dielectric and σ_U is induced charged at the conductive electrodes. In open circuit condition σ_U is zero and *Voc* becomes:

$$V = \phi_1 - \phi_2 \tag{4.17}$$

In short circuit conditions electrodes are at the same potential, thus:

$$V = \phi_1 - \phi_2 = 0 \tag{4.18}$$

$$\sigma_U = \frac{\sigma_T \left[\frac{1}{\varepsilon_1}\int_{x_1}^{x_1+z} f(x)dx + \frac{1}{\varepsilon_2}\int_{x_2}^{x_2+z} f(x)dx\right]}{\left(\frac{1}{\varepsilon_1}+\frac{1}{\varepsilon_2}\right)\int_{0}^{x_1+x_2+z} f(x)dx} \tag{4.19}$$

$$I_{SC} = A\frac{d\sigma_U}{dt} \tag{4.20}$$

DDEF was the first proposed model based on classical electromagnetic theory (Maxwell equations) which is very important in that regards. However, the validity of this model has been proven only when the moving part of the TENGs is in vertical direction. Horizontal movement of the TENGs has not yet been investigated with the DDEF model.

4.3.2.2.2 3D Mathematical (Finite-Sized Charged Plane (FSCP)) Model

Shao and coworkers later proposed 3D mathematical model (based on classical electromagnetic theory) which overcome the limitation of the DDEF model [124].Consider we have two different tribo-charged surfaces and a medium composed

of two electrodes having free charges as schematically provided in Figure 4.10 (a). The Maxwell-Poisson equation is:

$$\nabla . D = \rho(r) \tag{4.21}$$

,where *D* is the electric displacement vector, *ρ* is the total charge density (composed of both tribo and induced charge). Electrical potential of the system containing point charges is:

$$\phi(r) = \frac{1}{4\pi\varepsilon_0}\int \frac{\rho(r')}{|r - r'|} dV \tag{4.22}$$

In this equation *r* is the point where potential is calculated and *ρ(r')* the charge density at point *r'*. Consider *N* number of finite sized planes having the same dimensions a and b placed in x and y-directions, respectively. All of these planes are centered at (x,y) = (0,0) and positioned at *z1*, *z2*,….., *zN* (as schematically provided in Figure 4.10 (b)). The surface charge densities of the planes are *σ1*, *σ2*, …...., *σN*, respectively. Electrical potential at point *r (x, y, z)* becomes:

$$\phi(x, y, z) = \sum_{i=1}^{N} \frac{\sigma_i}{4\pi\varepsilon_0} \int_{-a/2}^{a/2} \int_{-b/2}^{b/2} \frac{dx'dy'}{\sqrt{(x - x')^2 + (y - y')^2 + (z - z')^2}} \tag{4.23}$$

Equation 4.23 is the same as Equations 4.15 and 4.16, when a TENG system is constructed as in Figure 4.10 (a). Unlike DDEF, the FSCP model is universal for all-operating modes of TENGs and for both vertical and horizontal movement directions. Therefore, it can be concluded that the DDEF model is a special case of the FSCP model for motion in vertical direction. Comparisons of aforementioned

models for performance outputs (*Voc, Qsc, Isc*) of vertical contact separation mode TENGs are provided in Figure 4.11 (a)-(d). It can be clearly seen that DDEF and FSCP models shows the same output performances for *Voc, Qsc and Isc*. However, the parallel plate capacitor model (CA) shows a significant deviation, especially at large separation distances (Figure 4.11 (b)). This deviation is mainly due to the edge effect, which is ignored in the CA model. However, DDEF and FSCP models also deviate from the experimental results for the output voltage of TENGs [122]. This deviation is attributed to limited impedance of the measurement instruments by which output voltages are measured. Therefore, Northons' model was proposed to overcome this aforementioned issue which is discussed in related section (4.3.2.1.2)

To sum up, one can conclude that displacement current is the driving force inside the TENG while the current on the load is the conduction current. The displacement current inside and conduction current outside of the TENG are equal in theory. These two currents are joining at the electrodes and form a complete loop. Electrical potential (ϕ), electric displacement vector (D), displacement current (I_D) can be calculated by using quasi-electrostatic models. On the other hand, output voltage (V), charge (Q) and conduction current (I) can be determined by using equivalent circuit models. Moreover, these two models can be linked with each other by using proper transport equations [117].

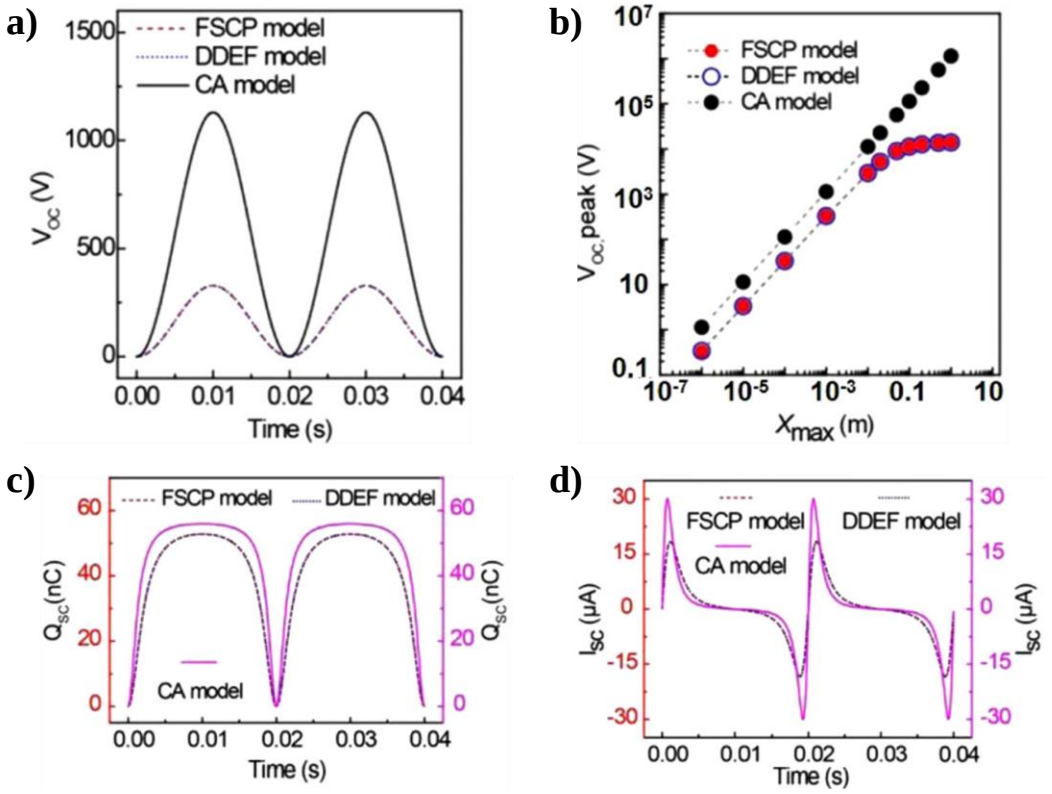

Figure 4.11 Comparison of theoretical models for output performance (a) *Voc*, (b) *Voc* at different separation contact materials, (c) *Qsc* and (d) *Isc* of a dielectric-dielectric TENG system working contact separation mode [124]. Adapted with permission of Elsevier.

4.4 Parameters Effecting the Output Performances of Triboelectric Nanogenerators

The output charge, voltage, current and power of TENGs can enhanced by different parameters depending on the working conditions, size and type of the materials. Effects of working conditions like tapping frequency, separation distance on *Isc*, *Voc* and output charges are experimentally investigated in the literature [126–129]. However, the changes can also be predicted via theoretically. For example, *Isc* increases with increasing tapping frequency. Since the change rate of the induced charge increases with the increasing tapping frequency which can be predicted from Equations 4.19

and 4.20. *Voc* and *Isc* increases with increasing separation distance, as can be figured out from Equations 4.15, 4.16, 4.17, 4.18, 4.19 and 4.20.

Increasing surface charge density as the result of contact electrification increases output voltage, charge, current and power of the TENGs. This can be deduced from both the instinctive and the derived equations in the previous sections. There are several ways to increase the surface charges. Materials selection for the tribo-charged materials is the starting point. Here, it is necessary to mention the concept of the triboelectric series. The exact mechanism of the contact electrification is still a mystery as discussed in the origin of contact electrification section (4.2). However, some materials are known to be negatively charged and others positively charged. More importantly, the amount of charge of each material is different from each other during contact electrification. This fact allowed researchers to create triboelectric series in which materials are ranked and placed in their relative positions. Measuring the surface charge of a material after contact electrification using liquid mercury was first proposed by Harper to establish the triboelectric series [130]. It is important to choose liquid mercury as the reference electrode, as the measured material gets in full contact with the liquid medium. Later, Wang research group provide a detailed triboelectric series including polymers and ceramics in two different research articles through the use of liquid mercury reference electrode [131,132]. Their obtained triboelectric series for polymers is provided in Figure 4.12. It is important to note that the greater the distance between the positions of the two contact materials in the series, the higher the surface charge.

Modification of the contact materials surfaces is proposed to increase tribo-charge. Changing the surface roughness is one of them [133,134]. Increasing surface roughness increases the active contact area which helps in escalating the output performances of TENGs. Chemical modifications of the dielectric surfaces have also been extensively investigated in the literature [135–137]. Chemical modification allows one to shift a material to a more tribopositive or tribonegative location in the triboelectric series. As a result of this shift, more surface charges can be generated at the time of contact, which improves the output performance of TENGs. The size of the contact

area of TENGs is also important since it effects all aforementioned parameters. Increasing the area increases total surface charge, current, voltage and eventually power. However, it should be noted that current, charge and power are generally reported in literature by normalizing them to surface area.

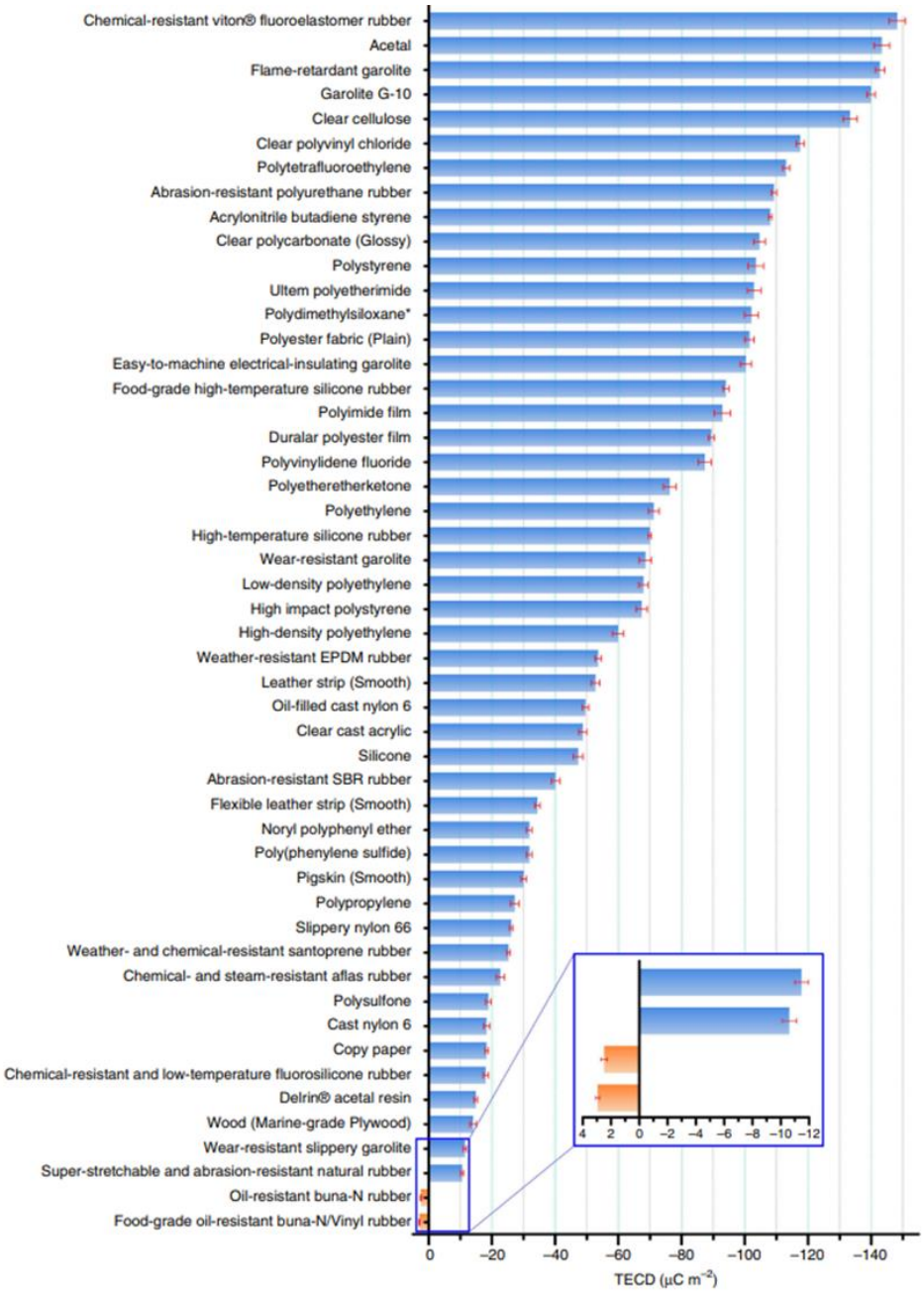

Figure 4.12 Triboelectric series of some polymers quantified using liquid mercury as counter electrode [131]. Reproduce with the permission of Nature Publishing Group

CHAPTER 5

FABRIC BASED WEARABLE TRIBOELECTRIC NANOGENERATORS FOR HUMAN MACHINE INTERFACE

5.1 Introduction

Wearable electronics received considerable attention from both the academia and industry, which resulted in the appearance of commercial products in the market by late 2000s. List of applications include but not limited to health monitoring, motion tracking, human-machine interfaces, internet of things (IOTs), wearable light emitting diodes (LEDs) [138–143]. These wearable electronics must not only be lightweight, flexible and stretchable but must also consume low power. Although their power consumption can be significantly reduced, they still need to be powered from an external power source such as a rechargeable electrochemical cell. However, integration of the electrochemical cells with those wearable electronics without reducing the users' comfort is almost impossible due to excessive weight, bulky structure, limited capacity and life time of the commercial products. In fact, biomechanical energy harvesters are considered as an alternative to electrochemical cells that circumvent aforementioned problems of wearable electronics. Following their invention in 2012 by Wang et al., extensive amount of research is still being carried out on triboelectric nanogenerators (TENGs) [144]. Early TENG devices in literature consisted mostly of polymer films on top of metallic foils or indium tin oxide (ITO) coated polyethylene terephthalate (PET) substrates with basic planar structures [145–147]. Lately, fiber-based structures were developed as light-weight, durable, comfortable and wearable TENGs [148–151]. For example, X. He and coworkers modified silicon rubber fibers with carbon nanotubes (CNTs) and copper wires to fabricate high performance stretchable TENGs with an output power of 6 μW [152]. In another study, Yang et al. designed coaxial TENGs and supercapacitor

fibers to be used as self-charging fabrics. Silicon rubbers and carbon fibers were deposited onto fiber-based supercapacitors to obtain 3 cm thick multifunctional TENG supercapacitor hybrid fibers [153]. Although fiber shape provides excellent mechanical stability for wearable TENGs, this design had two major shortcomings. Firstly, complex production routes are employed, which are not too much suited for mass production and secondly, fiber-shaped TENGs tend to be very thick and thus heavy, due to their multi-layered structure.

Conductive fabrics are also utilized as electrodes and substrates for wearable TENGs. Typical approaches to fabricate conductive fabrics include metal (Ag, Ni and Cu etc.), CNTs, graphene and two-dimensional (2D) transition metal carbides and nitrides (MXenes) deposition onto conventional fabrics [154–157]. Elastomers such as polydimethylsiloxane (PDMS) and Ecoflex are then deposited onto these conductive fabrics as the dielectric layers utilizing dipping methods [158,159]. However, PDMS and Ecoflex are known to lose their flexibility and stretchability upon prolonged ambient exposure. Thermoplastic polymers are also utilized for TENGs since they can be fabricated in fiber form via electrospinning or solution blowing [160–162]. Fiber forms of the dielectric layers are demonstrated to substantially increase TENG performance. Ho and coworkers recently fabricated β-phase poly(vinylidenefluoride)-co-hexafluoropropylene [P(VDF-HFP)] fibers via solution blowing method and demonstrated that the surface potential of [P(VDF-HFP)] fibers is one and a half times that of thin films (-489 mV vs -743 mV). This resulted in a dramatic increase in TENG performance [161]. However, wearable TENG devices based on polymeric materials are not washable, which hinders their future utilization in wearable technologies. In fact, the lack of wash stability is a serious concern not only for TENGs but also for any type of wearable electronics. For example, in Chapter X, it was demonstrated that silver nanowire (Ag NW) modified fabrics can be used as high-performance wearable heaters; however, their performance was found to diminish after several washing cycles [16].

Three major problems arise in the fabrication of electronic textiles and devices over large areas. Firstly, fabrics should be homogenously decorated with active materials

in order to be fully functional. Secondly, fabrics must retain their performance after a certain number of wash cycles. Lastly, the power consumption of fabrics increases with device area, so higher capacity, bulkier batteries are needed for long-term use of these devices. Significant portion of the reported solutions in literature involve complex production steps, which reduce applicability and limit realization of fully functional wearable devices. Herein, this thesis demonstrates the use of laminated TPU films as dielectric layers on Ag NW modified fabrics for the realization of washable and wearable TENGs as a combined solution. TPU films are firstly produced via doctor blading and then laminated onto Ag NW modified cotton fabrics via simple, cost effective and scalable hot-pressing method. Upon fabrication, resistance change and heating uniformity of the Ag NW modified and TPU laminated fabrics were systematically investigated to monitor their washing stability. Very high output performance was obtained from the fabricated TENGs. In order to demonstrate the true potential, fabricated washable and wearable TENG electrodes were utilized for charging a capacitor, illuminating LEDs, motion detection and interfacing humans and machines.

5.2 Experimental Procedure

5.2.1 Fabrication of Silver Nanowire Modified Conductive Fabrics

The 100 % cotton textiles with a biaxial woven structure were used for the experiments. All glassware and textiles used in the experiments were cleaned using acetone (99.8%), isopropyl alcohol (99.8%). Ag NW synthesis chemicals were purchased from Sigma-Aldrich and used without further purification. Ethylene glycol (anhydrous, 99.8%), polyvinylpyrrolidone (PVP) (monomer-based calculation MW = 55000), sodium chloride (NaCl, 99.5%) and silver nitrate ($AgNO_3$, ACS reagent, ≥99.0%) were used for the polyol synthesis of Ag NWs. Ag NWs were synthesized according to a procedure described previously by our research group [51]. Following synthesis, nanowires were purified through washing

with ethanol several times followed by centrifugation. The final product was then dispersed in ethanol for further processing.

Simple dip and dry method was used to fabricate conductive fabrics [163]. Basically, 100 ml ethanolic dispersions of Ag NWs with different Ag NW content (0.5 mg/ml and 2.0 mg/ml) were prepared. Afterwards, pre-cleaned bare cotton fabrics (2 × 2, 3 × 3 and 4 × 4 cm^2) with different fabric densities (54 g/m^2 and 160 g/m^2) were immersed into this solution for 5 minutes and dried at 80°C for 10 minutes. This procedure was repeated until an edge-to-edge resistance of 3-4 ohm was obtained from the samples. Conductive silver inks were applied as stripes onto the edges of the fabrics to monitor changes in resistance after each washing cycle and to apply voltage for fabric heaters. Bending stability of the fabrics were investigated using a custom-made bending machine.

5.2.2 Fabrication of Triboelectric Nanogenerators Electrodes

TPU granules were purchased from LUBRIZOL (ESTANE 58887) and kept at 60°C for 12 hours to remove moisture. 10 g of TPU was dissolved in 25 ml of N-N Dimethylformamide (DMF) at 70 °C in a closed beaker. After that TPU/DMF solutions were doctor bladed onto glass substrates to fabricate 70 and 90 μm thick films. TPU films on glass substrates were kept at 110 °C for 12 hours to remove excess solvent. Afterwards, TPU films were peeled off from the glass substrates. Fabricated TPU films were then laminated onto Ag NW modified conductive textiles via simple and scalable hot-pressing method practiced at 160 °C for 1 minute with an applied pressure of 25kPa. For simplicity, from now on 70 μm thick TPU laminated fabrics with densities of 54 and 160 g/m^2 will be referred as 70TPU/54F and 70TPU/160F, respectively. Likewise, 90 μm thick TPU laminated fabrics with densities of 54 and 160 g/m^2 will be referred as 90TPU/54F and 90TPU/160F, respectively.

Following structures were fabricated and used as the top TENG electrodes. Commercially available polyimide (PI) tapes (Kapton tape) were carefully attached to 30 μm thick aluminum (Al) foils. PDMS (Sylgard 184 Silicon elastomer, Corning) solution was prepared using PDMS base part A and curing agent part B with a ratio of 10:1. Prepared solution was hand mixed and degassed under vacuum for 10 minutes to eliminate air bubbles. Prepared solution was spread on the Al foil electrode using a doctor blade. The applied PDMS layer was cured at 90 °C for 30 minutes. Ecoflex 00-30 was purchased from Smooth-On and processed as instructed by the manufacturer. 2 g of part A was mixed manually with 2 g of part B (mixing ratio of 1:1). Then the mixture was doctor bladed onto Al foil and cured under 100 °C for 3 hours. Polylactic acid (PLA) granules used in this study was provided by NaturePlast (PLI 003). PLA films were fabricated according to the procedure described elsewhere [164,165]. Briefly, 1 g of PLA powders were dissolved in 10 ml of chloroform at room temperature using a magnetic stirrer operated at 1000 rpm for 12 hours. The solution was doctor bladed onto Al foils as a 30 μm thick film. Finally, the films were dried at 60 °C for 12 hours to remove excess solvent.

5.2.3 Characterization

The surface morphologies of bare, Ag NW modified and TPU laminated fabrics were investigated using a scanning electron microscope (SEM). SEM studies were performed on a FEI NOVA NANO SEM 430 microscope operated under low voltage to prevent fabric damage. Prior to SEM analysis, samples were coated with a few nanometers thick gold (Au) layer to impart conductivity. 3D maps of the bare and TPU laminated fabrics were obtained via Huvitz HRM 300 optical microscope. Fourier transform-infrared (FTIR) spectroscopy analyses were conducted via attenuated total reflectance (ATR) unit of FTIR spectrometer (Bruker Alpha) with a resolution of 4 cm^{-1} within a wavenumber range of 400-4000 cm^{-1}. Keithley 2400 source meter was used for resistance measurements. Washing tests on the Ag NW modified and TPU laminated fabrics were performed according to ISO 6330:2012

(Textiles - Domestic washing and drying procedures for textile testing) standard using a commercial washing machine. No detergent was used during the washing tests. Heating performance of the fabrics were investigated via Optris PI 400 thermal camera. A homemade, 3D printed apparatus was used to investigate TENG performance of the fabricated electrodes in contact separation mode via hand tapping at a frequency of 5 Hz. Open circuit voltage (*Voc*), short circuit current (*Isc*) and short circuit charge (*Qsc*) of the TENGs were measured using a Keithley 6514/E-Electrometer, a LabView code was used for data collection. *Voc* of the 90TPU/160F bottom electrode and PLA/Al foil top electrode TENG was theoretically calculated using AC/DC module of COMSOL Multiphysics. The analysis was made according to Gauss's law, which gives the relationship between fundamental electromagnetic quantities.

5.3 Results and Discussion

SEM image of purified Ag NWs is provided in Figure 5.1 (a). The average length and diameter of the NWs utilized in this work were 8 μm and 50 nm, respectively. Changes in resistance with the number of dip and dry cycles are provided in Figure 5.1 (b). Two different concentrations of Ag NW/ethanol dispersions (0.5 and 2 mg/ml) were used for dipping. It was observed that the target resistance in fabrics with a density of 54 g/m^2 can be much quickly attained with less dip and drying cycles compared to the fabrics with a density of 160 g/m^2. This was attributed to the facile infiltration of Ag NWs into the textiles through inner fibers, allowing easy and highly efficient fabrication of Ag NW modified textiles. Moreover, as expected, through the use of higher concentration Ag NW/ethanol dispersion, textiles quickly reached the target resistance using a smaller number of dip and dry cycles.

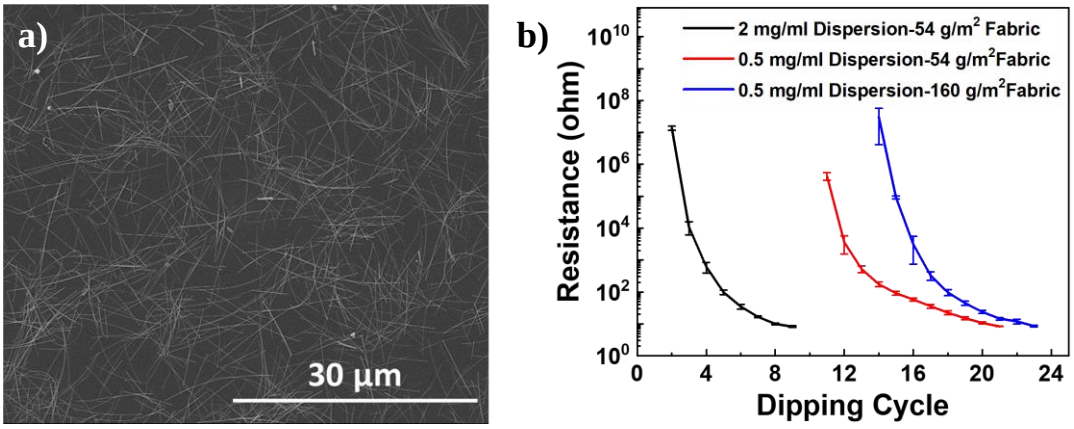

Figure 5.1 (a) SEM image of purified Ag NWs. (b) Resistance changes of the fabrics with different densities decorated with two different concentrations of Ag NW/ethanol dispersions.

Fabrication steps of TPU laminated Ag NW modified fabrics is schematically shown in Figure 5.2 (a). SEM images of Ag NW modified cotton fabrics with densities of 54 g/m^2 and 160 g/m^2 are provided in Figure 5.2 ((b-i), (b-ii)) and ((c-i), (c-ii)), respectively. The difference in the weaving density can be observed from the Figure 5.2 (b-i) and (c-ii) for the fabrics with densities of 54 and 160 g/m^2, respectively. SEM images of the fabrics show that the fiber diameters were the same but yarn count was different for each fabric density. The magnified images of Ag NW modified fabrics revealed conformal deposition of Ag NWs onto the fabric fibers (Figure 5.2 (b-ii), (c-ii)). As fabricated TPU films showed very smooth surfaces without any surface textures (Figure 5.2 (d)). Cross-sectional SEM images of the fabricated TPU films with thicknesses of 70 and 90 µm are provided in Figure 5.2 (e) and (f), respectively. Cross-sectional SEM image of TPU laminated fabric is provided in Figure 5.2 (g). It is clear that the TPU films were conformably laminated onto fabrics with the utilized hot-press pressure and temperature.

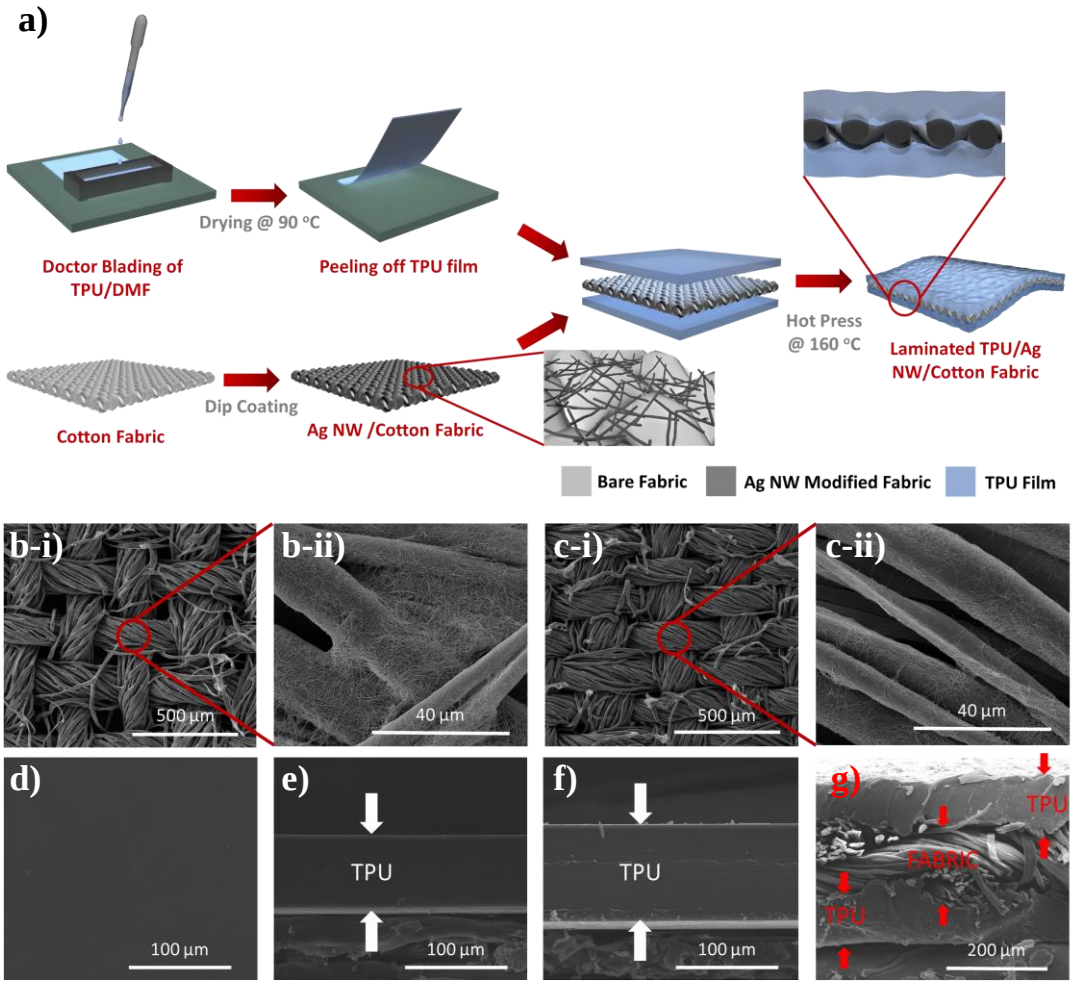

Figure 5.2 (a) Schematic representation of the fabrication steps of TPU laminated Ag NW modified cotton fabrics. SEM images of Ag NW modified fabrics with a density of (b-i, b-ii) 54 g/m^2 and (c-i, c-ii) 160 g/m^2. (d) Top-view SEM image of as-fabricated TPU. Cross-sectional SEM images of as-fabricated TPU with the thicknesses of (e) 70 µm and (f) 90 µm. (g) A cross-sectional SEM image of TPU laminated fabric (90TPU/160F).

While the fabrication of TPU films was successfully achieved, it was equally important to chemically characterize the resulting TPU films. This was because their quality determines the end product quality and performance of the fabricated TENGs. For this purpose, chemical structure of the films was investigated via FTIR analysis, results of which is provided in Figure 5.3 (a). IR bands of TPU films are

summarized in Table 5-1. Distinctive IR bands were obtained at 771 cm^{-1} (CH2 rocking (polyeter)), 816 cm^{-1} (C-H out of plane (aromatic ring)), 1079 cm^{-1} (C-O stretch (urethane)), 1104 cm^{-1} (C-O stretch (polyeter)), 1221 cm^{-1} (C-O stretch (urethane)), 1310 cm^{-1} and 1414 cm^{-1} (C-H bend), 1529 cm^{-1} (N-H bending), 1597 cm^{-1} (C=C in plane (aromatic ring)), 1699 cm^{-1} and 1731 cm^{-1} (C=O stretch), 2853 cm^{-1} and 2940 cm^{-1} (C-H stretch), 3330 cm^{-1} (N-H stretch) [166,167]. Thermal degradation behavior was investigated via thermogravimetric analyses performed under thermo-oxidative conditions (air). A typical three stage decomposition process was observed from TGA and DTG curves for TPU (provided in Figure 5.3 (b), (c), respectively). The first and the second peaks at 349 °C and 434 °C were assigned to scission of TPU chains and degradation of polyols and isocyanates, respectively [168]. The third peak at 570 °C was assigned to the degradation of the previously formed char [169]. Differential scanning calorimeter (DSC) curve of fabricated TPU films is provided in Figure 5.3 (d). Two different glass transition temperatures were observed at -46.5°C and 103 °C, which were corresponding to soft (T_g SS) and hard segments (T_g HS) of TPU, respectively. Endothermic melting peak observed at 154 °C was attributed to the melting of hard segment (T_m HS). Second endothermic melting peak, corresponding to micro phase mixing of soft and hard segments was observed at 190 °C [170].

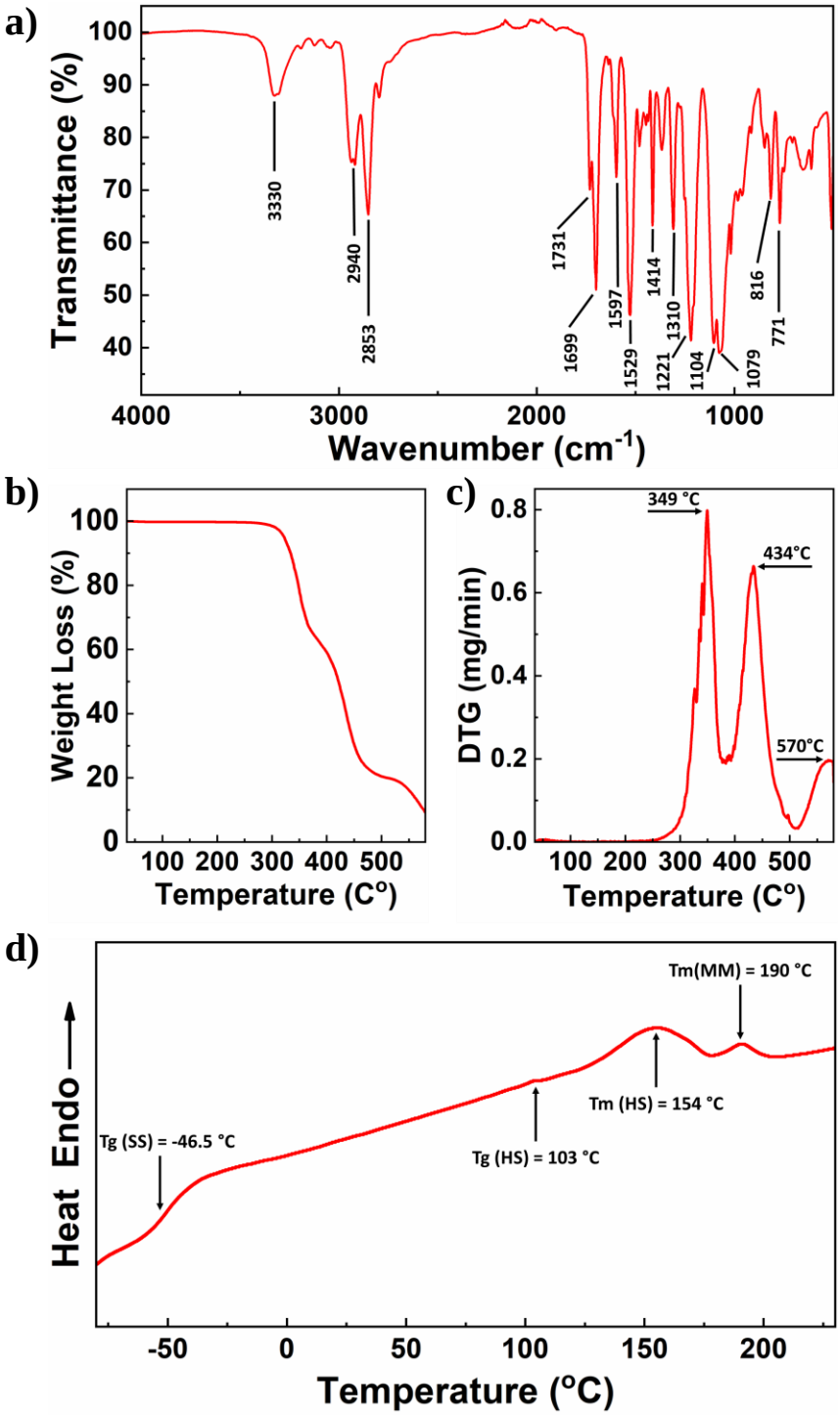

Figure 5.3 Characterizations of fabricated TPU films. (a) FTIR spectrum, (b) Results of TGA analysis obtained under air. (c) Derivative of thermogravimetric analysis results. (d) Results of DSC analysis performed under nitrogen.

Table 5-1 Position and assignments of distinctive IR bands of fabricated TPU films.

Peak Location (cm^{-1}) in this work	**Vibration Mode**
3330	N-H and O-H
2940	C-H stretch
2853	C-H stretch
1731	C=O stretch
1699	C=O stretch
1597	C=C in plane (aromatic ring)
1529	N-H
1414	C-H bend
1310	C-H bend
1221	C-O stretch (urethane)
1104	C-O stretch (polyeter)
1079	C-O stretch (urethane)
816	C-H out of plane (aromatic ring)
771	CH_2 rocking (polyeter)

Most of the studies on the washing stability of e-textiles are conducted using a simple beaker and magnetic stirrers [171–173]. Although simulating washing conditions using magnetic stirrers and a beaker gives a general idea, it cannot represent real washing conditions and may lead to misinterpretation of the results for real-life applications of electronic textiles. Thus, as stated before, washing stabilities of these kind of electronic textiles should be investigated using washing machines. Resistance changes upon washing cycles for the fabrics with different densities and different TPU thicknesses are provided in Figure 5.4. It was observed that Ag NW modified fabrics without TPU lose their conductivities dramatically after 2nd washing cycle. It was mainly due to loss of NW network on textile fibers (as observed in the SEM image inset in Figure 5.4) as the result of combined effects of water and friction

arising from washing conditions. This loss of conductivity of Ag NW modified fabrics is one of the main obstacles for market infiltration. Therefore, TPU films with two different thicknesses were laminated onto Ag NW modified fabrics to increase their washing stability. It is worth mentioning that, the thinnest possible TPU layer should be laminated onto textiles to prevent any loss in fabric touch. Therefore, firstly, 70 μm thick TPU films were laminated onto the modified textiles followed by the investigation of their washing stability. Fabrics with 70 μm thick TPU retained their conductivity up to a certain level for the first 5 washing cycles. Initial resistances of the fabrics were 4 ohms and it was increased to 6 ohms and 10 ohms after 5 washing cycles for 70TPU/160F and 70TPU/54F, respectively. After 5th cycle, delamination of TPU films were observed which is shown in the inset images of Figure 5.4. To further improve the washing stability, thickness of the TPU films were increased to 90 μm. Fabrics with 90 μm TPU preserved their conductivity even after 15 washing cycles. After 20 washing cycles, the conductivity of the fabrics was found to increase significantly and TPU films were delaminated from the fabrics.

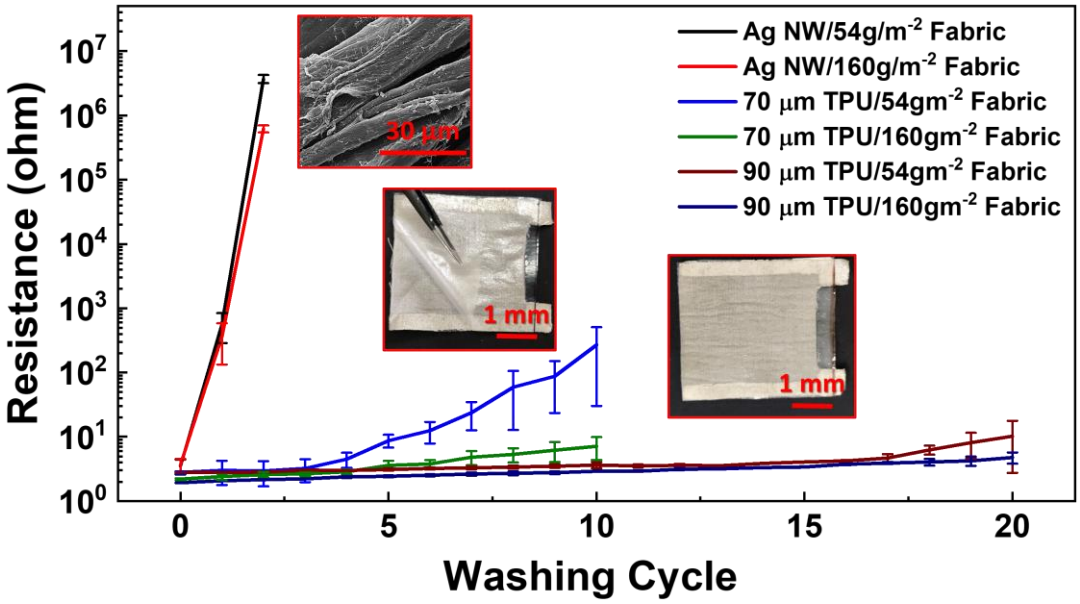

Figure 5.4 Resistance changes of Ag NW modified fabrics (densities of 54 and 160 g/m^2) with respect to washing cycles with and without TPU (70 and 90 μm) lamination.

Monitoring the resistance change in fabrics after each washing cycle is an important way to understand their washing stability. However, it is not enough to understand how the washing cycles affect the homogeneity of the coatings. Only one bridging Ag NW might provide 3D percolation on fabric surface; however, this will significantly alter the triboelectric performance of the fabrics. Heat distribution throughout the fabric (fabrics were used as heaters as in Chapter 3) was also monitored after each washing cycle to deduce the stability of the network. Time dependent heating performance of the fabrics with a density of 54 g/m^2 (70TPU/54F) and 160 g/m^2 (70TPU/160F) after washing cycles with 70 μm TPU lamination is provided in Figure 5.5 (a) and (b), respectively. Applied voltages and corresponding currents can be found within the graph. Initially, the same power was applied to each fabric (between 1 and 1.1 Watt). Then, the initial voltage was applied for the Joule heating measurements (1.7 V for 70TPU/54F, 1.7 V for 70TPU/160F, 1.6 V for 90TPU/54F, 1.8 V for 90TPU/160F). Although homogeneity of heat distribution across the sample for 70TPU/54F was not lost totally, steady state temperature value remarkably diminished after 5th washing cycle (40% decrease in the steady state temperature). Hot spot formation was observed after 10th washing cycle. When Ag NW network starts to break down due to washing, conduction gets facilitated through less narrow and less resistive paths. This results in the formation of hot spots. Higher degree of current flows within that specific region compared to the remaining higher resistance regions in the fabric. Therefore, temperature of that region is significantly increased according to the Joule heating principle. These hot spots may eventually become a serious problem for wearable heaters since the localized heating spots may result in ignition. Inhomogeneity of the functional material decoration also effect other electronic textile applications such as wearable sensors and antennas. Although slightly better protection was obtained for 70TPU/160F than 70TPU/54F, significant performance and homogeneity loss were observed after repeated washing cycles (12% decrease in steady state temperature after 5 washing cycles and 31% decrease in steady state temperature after 10 washing cycles).

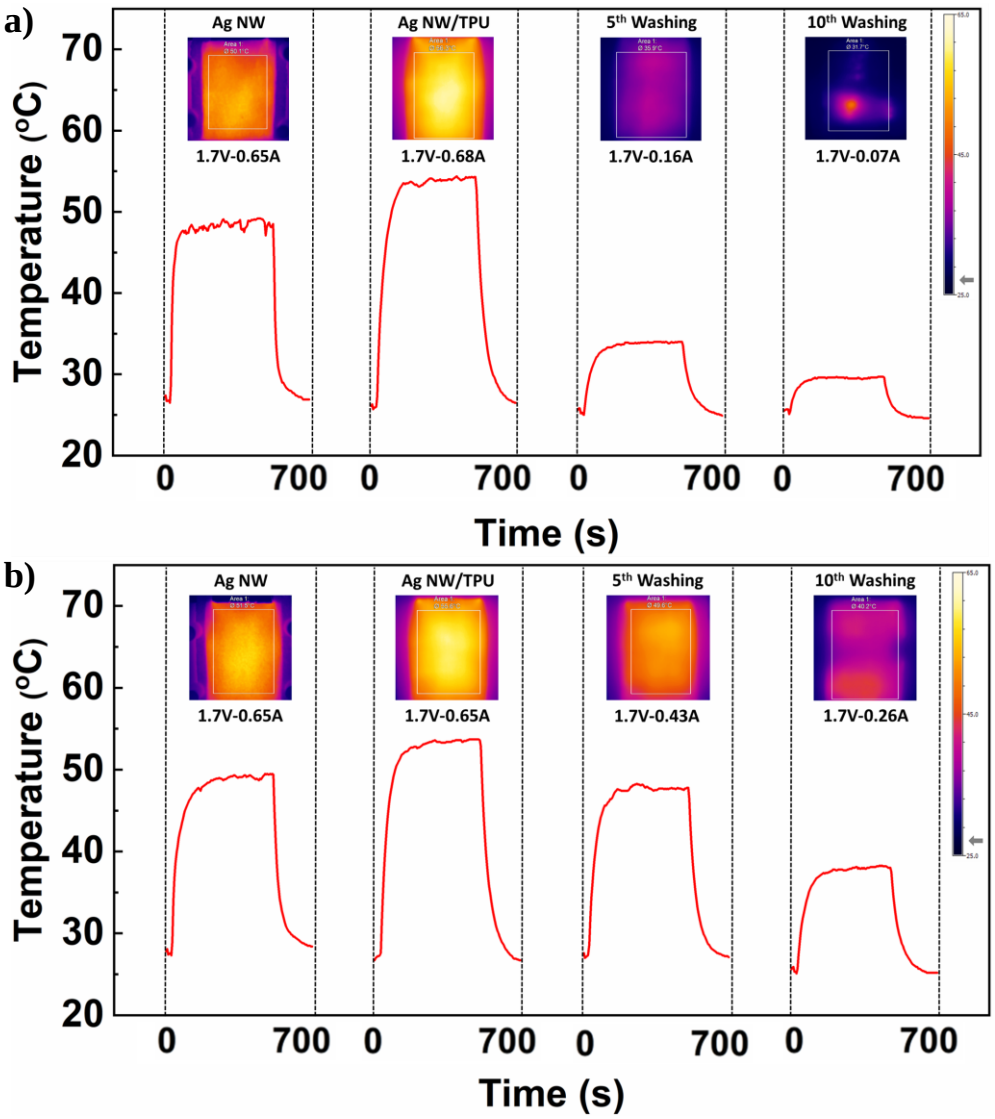

Figure 5.5 Heating performance of as fabricated and washed, 70 μm thick TPU laminated Ag NW modified fabrics with fabric densities of (a) 54 g/m^2 (70TPU/54F) and (b) 160 g/m^2 (90TPU/160F).

Heating performances of the 90TPU/54F and 90TPU/160F fabrics with 90 μm thick TPU upon washing are provided in Figure 5.6 (a) and (b), respectively. 90 μm thick TPU was found to provide superior washing stability to both fabrics with different densities. Heating homogeneity without any hot spot formation was observed even after 15 washing cycles, as can be seen from the provided thermal camera images.

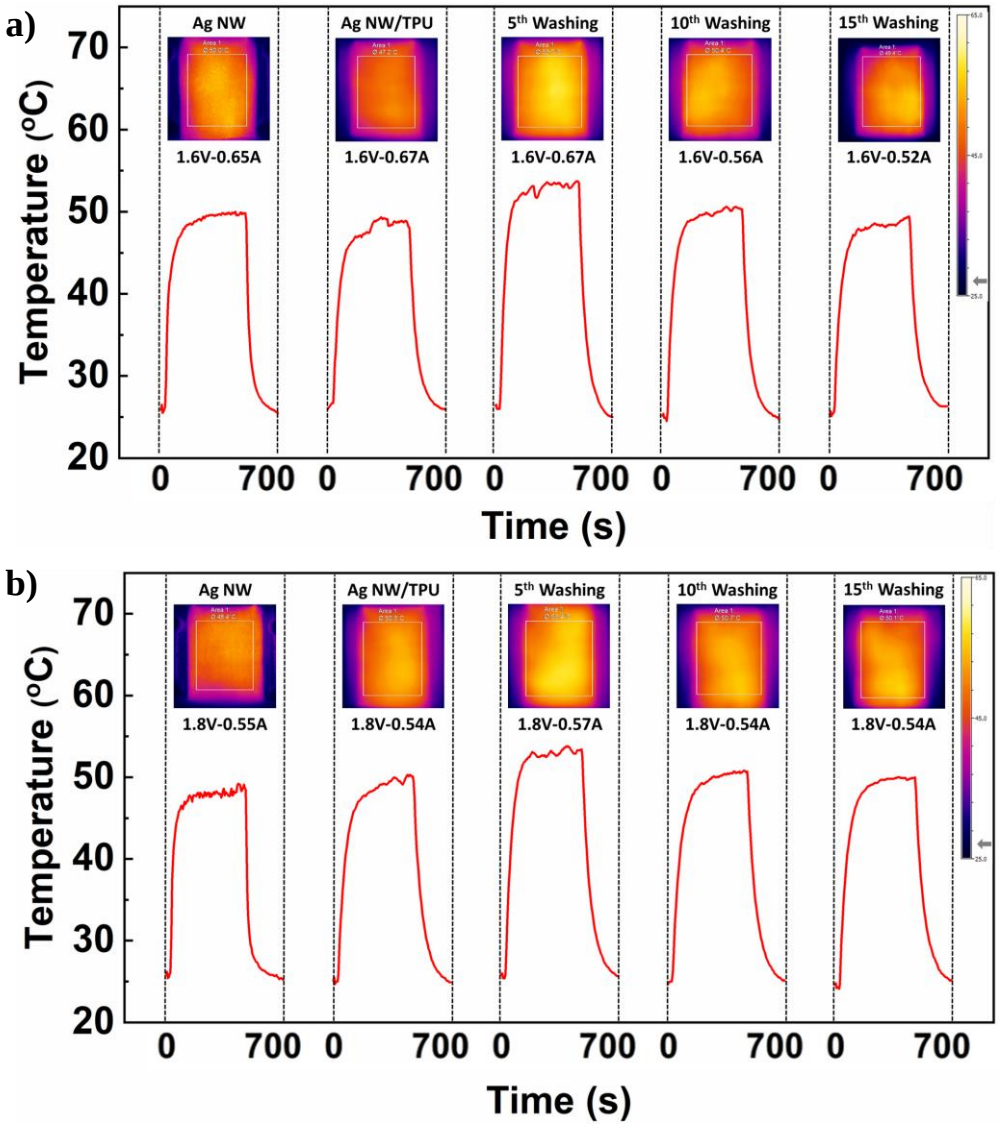

Figure 5.6 Heating performances of the 90 μm TPU laminated fabrics with a density of (a) 54 g/m^2 (90TPU/54F) and (b) 160 g/m^2 (90TPU/160F) with respect to washing cycles.

Joule heating performances of the fabrics were also investigated after 20 washing cycles. Delamination of the TPU layers was found to drastically decrease the steady state temperatures. Hot spot formation was also observed for 90TPU/54F, as shown in Figure 5.7 (a). Although hot spot formation was not observed for 90TPU/160F after 20 washing cycles, steady state temperature was found to decrease as shown in

Figure 5.7 (b). These results show that TPU lamination, that is industrially used by the outdoor wear companies, is a highly promising solution for improving the washing stability of Ag NW modified heated fabrics.

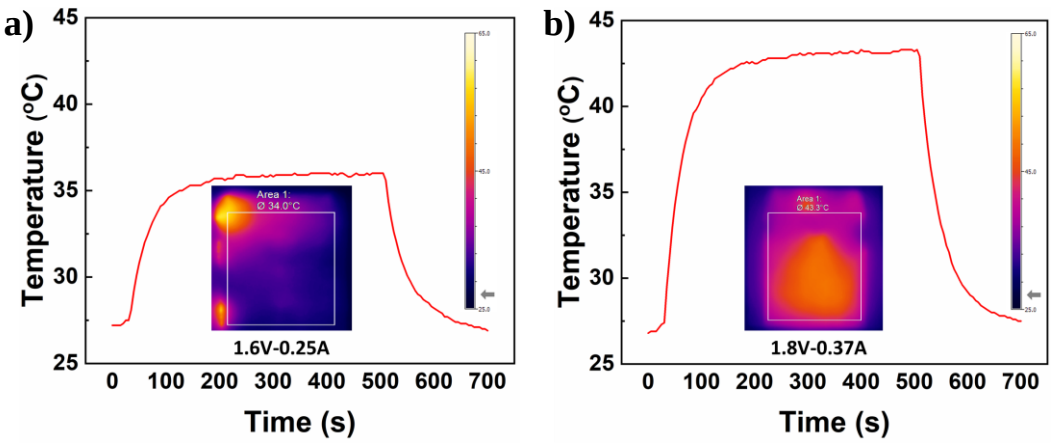

Figure 5.7 Heating performance of 90 µm thick TPU laminated Ag NW modified fabrics with fabric densities of (a) 54 g/m^2 (90TPU/54F) and (b) 160 g/m^2 (90TPU/160F) after 20 washing cycles.

Operating mechanisms of the TENGs used in this study is schematically presented in Figure 5.8. Bottom electrode of the TENG was consisted of TPU laminated Ag NW modified fabrics. PLA films doctor bladed on top of Al foils were used as the top electrodes. Charge is induced due to triboelectrification after two adjacent electrodes contact each other. Therefore, initially there is no potential difference in the system (I). Electrode surfaces are charged once these two electrodes are contacted via hand tapping. The sign (negative or positive) of the charge depends on the positions of the dielectric materials in the triboelectric series. Increasing the gap between the electrodes leads to charge separation with the opposite polarity. However, due to insulative nature of the polymer, charges are preserved on the surface for a long time. Therefore, there is no practical electrical potential difference between the two electrodes at this point (II). When the two electrodes start to get separated, it then starts to build up a potential difference, which then hits a maximum. As the electric potential increases, induced electrons start to flow from one electrode

to the other (III) when the electrodes are shorted. This electron flow causes a current flow that passes through the external circuit until electrostatic charge equilibrium is sustained (IV). Electrons start to flow in the opposite direction, while the gap between the electrodes are started to be closed (V). This periodic connection and separation generate alternating currents. Open circuit voltage (*Voc*) of the TENG system depends also on the separation between two electrodes. Following formulas were used to calculate *Voc* of the system: $\nabla D = \rho$ and $E = -\Delta V$, where D, ρ, E and V are electric displacement, electric charge density, electric field intensity and voltage, respectively. Surface charge density was taken as +/-5.43e-5 C/m^2 for triboelectric layers. For the sake of simplicity both electrode layers were considered flat and homogeneously conducting with a layer thickness of 2 mm. Thicknesses of the triboelectric layers were taken as 30 and 90 µm for PLA and TPU, respectively. *Voc* was calculated as 3×10^3, 9×10^3 and 1.3×10^4 V when the separation distance was set as 1, 3 and 6 mm, respectively.

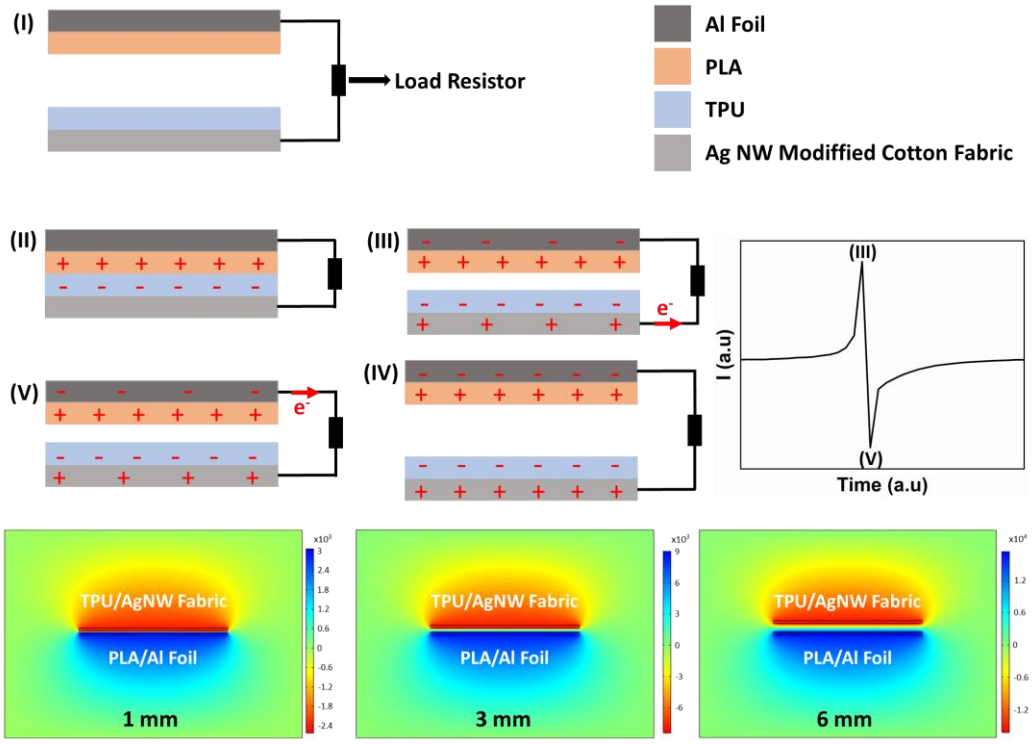

Figure 5.8 Operating mechanism and simulations of the separation dependent open circuit voltages of the TENG electrodes used in this study.

90 μm TPU lamination were preferred for the fabrication of TENG electrodes, since it imparted superior washing stability to the fabrics with both densities. *Voc*, *Isc* and *Qsc* of the TENG electrodes are provided in Figure 5.9 (a), (b) and (c), respectively. *Voc*, *Isc* and *Qsc* values of 90TPU/54F and 90TPU/160F electrodes are also summarized for each top electrode (PDMS, PI, Ecoflex and PLA) in Table 5-2. *Voc*, *Isc* and *Qsc* was higher for 90TPU/160F than 90TPU/54F for all top electrodes (PDMS, PI, Ecoflex and PLA). *Voc* of 90TPU/160F bottom electrodes were recorded as 41, 42, 78 and -162 V for PDMS, PI Ecoflex and PLA top electrodes, respectively. *Isc* of 90TPU/160F bottom electrodes were recorded as 8, 15, 41 and -42 μA for PDMS, PI, Ecoflex and PLA top electrodes, respectively. *Qsc* of 90TPU/160F bottom electrodes were recorded as 19, 20, 52 and -87 nC for PDMS, PI, Ecoflex and PLA, respectively. The difference in the *Voc*, *Isc* and *Qsc* for each top electrode was mainly due to the positions of the polymers in the triboelectric series [174]. The output voltages and charges for PI/Al top electrode were expected to be higher than that of PDMS/Al electrodes, according to positions in the triboelectric series. However, it should be considered that the positions in the triboelectric series are determined by the surface charge of the materials when they are contacted between liquid metals like mercury. In case of using solid contacts like in our system, difference in the surface roughness and the mechanical properties may cause improper contact touch, which may cause deviation from the ideal output voltage and current changes. Highest and the most promising *Voc*, *Isc* and *Qsc* results were obtained from the PLA/Al foil top electrodes. It is worth noting that the use of TPU and PLA couple as the dielectric layers in TENGs that operate in contact separation mode holds great potential to be further investigated.

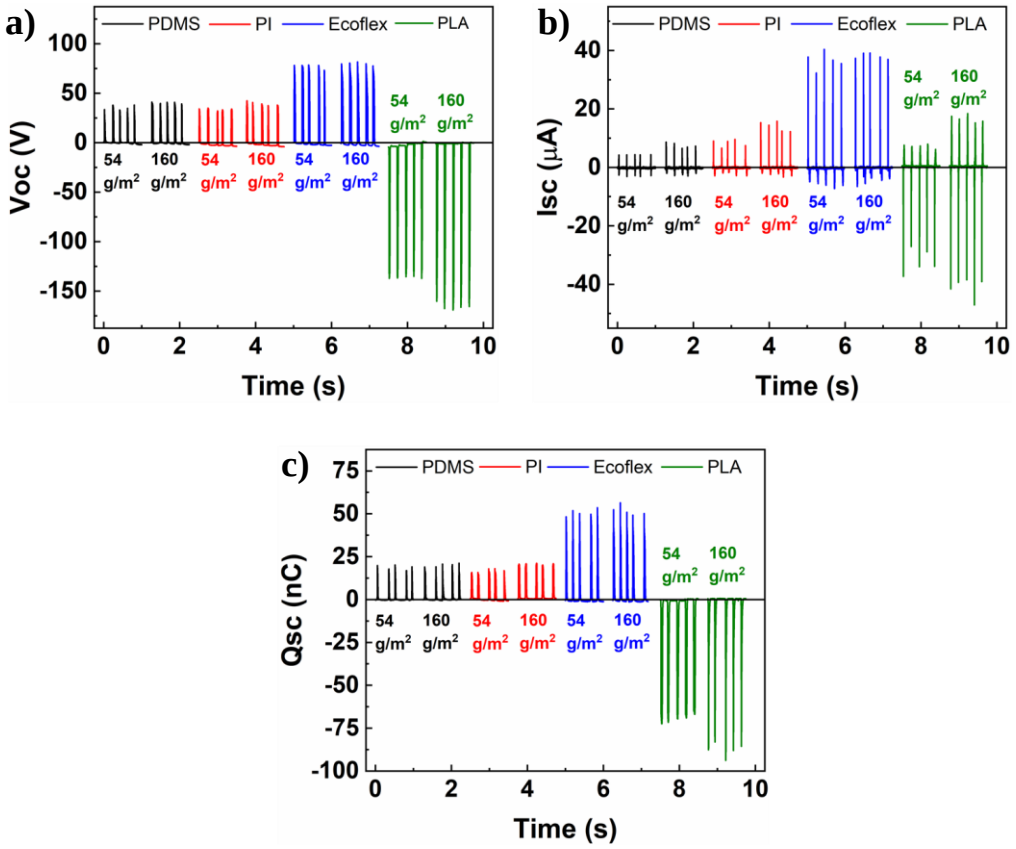

Figure 5.9 (a) Voc, (b) Isc and (c) Q_{SC} of 90TPU/54F and 90TPU/160F bottom electrodes and PDMS, PI, Ecoflex and PLA/ Al foil top electrodes. (A tapping force and frequency of approximately 2 N and 5 Hz, respectively).

Table 5-2 Voc, Isc and QSC values of TENG devices with 90TPU/54F and 90TPU/160F bottom electrodes and PDMS, PI, Ecoflex and PLA top electrodes.

	PDMS/Al foil			**PI/Al foil**			**Ecoflex/Al foil**			**PLA/Al foil**		
	V_{oc} (V)	I_{sc} (μA)	Q_{sc} (μA)	V_{oc} (V)	I_{sc} (μA)	Q_{sc} (μA)	V_{oc} (V)	I_{sc} (μA)	Q_{sc} (μA)	V_{oc} (V)	I_{sc} (μA)	Q_{sc} (μA)
90TPU/54F	37	4	17	37	11	16	74	40	48	-137	-34	-72
90TPU/160F	41	8	19	42	15	20	78	41	52	-162	-42	-87

Output voltages and currents were also measured with different load resistors connected to the circuit for the TENG systems consisting of PLA/Al foil top electrodes and 90TPU/54F, 90TPU/160F bottom electrodes (Figure 5.10 (a) and (b),

respectively). Higher output voltages were obtained in TENG devices with TPU films laminated onto fabrics with higher densities. In addition, slightly higher output currents were measured in TENG devices with higher density fabrics. Output power with respect to resistance load was also calculated and provided in Figure 5.10 (c). A maximum power of 1.25 W/m^2 was calculated when a 50 Mohm load resistor was connected to the system. The output power of the TENGs was also higher when they were fabricated using higher density fabrics.

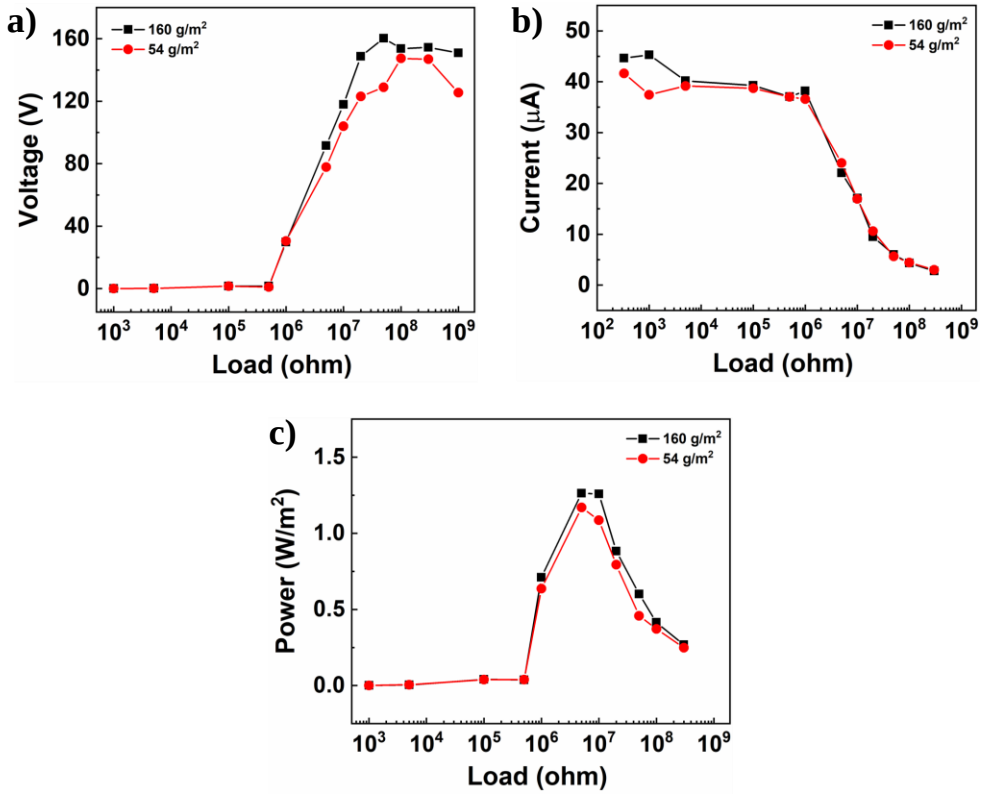

Figure 5.10 Output (a) voltage, (b) current, (c) power of 90TPU/54F and 90TPU/160F bottom and PLA/ Al foil top electrodes under different load resistors. Lines are for visual aid. (A tapping force and frequency of approximately 2 N and 5 Hz, respectively).

The increase in TENG performance with increasing fabric density was attributed to surface roughness differences between fabrics. Fabrics with a density of 160 g/m^2 have higher surface roughness than those with a density of 54 g/m^2, as can be seen

from Figure 5.11 (a) and (b). This initial difference in the roughness of the fabrics also effects the final roughness of the electrodes after 90 µm thick TPU lamination onto the fabrics, as shown in Figure 5.11 (c) and (d).

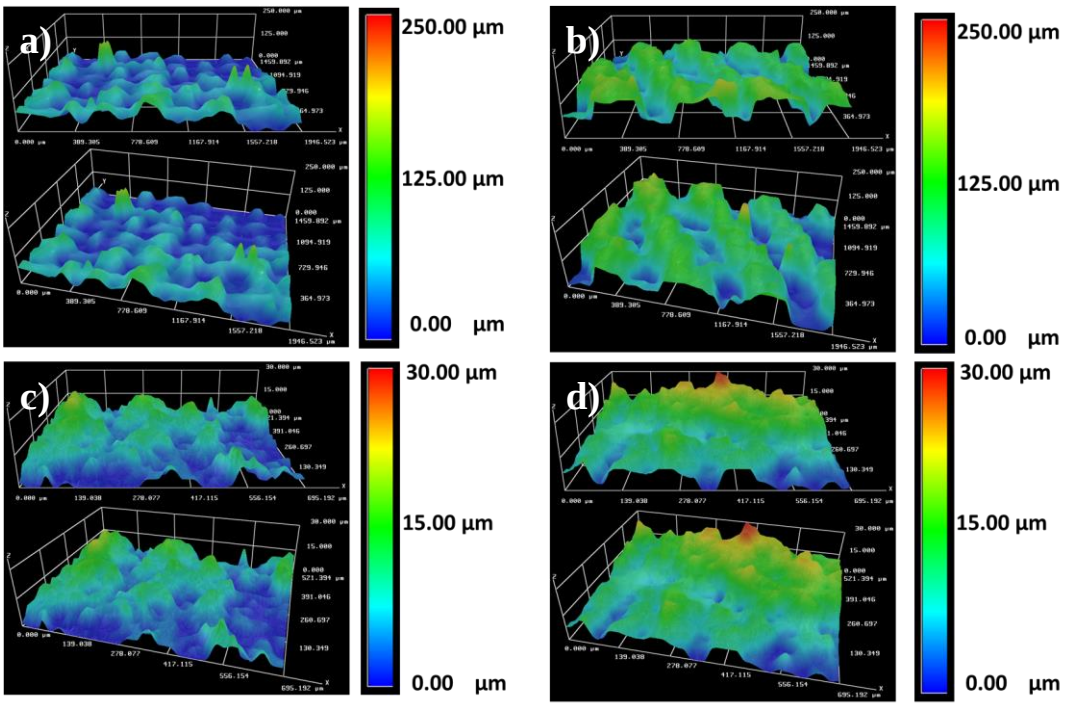

Figure 5.11 3D morphologies of the cotton fabrics with fabric densities of (a) 54 and (b) 160 g/m^2. 3D morphologies of the 90 µm thick TPU laminated cotton fabrics with fabric densities of (c) 54 and (d) 160 g/m^2.

Durability of the TENG system consisting of 90TPU/160F fabric bottom and PLA/Al foil top electrodes were investigated for a time period of 130 s. Open circuit voltage during 130 s hand tapping are provided in Figure 5.12 (a). It was observed that the electrodes are quite durable and show stable *Voc*. It is also crucial for wearable TENGs that; the electrodes should withstand repeating mechanical forces. Therefore, *Voc* was measured after repeated bending cycles and results are provided in Figure 5.12 (b). It was observed from the measurements that the 90TPU/160F electrodes showed very stable characteristic against repeated bending cycles (no voltage drops upon bending). *Voc* of the 90TPU/160F fabric with respect to washing cycles is provided in Figure 5.12 (c). Similar to resistance and heating performance,

output voltages of the electrodes were also preserved for 15 washing cycles. It was observed from resistance changes and Joule heating tests that the TPU layer impart washing resistance to the Ag NW network on fabrics. It was also observed from the TENG measurements that (no voltage drops upon washing), TPU layer itself was highly stable.

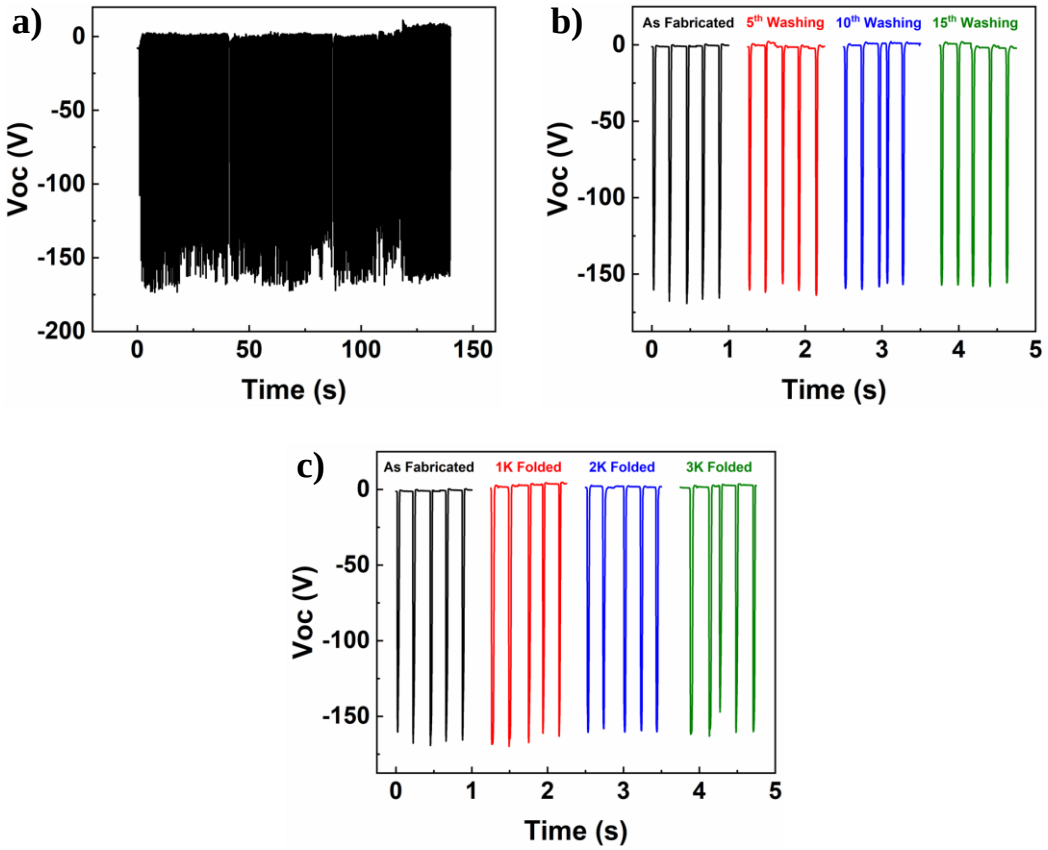

Figure 5.12 (a) Durability of the TENG system consisting of 90TPU/160F bottom and PLA/ Al foil top electrodes. (b) Bending stability of the TENG system consisting of 90TPU/160F bottom and PLA/ Al foil top electrodes. (c) Washing stability of 90TPU/160F bottom electrode with PLA/Al foil top electrode. Top electrodes were not subjected to washing cycles (A tapping force and frequency of approximately 2 N and 5 Hz, respectively).

Separation distance between the electrodes is another important parameter determining the output performance of TENGs. Output performances (*Voc*, *Isc* and

Qsc) of the TENG system consisting of 90TPU/160F bottom and PLA/Al foil electrodes were also experimentally investigated, in addition to simulations (Figure 5.8), using the separation distances of 1, 3 and 6 cm and the results are provided in Figure 5.13 (a), (b) and (c), respectively. All the performance metrics (*Voc*, *Isc* and *Qsc*) were found to increase with the separation distance as confirmed by the simulations. Effect of the electrode size on the output TENG metrics were also investigated for 90TPU/160F bottom and PLA/Al foil electrodes.

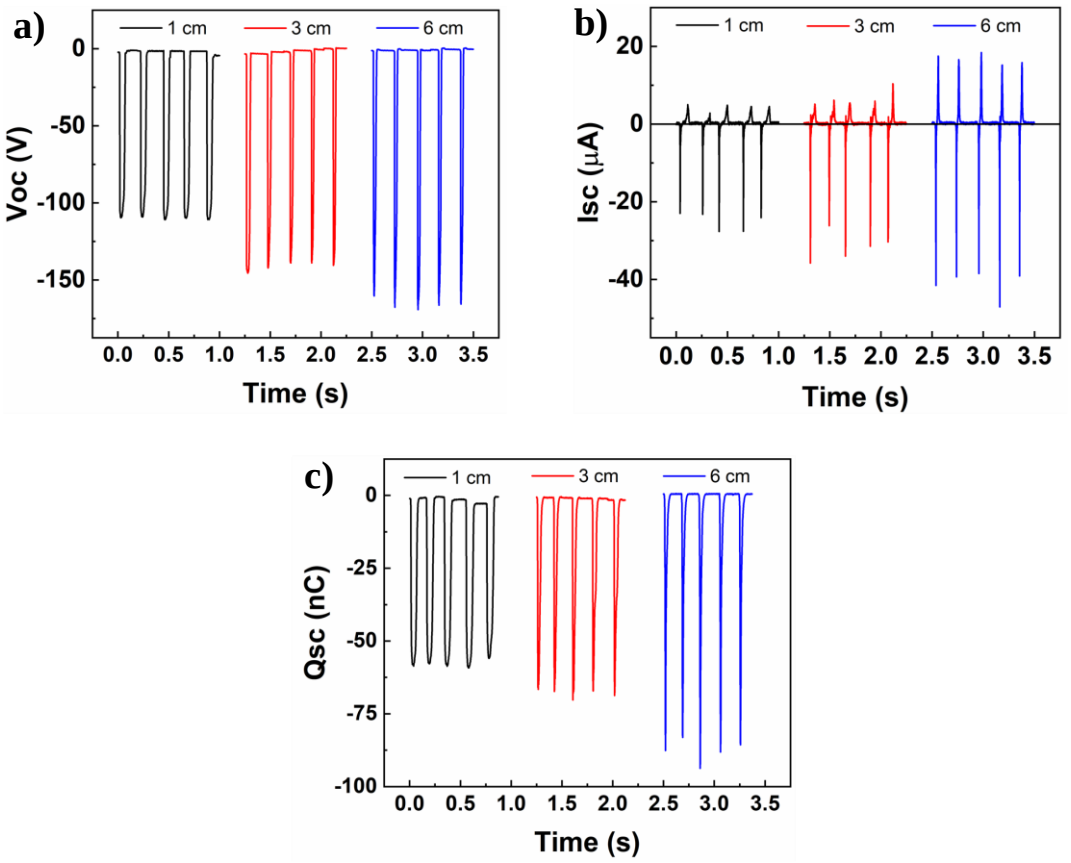

Figure 5.13 Effect of separation distance on (a) Voc, (b) Isc, and (c) Qsc for 90TPU/160F bottom and PLA/Al foil electrodes. (approximately 2 N tapping force, 5 Hz tapping frequency).

Three different electrode sizes were explored (2 × 2, 3 × 3 and 4 × 4 cm^2). *Voc*, *Isc* and *Qsc* values for different electrode sizes are provided in Figure 5.14 (a), (b) and (c), respectively. It was observed that all metrics increase with the electrode size.

Voc of the electrodes with the sizes of 2 × 2, 3 × 3 and 4 × 4 cm^2 were measured as -30, -47 and -162 V, respectively. *Isc* were recorded as -7, -23 and -42 µA for the electrodes with the sizes of 2 × 2, 3 × 3 and 4 × 4 cm^2, respectively. On the other hand, *Qsc* of the electrodes with sizes of 2 × 2, 3 × 3 and 4 × 4 cm^2 were measured as -12, -26 and -87 nC, respectively.

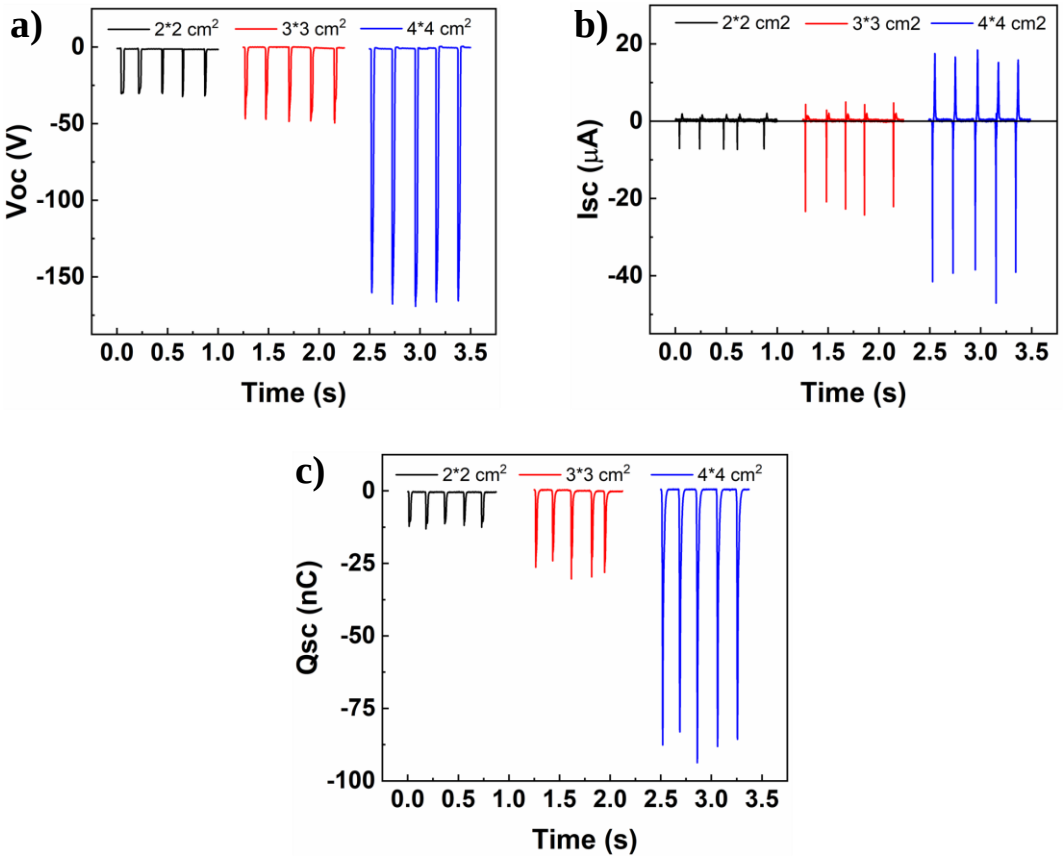

Figure 5.14 Effect of electrode sizes on (a) Voc, (b) Isc and (c) Qsc for 90TPU/160F bottom and PLA/Al foil electrodes (approximately 2 N tapping force, 5 Hz tapping frequency).

Fabricated TENG device consisting of 90TPU/160F and PLA/Al foil electrodes was used to charge capacitors to be used as an energy storage device. Circuit schematics used to charge capacitors and to power up a chronometer is provided in Figure 5.15 (a). Alternating current generated from TENGs was rectified via a rectifying bridge, which was connected to a capacitor. Voltage changes of the capacitors with different

capacitance values are provided in Figure 5.15 (b). The capacitors were charged by the rectified current generated as the result of contact and separation cycles practiced by hand tapping. The charges were transferred to the capacitor and stored until it reaches saturation. Time or tapping cycles required to reach the threshold was directly related to the capacitance of the capacitors. Following charging, the capacitor was connected to a chronometer to power it up (provided in Figure 5.15 (c)). The same TENG electrodes were also used to illuminate green LEDs according to circuit schematics provided in Figure 5.15 (d). Current generated as a result of hand tapping successfully illuminated 185 serially connected LEDs and 86 serially connected LEDs arranged in METU letters as shown in Figure 5.15 (e), (f) respectively. Our results showed that this TENG system can generate enough energy for lighting at night through making use of mechanical energy generated by walking. At the same time, fabricated electrodes were also used to monitor body motion like walking, running and jumping. For this purpose, a 90TPU/160F bottom electrode was placed into a slipper and PLA/Al foil top electrode was placed on the heel of the foot of a volunteer as shown in Figure 5.15 (g). Output voltages of the system while walking, running, resting and jumping is provided in Figure 5.15 (h). Output voltage was measured as around 90, 120 and 180 V for walking, running and jumping, respectively. The increasing trend was attributed to increased pressure and frequency while running and jumping compared to walking. Therefore, the output voltages were found to differ significantly. These results indicate that the TENG systems used in this work can be easily used as a self-powered pedometer.

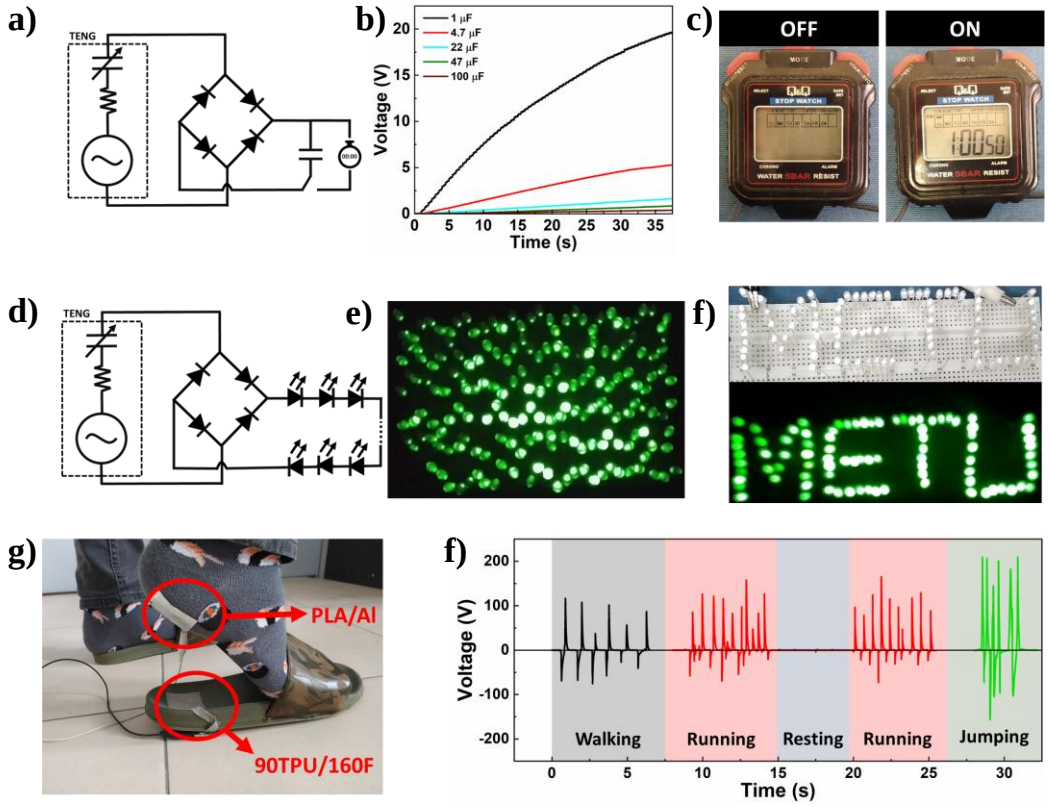

Figure 5.15 (a) Schematic representation of the overall circuit used for charging capacitors and powering up a chronometer. (b) Capacitor charging via fabricated TENG electrodes with different capacitance values (1 μF – 100 μF). (c) Schematic representation of overall circuit used to illuminate serially connected green LEDs. Photographs showing illuminated (e) 186 serially connected LEDs and (f) 86 serially connected LEDs arranged as METU letters. (h) Photograph showing TENG electrodes placed into slipper and on the heel of the foot. (g) Output voltages read out from the TENG electrodes placed into slipper and on heel when the volunteer walks, runs, rests and jumps.

A self-powered e-wristband consisting of 90TPU/160F bottom and PLA/Al foil top electrodes was fabricated and utilized as a human machine interface. Circuit schematics of the e-wristband is provided in Figure 5.16 The e-wristband consisted of four buttons that were separately fabricated and controlled.

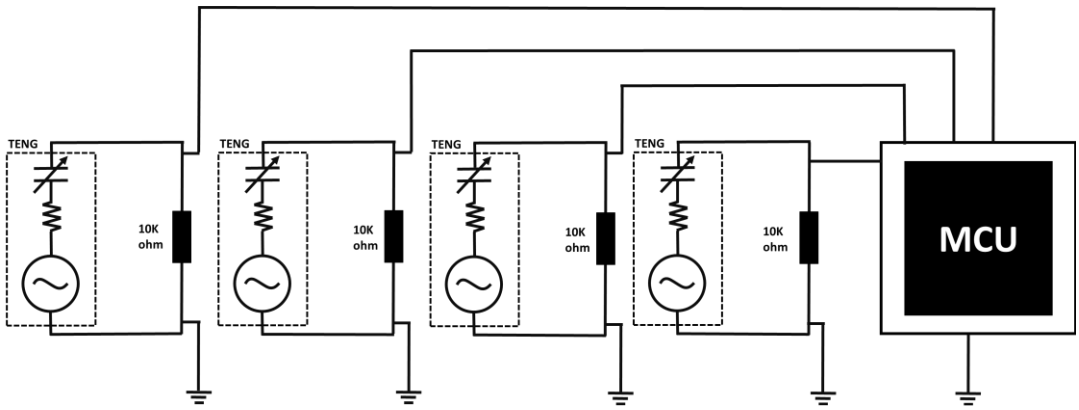

Figure 5.16 Schematic representation of the overall circuit used for e-wristband.

Electrode layers, fabrication steps, and a photo of the self-powered e-wristband is provided in Figure 5.17 (a). 5 mm thick sponge spacers were used to separate top and bottom electrodes. The assembly was then fixed to the textile via double sided tape. Current carrying cables were soldered onto conductive sides of the electrodes. Finally, another textile layer was fixed and used as a cover. 10 Kohm pull-down resistors were connected to get rid of noises that might be generated as fake signals. Top electrode of the TENGs were connected to the separate pins on the micro controller unit (MCU), while the bottom electrodes of the TENGs were grounded. MCU was serially connected to a computer. Output voltages of the four buttons were recorded separately and provided in Figure 5.17 (b). Voltages were measured between 5-7 V for each TENG upon pressing the buttons. The e-wristband was used to control Spotify, as shown in Figure 5.17 (c). Play button was responsible to play and pause the song. The next and previous arrow buttons were used to change the song that was played. It is clear that the potential of fabricated e-wristband is not limited with the demonstrated application. Recent progress in the Industry 4.0 increases the importance of the human machine interfaces. The e-wristband demonstrated in this work can be easily adapted to the production lines of the factories to increase productivity and reduce human errors. The ergonomic and self-powered e-wristband demonstrated in this work is a very strong alternative to current solutions that require external power sources.

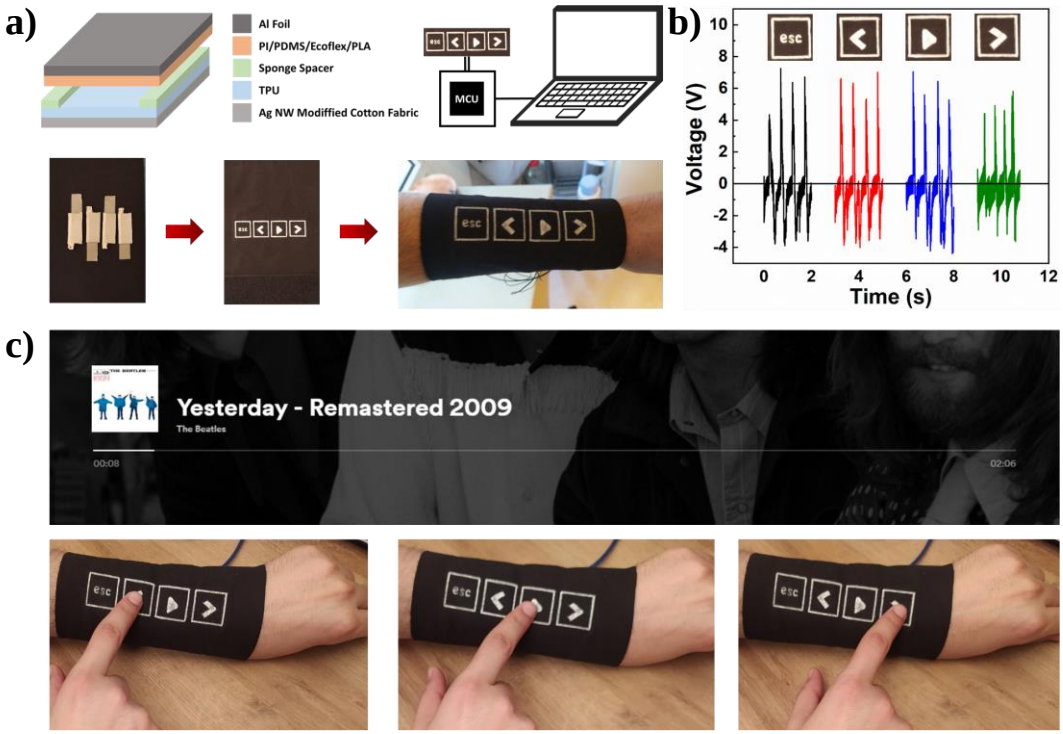

Figure 5.17 (a) Fabrication steps, schematic circuit design, layers and a photo of the e-wristband. (b) Output voltages of each button of the e-wristband. (c) Pictures of fabricated e-wristband in operation while controlling Spotify.

Recently published wearable TENG devices with their performance metrics have been tabulated and provided in Table 5-3. Results obtained in this work is also provided in the same table. Non-woven fibers provide higher output power density; however, they are not washable. This limits them in real case scenarios. On the other hand, washable structures were reported to provide limited output power densities. With a maximum output power of 1.25 W/m^2, PLA/Al foil top and 90TPU/160F bottom electrode TENG system fabricated in this work is one of the highest performance fiber/fabrics based TENGs among the previously reported ones.

Table 5-3 Performance comparison of recently published wearable TENGs structures.

Type	Electrode I	Electrode II	Voc (V)	Isc (μA)	Power Density (W/m^2)	Washable	Ref
FS	-Cotton yarn -Ag plated nylon fibers	-Expanded PTFE	900	19	0.02	Yes	175
CS	-PTFE tubes -Liquid Metal	-Silk Fabric -Cu Fabric	100	6	0.03	-	176
CS	-PVDF NP PDMS - Silver Fabric	- Silver Fabric	105	5.39	0.83		177
CS	-PTFE yarn -Ag coated nylon yarn	-PA66 yarn -Ag coated nylon yarn	35	1.8	7.5×10^{-3}	Yes	178
SE	-SEBS /PVDF Nanofibers -Ag Flakes/Liquid Metal	Skin	85	4	0.22	Yes	179
SE	-PMA -PNA hydrogel fiber	PTFE film	36	0.7	8.8×10^{-3}	-	180
SE	-PDMS -RGO coated Carbonized Cotton Fabric	Acrylic Plate	17.8	0.83	8×10^{-3}	-	181
SE	-Silicone Rubber -Ag coated PA Fiber	PET film	40	0.1	1.6×10^{-3}	Yes	182
CS	-PTFE -Stainless Steel Yarn	-Nylon -Stainless Steel Yarn	2.17	-	9.9×10^{-6}	Yes	184
FS	-PDMS -Ni Coated Fabric	Bare fabric	49	1.8	0.095	-	185
CS	-Melt blow PA -Ni Coated Fabric	-Melt blow PP -Ni Coated Fabric	150	15	0.902	-	154
SE	-Hydrophobic cellulose oleoyl ester/ black phosphorus -Ag NF Coated Fabric	Skin	880	16	5.2	Yes	173
CS	**-TPU -Ag NW Coated Fabric**	**-PLA -Al Foil**	**155**	**41**	**1.25**	**Yes**	**This Work**

5.4 Conclusions

In summary, washable TENG electrodes were fabricated using TPU laminated Ag NW modified fabrics. Both the Ag NW modification and TPU lamination was practiced using simple and scalable methods. Heat distribution of the Ag NW modified fabric heaters was monitored to investigate the washing stability of the TENGs, complementary to typical resistance change monitoring. It was observed that 90 μm thick TPU film lamination preserved resistance, the heating behavior and homogeneity of the fabrics up to 15 washing cycles. The laminate structure was also used as TENG electrodes working in contact separation mode. Four different top electrodes were prepared with PI, PDMS, Ecoflex and PLA dielectric layers coated onto Al foil. It was found that fabrics with a density of 160 g/m^2 provide higher *Voc* and *Isc* values for each TENG couple than the fabrics with a density of 54 g/m^2. *Voc*, *Isc* and maximum power outputs were measured as 162 V, 41 μA and 1.25 W/m^2, respectively, for the systems consisting of 90TPU/160F bottom and PLA/Al foil top electrodes. The same system was also used to charge conventional capacitors and to power up a chronometer. It was also shown that the fabricated TENGs can illuminate 186 serially connected LEDs with gentle hand tapping. Moreover, electrodes were used as a self-powered pedometer to monitor walking, running and jumping of a volunteer. Finally, in order to demonstrate the true potential of fabricated TENGs a self-powered e-wristband with four control buttons was fabricated and used as a wearable human machine interface to control simple computer operations.

CHAPTER 6

WET SPUN CORE-SHELL FIBERS FOR SELF POWERED WEARABLE SENSORS

6.1 Introduction

Clothing has been used only for protection from environmental conditions such as rain, heat and cold [175]. The developments in technology in the last two decades have caused the inadequacy of clothes to meet human needs. Extra features have been requested as well as providing protection from clothing. Especially, the advancements in communication technologies and the cooperation of different disciplines such as the internet of things, artificial intelligence and data science have made a significant contribution to the development of wearable electronic devices [176–179]. These devices have begun to touch human life in many different applications including healthcare monitoring, human machine interface and virtual reality technology [126,180–183]. However, there is still a long way to go before these devices reach their full potentials. Even though these wearable devices operate at low-power they still require power sources to function. Rechargeable batteries and capacitors are currently used to power up these devices. However, the shortcomings of these power supplies limit the use of wearable electronics. First of all, they are heavy and bulky that reduce comfort. In addition, their capacity is limited. They require frequent charging and they carry potential risks.

Triboelectric nanogenerators (TENGs) have significant potential to be used as a reliable, inexhaustible, sustainable and economically feasible power source. In addition, TENGs can also perform as self-powered sensors for wearable electronics [184]. Combined effect of triboelectricity and electrostatic induction enable TENGs to harvest mechanical energy and convert that to electrical energy with high conversion efficiency especially at low frequencies such as human motion. However, most of

the early TENGs consist of planar polymeric films as the triboelectric layers [145,185]. Such structures are important as proof of concepts, but far from the what wearable electronics have to offer. First of all, since they provide limited air permeability, they do not offer comfort to the user. In addition, covering the textile with a planar film disrupts the fabric texture and reduces its flexibility. Electrospun fibers have been coated onto conductive textile to overcome lack of air permeability, flexibility and loss of textile texture problems [160–162]. However, washing instability can be a serious problem for such structures. Therefore, more suitable structures must urgently be developed to realize truly wearable TENGs. Fiber-based TENGs stand out as a promising solution to the aforementioned problems and it has been explored in the literature [186–188]. However, some of these fiber-based TENGs involve very complex manufacturing steps and non-textile parts (like springs, Teflon tubes) that hinder their applicability in real case scenarios [189–193]. More suitable materials and production techniques have also been proposed for fiber based TENGs in literature [194–200]. Most of these studies are based on the same approach. Commercial bulk metal fibers and/or metal coated polymer fibers were directly used in some of these works. Then polymeric fibers were coated/wrapped onto these conductive fibers via dip coating or winding techniques. These approaches enable the development of promising wearable TENGs with high power output and real-case applicability. However, there are also some restrictions of these structures. First of all, the conductive fibers used in these studies are not mechanically stable to repetitive forces [84]. In addition, they are not sufficiently stretchable, preventing their use in some cases. They also require an additional manufacturing step to coat and/or wind the dielectric fibers onto the conductive fibers. Liquid metals were utilized as the conductive core layer for core-shell fiber based TENGs to overcome mechanical instability issues [192]. However, these core-shell structures pose a potential risk in case of rupture, as the liquid metals are toxic. In addition, in such structures, solid cables are required to contact liquid metals with power management circuits. This will cause connection problems in real use.

Here in this study, scalable, economically feasible and practical core-shell fibers are developed to overcome aforementioned problems of fiber based TENGs. It has been shown that wet spinning of the core-shell structure with a conductive core and a dielectric shell has great potential. Thermoplastic polyurethane (TPU) is used as a matrix material for core fibers. Carbon black (CB) and silver nanowires (Ag NWs) are added into TPU matrix to develop conductive core fibers. A bare TPU layer was used as shell fiber acting as the triboelectric layer. The fabricated core-shell fiber TENGs showed excellent performance and hold a great potential to be used in self-powered smart wearable sensors for futuristic applications.

6.2 Experimental Procedure

6.2.1 Synthesis of Nanomaterials

All glassware used in the experiments were cleaned using acetone (99.8%), isopropyl alcohol (99.8%) and DI water. Ag NW synthesis chemicals were purchased from Sigma-Aldrich and used without further purification. Ethylene glycol (anhydrous, 99.8%), polyvinylpyrrolidone (PVP) (monomer-based calculation MW = 55000), sodium chloride (NaCl, 99.5%) and silver nitrate (AgNO3, ACS reagent, ≥99.0%) were used for the polyol synthesis of Ag NWs. Ag NWs were synthesized according to describe in previous chapters. Following synthesis, nanowires were purified through washing with ethanol several times followed by centrifugation. The final product was then dispersed in water for further processing.

6.2.2 Wet Spinning of Core Shell TENGs Electrodes

A coaxial needle with 22G inner and 18G outer size was used to fabricate core-shell fibers. TPU granules were purchased from LUBRIZOL (ESTANE 58887) and kept at 60°C for 12 hours to remove moisture. For all fiber types, (unless otherwise stated) 0.2 g of solid content was dissolved/dispersed in 1 ml of N-N Dimethylformamide

(DMF) at 40 °C in a closed beaker. Different amounts of CB (10-50 wt% wrt. solid content) were mixed with TPU/DMF to optimize core layer. 10 wt.% of Ag NWs were also added to increase the conductivity of core fibers. Then the solution was transferred to a 10 ml syringe. Initially three different TPU/DMF solutions were prepared with different TPU concentrations (0.05 g/ml, 0.1 g/ml and 0.2 g/ml) to investigate TPU concentrations within the shell layer. The shell solutions were transferred to 10 ml syringes. Deionized water was used as the coagulation bath. Both core and shell solutions were injected to water coagulation bath via different injection pumps with an injection rate of 3 ml/h for core layer and 4 ml/h for the shell layer. Then the fibers were directly transferred into different water bath for 24 h to improve solvent exchange between DMF and water. Then fibers were dried at room temperature in vacuum furnace for another 24 h.

6.2.3 Characterizations

The surface morphologies of the wet spun fibers were investigated using a scanning electron microscope (SEM). SEM studies were performed on a FEI NOVA NANO SEM 430 microscope operated under low voltage to prevent fabric damage. Prior to SEM analysis, samples were coated with a few nanometers thick gold (Au) layer to impart conductivity. Tensile test was carried out with a universal testing machine (Zwick/Roell Z25) with a crosshead speed of 30 mm/min. Keithley 2400 source meter was used for resistance measurements. *Voc*, *Isc* and *Qsc* of the fibers were measured using a Keithley 6514/E-Electrometer, a LabView code was used for data collection.

6.3 Results and Discussion

Schematic illustration for the fabrication of wet spun core-shell fibers is provided in Figure 6.1 (a). The TPU chains and Ag NWs align as a result of injection of the feed solvent and coagulation of the fibers. Photo of CB/AgNW/TPU conductive core

carrying 500 g weight is provided in Figure 6.1 (c). Photo of wet spun core shell fiber carrying 500 g weight is provided in Figure 6.1 (d). These photos indicating that, both single core and core-shell fibers show superior mechanical stability to be used in wearable applications. Photo provided in Figure 6.1 (e) showing the junction of core and shell fibers. The core fiber is produced by itself before the core shell fiber will allow it to be easily connected to microcontrollers later on. This is a very important feature in terms of ease of use for later integration.

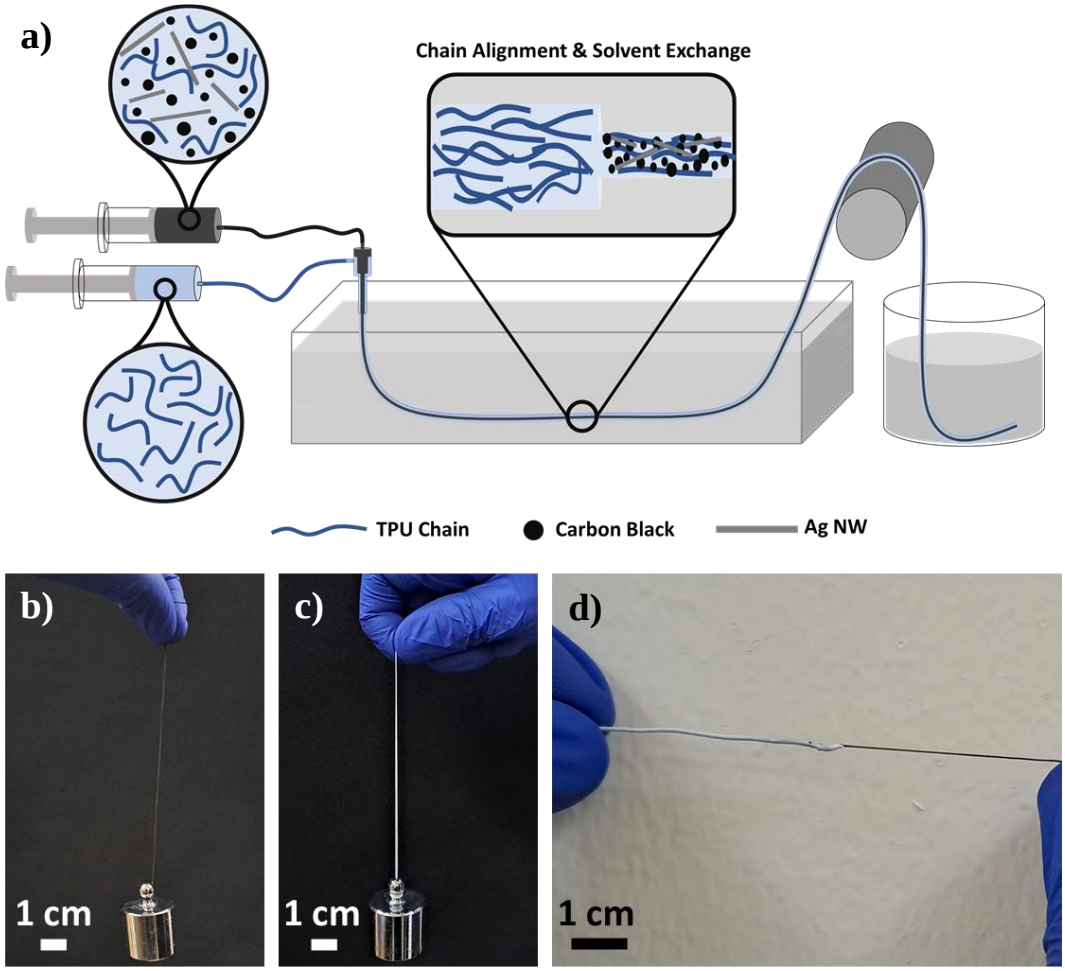

Figure 6.1 (a) Schematic illustration for the fabrication of wet spun core shell fibers. (b) Photos of wet spun core fiber carrying 500 g weight (c) Photo of wet spun core shell fiber carrying 500 g weight. (d) Photo of core shell fiber showing the junction of core and shell.

The conductivity of the electrode (core) fibers should be as high as possible, since the induced electrons flow through these fibers. On the other hand, these fibers also needed to be mechanically stable. Therefore, conductive filler (CB and Ag NWs) amounts must be optimized accordingly. The effect of CB amount on the conductivity was firstly investigated. The SEM images of CB added wet spun TPU fibers having CB amounts of 17, 23, 33, 38 and 50 wt.% are provided in Figure 6.2 (a)-(e), respectively. Columnar pore formation can be observed for the samples except for 50 wt.%. This was attributed to the fast solvent exchange during the coagulation process. Magnified SEM image of 50 wt.% CB/TPU composite fiber is provided in Figure 6.2 (f). It can be concluded that even with the addition of high amount of CB, the CBs are well dispersed in the structure. This is important for wet spinning, because agglomeration can significantly reduce fiber length by disrupting the continuity of the spinning process. The spinning solution including higher amount of CB were also investigated. Fiber formation was observed up to a CB content of 80 wt.%. However, the wet spun fibers were not mechanically stable above a CB addition of 50 wt.%. Therefore, 50 wt.% additive content were decided as our limit to produce the conductive cores. Ag NWs were preferred as one-dimensional additives to CB/TPU fibers to further increase conductivity and mechanical properties of the composite fiber. It has been previously shown in the literature that the addition of one-dimensional nanostructures increases the conductivity of composites by acting as a bridge between spherical particles [201,202]. Electrical conductivity upon stretching is also preserved by the addition of one-dimensional nanostructures. However, excess amount of Ag NW addition will increase the cost of the fiber. Therefore, 10 wt.% Ag NWs were added to CB/TPU wet spun fibers with different CB amounts. SEM images of CB/Ag NW/TPU wet spun fibers is provided in Figure 6.3 (a)-(e). Magnified image of the composites with 10 wt. % Ag NW and 40 wt.% CB is provided in Figure 6.3 (f). It can be observed from the figure that Ag NWs were well dispersed within the matrix.

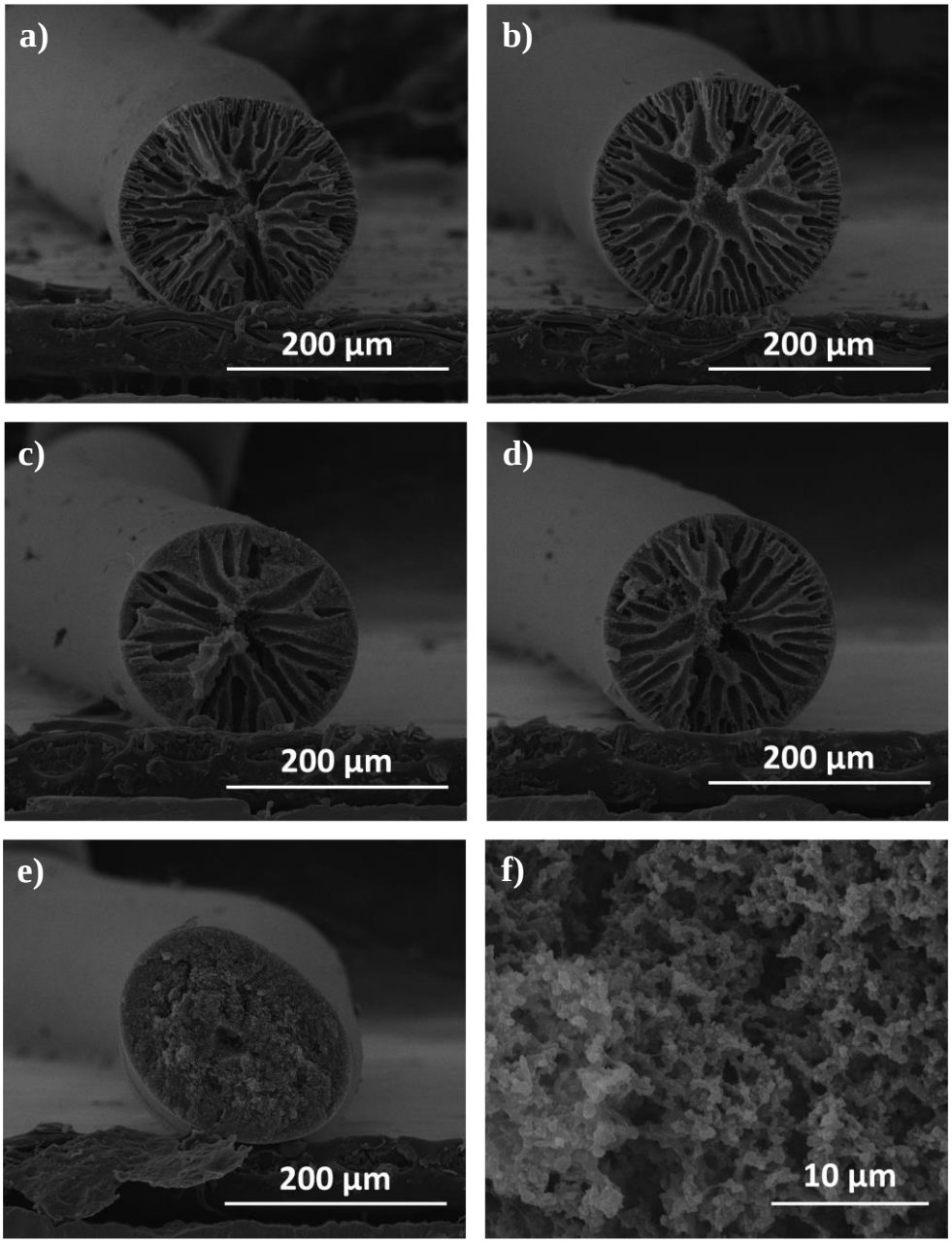

Figure 6.2: SEM images of CB/TPU wet spun fibers with CB contents of (a)17, (b) 23, (c) 33, (d) 38, and (e) 50 wt.%. Magnified image of 50 wt.% CB/TPU wet spun fibers.

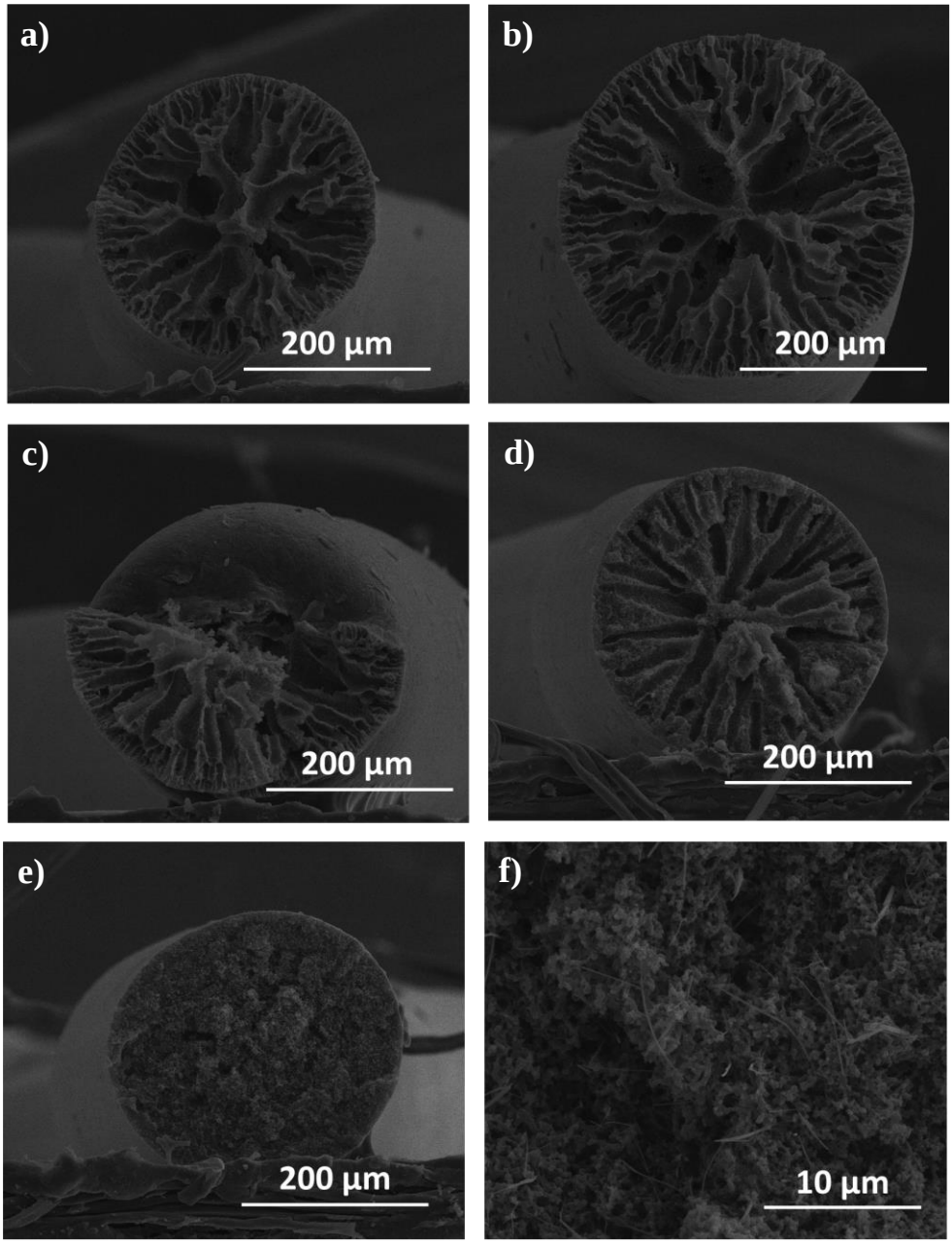

Figure 6.3: SEM images of Ag NW/CB/TPU fibers with 10 wt.% Ag NWs and CB contents of (a) 5, (b) 10, (c) 20, (d) 30, and (e) 40 wt. %. (f) Magnified image of the fiber with 10 wt.% Ag NW and 40 wt.% CB.

Electrical conductivities of the fabricated wet spun fibers are provided in Figure 6.4 (a) below. Electrical conductivity began to be measured for 17 wt.% CB/TPU fibers. Below this CB content, the conductivities were below the measurement limit of the

instrument. It may be a good assumption that percolation threshold is 17 wt.% CB for CB/TPU fibers. Electrical conductivity increased upon increasing CB content and reached 10 S/m at 50 wt.%. On the other hand, 10 wt.% Ag NW addition significantly reduced the percolation threshold and increased conductivity of the wet spun fibers. It should be noted that 10 wt.% Ag NWs were added to maximum of 40 wt.% CB in order not to exceed a total additive content of 50 wt.%. Electrical conductivity was measured as 30 S/m for the fiber with 10 wt.% Ag NWs and 40 wt.% CB. Representative tensile stress-strain curves of the conductive fibers are provided in Figure 6.4 (b). Fracture strain of the fibers was found to decrease with increasing CB content. However, it was possible to stretch 10 wt.% Ag NW/40 wt. % CB/TPU fibers up to 100% of their initial length, which is highly ideal for wearable applications. As the result of conductivity measurements and mechanical tests, core fiber composition was decided as 10 wt.% Ag NW, 40 wt. % CB and 50 wt. % TPU. This composition was used for the all the core-shell fiber based TENGs electrodes.

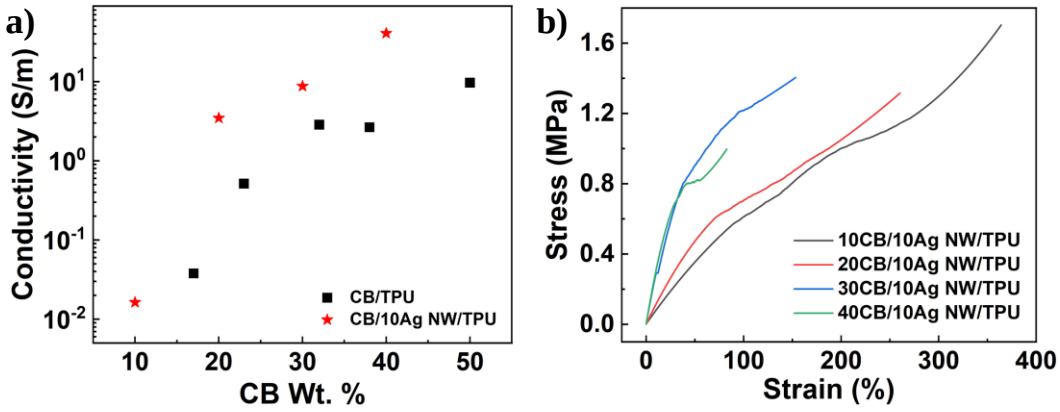

Figure 6.4 (a) Changes in conductivity of the wet spun CB/TPU and Ag NW/CB/TPU fibers with CB content. (b) Representative stress strain curves of the wet spun Ag NW/CB/TPU fibers.

Production parameters of the shell layer was optimized according to the injection rate and TPU mass within the spinning solution. The SEM images of the core shell fibers fabricated with the spinning solution having 0.05, 0.1 and 0.2 g/ml TPU concentrations are provided in Figure 6.5 (a), (b) and (c), respectively. The core

solution was the same for all the core shell fibers as mentioned above. From the Figure 6.5 it can be observed that decreasing the TPU concentration reduces the shell thickness as expected. As the TPU concentration in the shell solution decreased, the microstructure of the core layer became more porous. This was attributed to the excess solvent of the shell layer dissolving the TPU in the core layer during the spinning process.

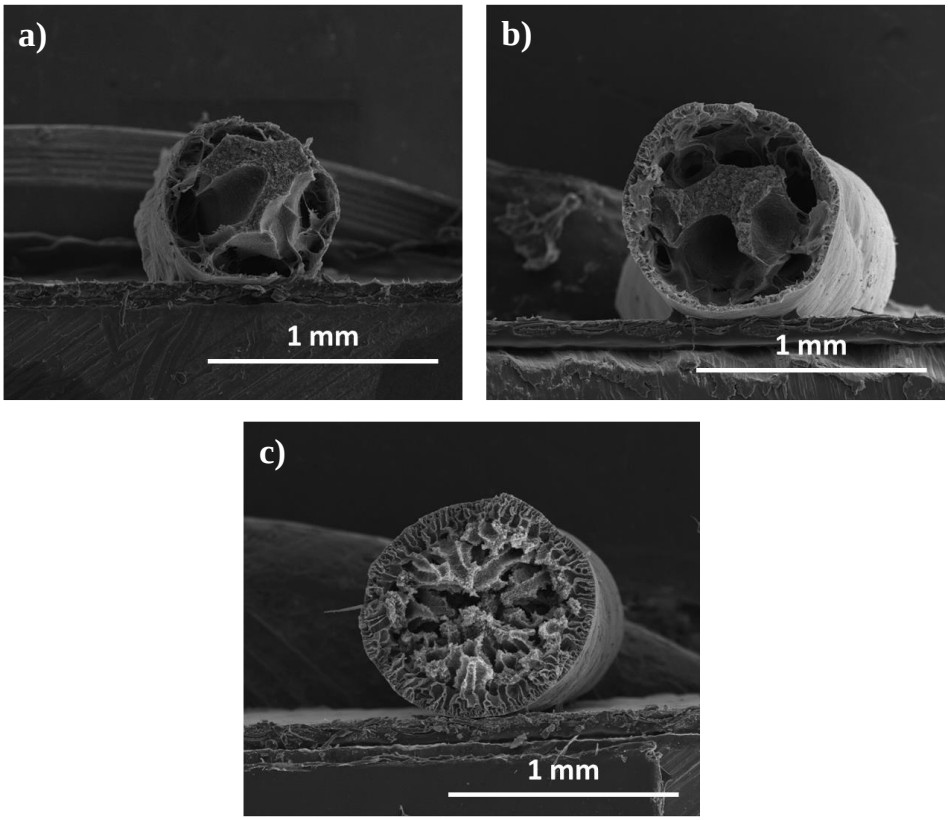

Figure 6.5 SEM images of wet spun core shell fibers fabricated with shell solution with TPU concentrations of (a) 0.05, (b) 0.1 and (c) 0.2 g/ml.

Output performance of these core-shell electrodes were investigated using PDMS/Al films as the counter electrode. *Voc*, *Isc* and *Qsc* results are provided in Figure 6.6 (a), (b) and (c), respectively. *Voc*, *Isc* and *Qsc* are 2.0 V, 42 nA and 1.6 nC, respectively for the core layers having a TPU concentration of 0.2 g/ml. All output parameters increased with the increase in TPU concentration. This contradicts the distance dependent model for TENGs reported in literature [122] . According to this

model, as the dielectric thickness increases, the overall electric field propagating within the dielectric layer decreases. Therefore, output voltage, charge and induced current decreases as thickness of the dielectric layer increases. On the other hand, in this model calculations are based on the same tribo-charge amount upon contact. The results would be different if the dielectric layers are charged with different amounts of tribo-charge upon contact. The relationship between tribo-charge amounts and dielectric layer thickness were reported by Wang et al. [203]. According to this study, tribo-charge increases with increasing dielectric thickness. The results obtained here are in agreement with Wang's work. Also, core and shell layers are loosely interconnected when the TPU concentration decreases as it can be observed in Figure 6.5. This might decrease the amount of induced charge in the core fiber.

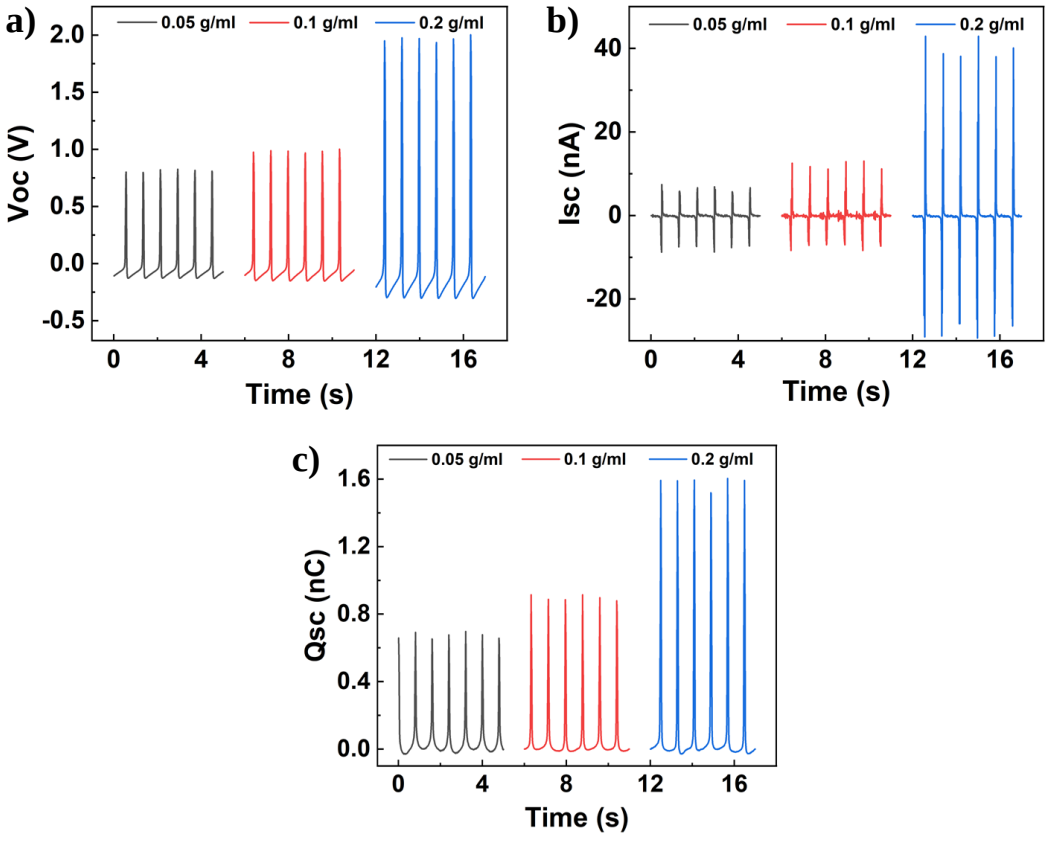

Figure 6.6 (a) *Voc*, (b) *Isc* and (c) *Qsc* of the wet spun core shell fibers having TPU concentration of 0.05, 0.1 and 0.2 g/ml within the shell solution.

The effect of the injection rate on the microstructure and output performance of the TENGs were also investigated. The SEM images of the core shell fibers fabricated with the shell layer injection rates of 4, 6, and 8 ml/h are provided in Figure 6.7 (a), (b) and (c), respectively. The TPU concentration of shell layer was 0.2 g/ml for all the injection rates. The ratio of shell and core thicknesses was found to increase with the injection rate. This was an expected result since more TPU was accumulated at the needle tip with the increased injection rate.

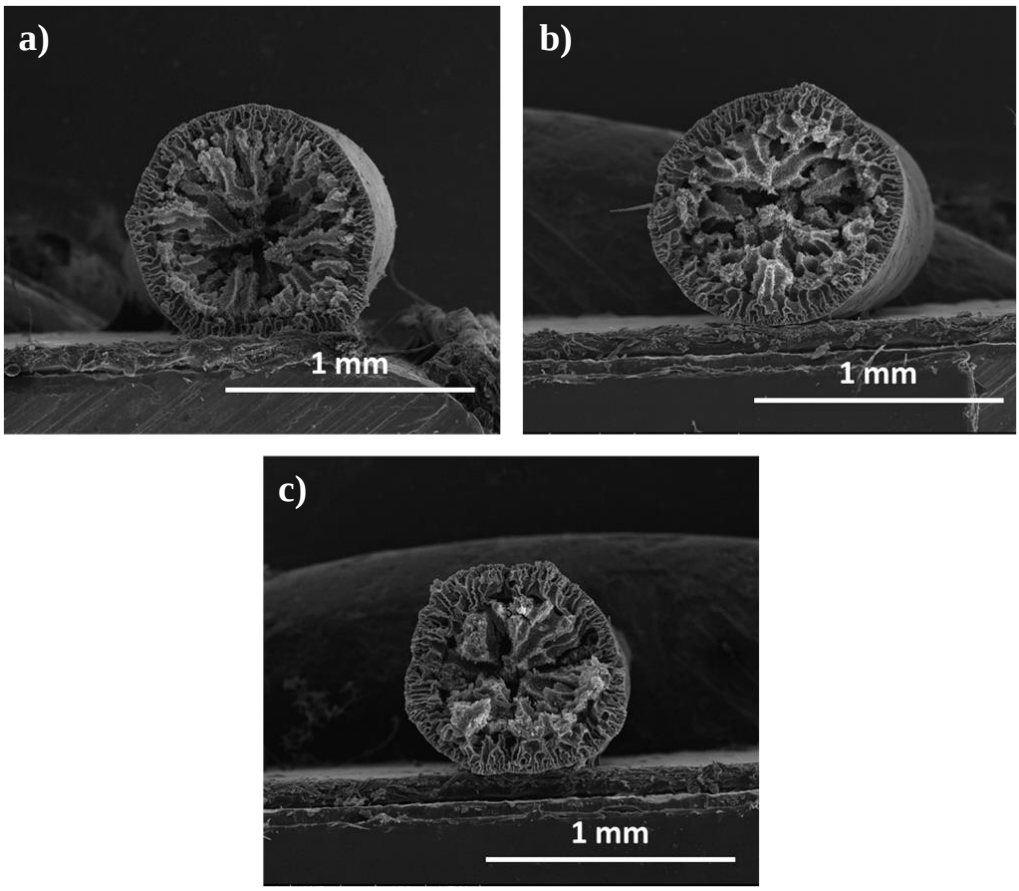

Figure 6.7 SEM images of wet spun core shell fibers fabricated with injection rates of (a) 4, (b) 6 and (c) 8 ml/h of the shell solution. (Injection rate of the core solution was 3 ml/h for all fibers.)

Output performance of the core shell fibers were recorded using PDMS/Al films as the counter electrode. It was found that *Voc*, *Isc* and *Qsc* do not change with increasing injection rate of the shell layer (Figure 6.8 (a), (b) and (c), respectively).

Optimum TPU concentration and injection rate were decided as 0.2g/ml for TPU concentration and 4 ml/h injection rate for the shell layer.

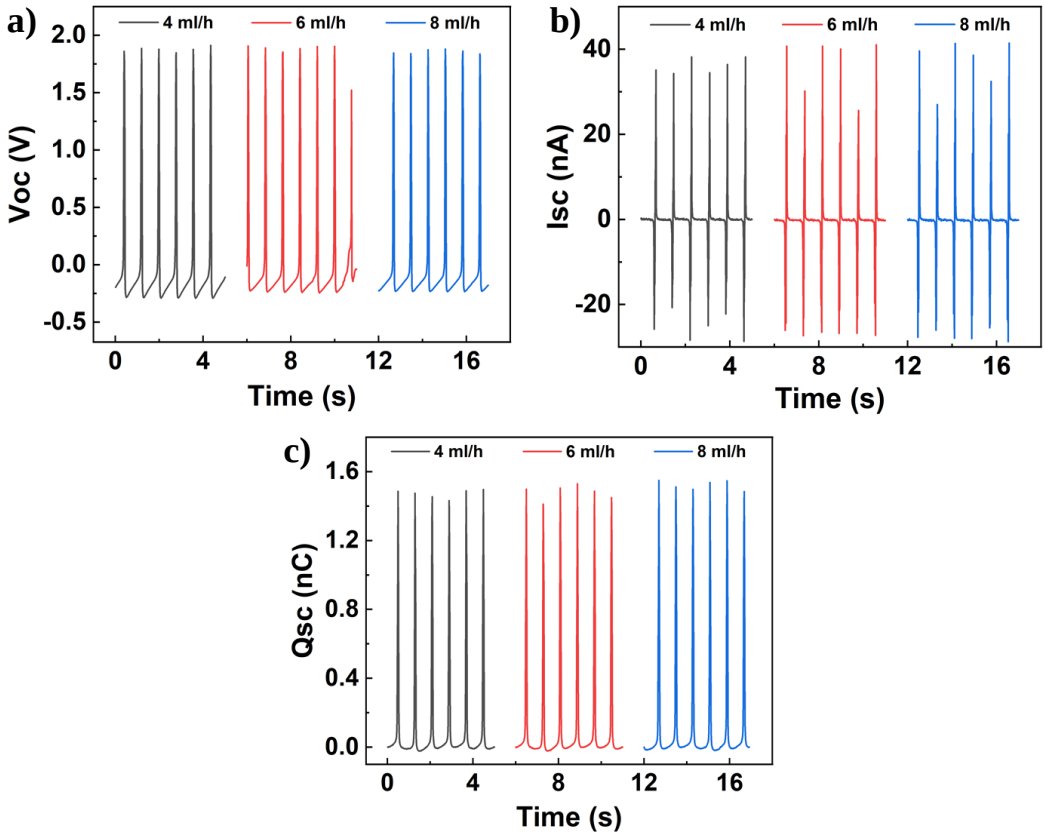

Figure 6.8 (a) *Voc*, (b) *Isc* and (c) *Qsc* of the wet spun core shell fibers fabricated with injection rates of 4, 6 and 8 ml/h of the shell solution. (Injection rate of the core solution was 3 ml/h for all fibers.)

Output voltages and currents were also measured with different load resistors connected to the circuit for the TENG systems consisting of core shell fiber electrodes and PDMS/Al foil electrodes (Figure 6.9 (a) and (b), respectively). When the electrodes are connected together with a small load resistance, the output voltage drops and the output current increases. This is because the induced charges are transferred from one electrode to the other easily. Upon connection of a high load resistance to electrodes, induced charge transfer was limited by the load. Therefore, output current decreased and output voltage increased. There was an optimum load

resistor maximizing the output power. In our case, the maximum power was obtained upon connection of a 300 Mohm resistor (Figure 6.9(c)).

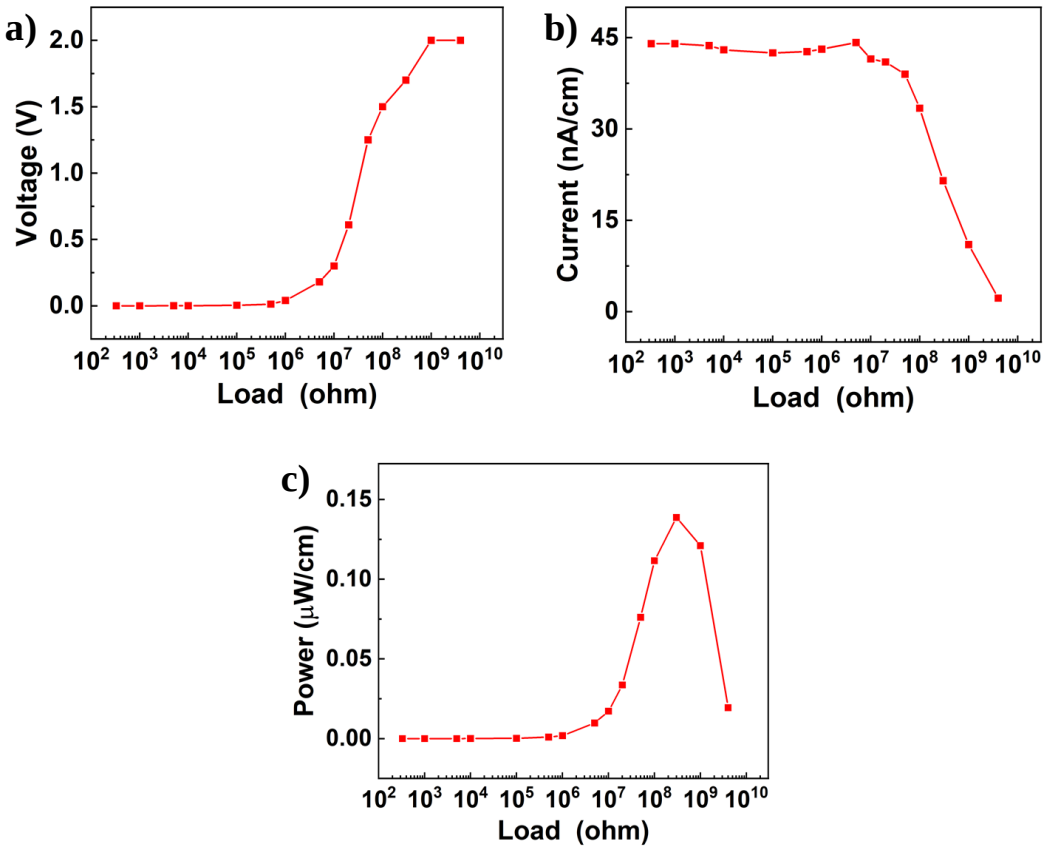

Figure 6.9 Effect of load resistance on the output (a) voltage, (b) current and (c) power of the core-shell fiber TENG electrodes.

The performance measurements reported above were conducted using a 1 cm long core-shell fibers to eliminate the size effect. However, it is possible to use longer fibers in real applications. It was already disused in Chapter 4 that, increasing electrode area increases the output performance of the TENGs. Therefore, the output performances of the long fibers were also measured, results of which are provided in Figure 6.10. The *Voc* values of 1, 2.5 and 5 cm long core-shell fibers were recorded as 2, 4.5 and 10 V, respectively (Figure 6.10 (a)). The *Isc* values of the 1, 2.5 and 5 cm long core-shell fibers were recorded as 43, 90 and 180 nA, respectively (Figure 6.10 (b)). The *Qsc* values of 1, 2.5 and 5 cm long core-shell fibers were recorded as

1.6, 3.8 and 6.5 nC, respectively (Figure 6.10 (c)). It can be concluded that the performance parameters increase almost linearly with increasing fiber length, as expected. Small deviations from the linearity can be explained with edge effects in the electric field.

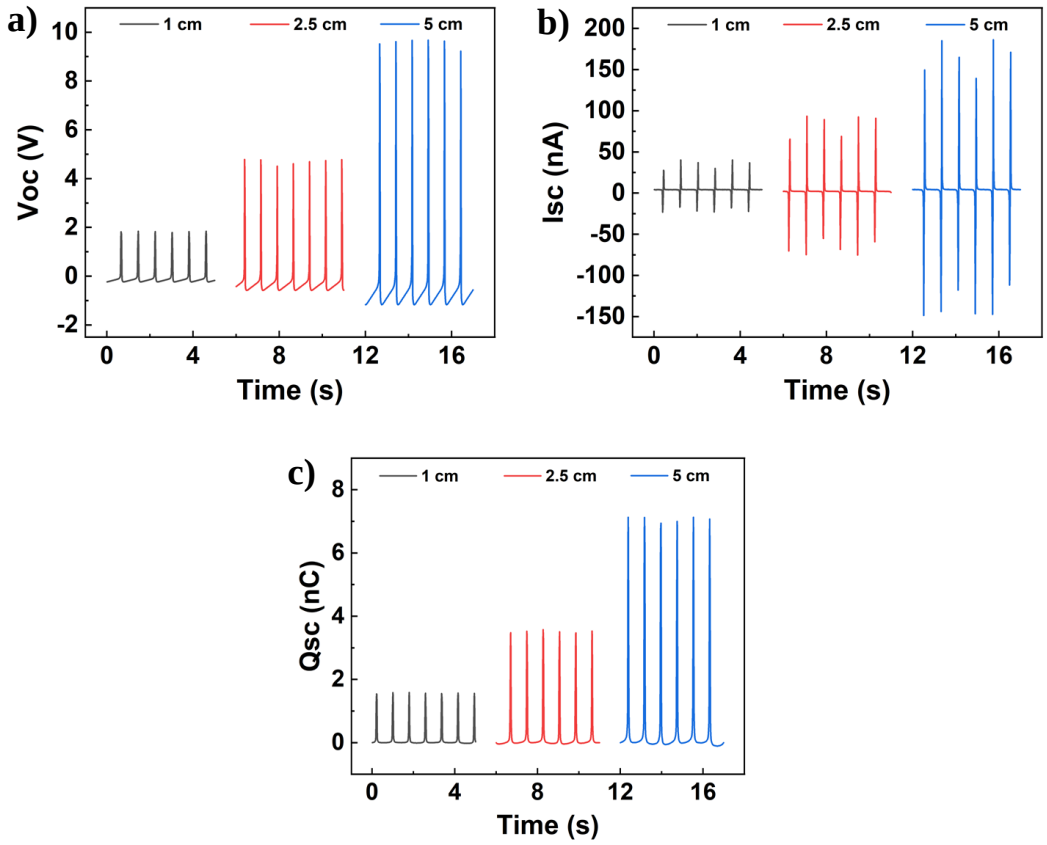

Figure 6.10 Effect of electrode length on the (a) Voc, (b) Isc and (c) Qsc of the core-shell fiber TENGs.

The effect of strain on the TENG performance of the core-shell fibers were also investigated provided in Figure 6.11 (a), (b) and (c) below. *Voc*, *Isc* and *Qsc* results were quite stable up to 50% strain. Then, all the performance metrics started to decrease upon further stretching. *Voc*, *Isc* and *Qsc* values decreased from 2 V, 40 nA and 1.6nC to 1 V, 20 nA and 0.7 nC at 100% strain. Then continue to drop to 0.7 V, 16 nA and 0.5 nC at 200% strain. The decrease in the output performance can be explained by the increase in the resistance of the core fiber. Upon stretching,

percolation network is damaged which may hinder the induced charge flow. Despite the performance degradation at high strain, the electrodes were quite stable up to 50% strain, which is sufficient for almost all wearable applications.

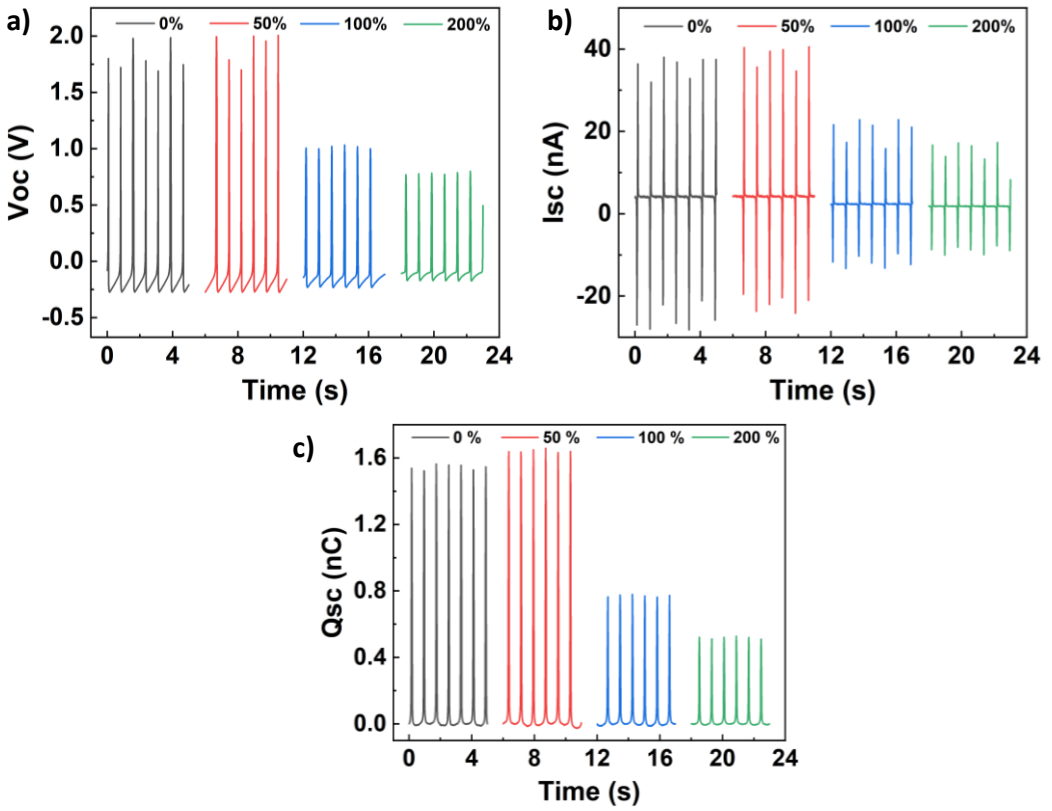

Figure 6.11 Effect of strain on the (a) Voc, (b) Isc and (c) Qsc of the core-shell fiber TENGs.

The resistance change of the core layer was also investigated under different cyclic tensile stresses as provided in Figure 6.12 (a). However, resistance change under 200% strain is not provided in the figure since the resistance of the core exceed the measurement limits of the instrument. Hysteresis behavior of resistance change when the core shell fibers were stretched and released with 100 % strain is provided in Figure 6.12 (b). These results demonstrate the potential to use the core-shell structure not only as TENGs but also as wearable strain sensors.

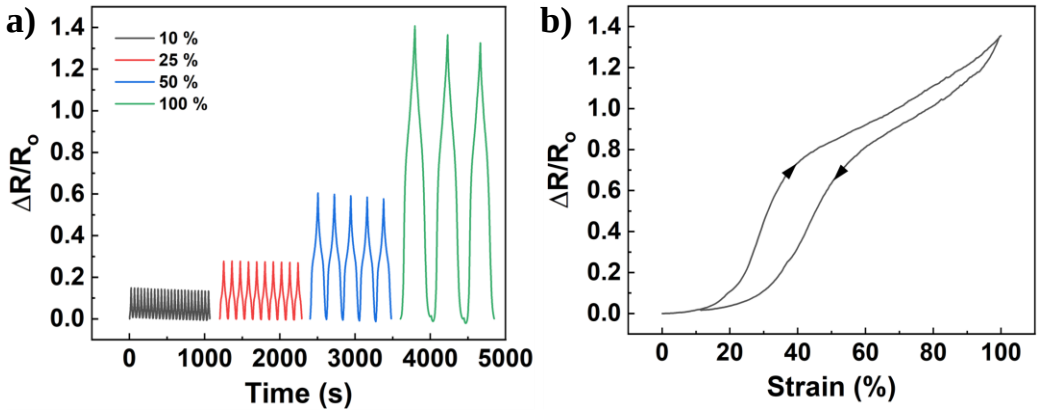

Figure 6.12 (a) Change in resistance of the core fiber under cyclic tensile force with different % strain. (b) Change in resistance of the core fiber with strain.

6.4 Conclusions

In summary, core-shell TENG electrodes were fabricated via co-wet spinning process for the first time in the literature. The core of the TENG electrodes were consisted of TPU matrix and CB and Ag NW additives. The core fibers were responsible to carry induced electrons as the results of contact electrification. The conductivity of the core fibers was recorded as 30 S/m when the composition was 40 wt. % CB-10 wt.% Ag NW and 50 wt.% TPU. The fabricated shell layer was bare TPU and acted as tribo-charged surface upon contact with PDMS/Al counter electrode. The effect of TPU concentration within the doping solution for the shell on the output performance of the TENGs were investigated. It was found that 0.2 g/ml TPU concentration showed the highest *Voc*, *Isc* and *Qsc* as 2 V, 40 nA and 16 nC, respectively. It was also found that injection rate of the shell layer is not effective on the TENGs performance. The maximum power output of the core shell fiber TENGs (PDMS/Al was the counter electrode) were recorded as 0.13 μW/cm when 300 Mohm load resistor was connected. A linear regression with the electrode length for the performance metrics (*Voc*, *Isc* and *Qsc*) was observed. The output performances of the core shell fibers were also quite stable up to 50 % strain. These

results indicated that, wet spun core-shell fibers carry great potential to be used in self-powered wearable sensors in real case applications.

CHAPTER 7

CONCLUSIONS AND FUTURE RECOMMENDATIONS

7.1 Conclusions

This thesis focuses on the utilization of Ag NWs in functional and/or electronic textiles. Polyol synthesized Ag NWs were used to modify conventional fabrics and fibers to impart different functions. The main motivation of this thesis was to find a combined solution for the common problems of the functional and/or electronic textiles. Initially, it was aimed to develop scalable, market ready and high-performance multifunctional textiles.

In the first part, the effects of Ag NW decoration onto conventional cotton fabrics on the antimicrobial performance was investigated. Simple dip and dry method was used for the decoration of Ag NWs. It was shown that a small amount of Ag NW addition provides superior antimicrobial performance against a Gram-positive coccus (*Staphylococcus aureus*), a Gram-negative bacillus (*Escherichia coli*), a Gram-positive and spore-forming bacillus (*Bacillus cereus*), and a yeast-like fungus (*Candida albicans*). It was also shown that, antimicrobial efficacy of the fabrics lasted 24 hours against *E. Coli*, *C. Albicans*, *B. Cereus* and 8 hours against *S. Aureus*. This result implied that Ag NWs can be promising candidates for the development of new generation antimicrobial textiles.

In the second part of the thesis, heating performance of the Ag NW modified fabrics was investigated. It was shown in this part that, Ag NW modified heatable fabrics operate under low input voltages. This enabled them to be used as wearable heaters for winter clothes. Moreover, the heatable fabrics showed superior mechanical stabilities. The heating performance of the fabrics remained unchanged after 5000 bending cycles. However, a significant performance drop was observed when the

fabrics were stored under ambient atmosphere for two months. Moreover, Ag NW modified heatable fabrics had limited stability. It was obvious that a proper coating should be developed to improve the environmental and washing stability of the fabrics.

In the third part of the thesis, TPU films were laminated onto Ag NW modified fabrics to increase the washing stability of the fabrics and to be used as wearable TENGs. It was observed that 90 μm thick TPU film lamination preserved resistance and the heating behavior of the fabrics up to 15 washing cycles. This structure also showed one of the highest power outputs (1.25 W/m^2) as fabric based TENGs in literature. Finally, a self-powered e-wristband was fabricated and used as a wearable human machine interface to control simple computer operations, demonstrating the true potential of the fabricated TENGs.

In the final part of the thesis, core-shell fiber based TENG electrodes were fabricated via co-wet spinning process for the first time in the literature. The conductive core and dielectric shell structures showed highly promising performance. *Voc*, *Isc* and *Qsc* of the electrodes were recorded as 2 V, 40 nA and 16 nC, respectively, when the electrode length was 1 cm. The maximum power output was recorded as 0.13 μW/cm when a 300 Mohm load resistor was connected. Overall, it is shown in this thesis that polyol synthesized Ag NWs carry great potential to be used various functional and electronic textiles applications.

7.2 Future Recommendations

The results and conclusions reported in the previous sections provide valuable insights into the use of Ag NWs for functional and/or electronic textiles. However, there are several issues that need to be addressed for Ag NWs to reach their full potential in functional and/or electronic textiles. Scalability has always been a concern for this thesis. Scaling up Ag NW synthesis is the first step in this sense. Scalable synthesis methods should be implemented. In addition to synthesis,

purification step of Ag NWs must also be scalable. Currently, as synthetized Ag NW/EG solutions are centrifuged with acetone and ethanol to remove the by-products, excess PVP and EG. However, these sequential centrifuge cycles are rate-limiting steps to prepare the coating dispersions. Although, there are bigger centrifuge systems that can handle solutions with much larger volumes, they are quite costly. Moreover, large amounts of as-synthesized Ag NW solution must be transferred to the centrifuge tubes, which is also slowing down the overall process. Therefore, alternative purification methods should be utilized at the end of large-scale synthesis of Ag NWs.

Modifications of commercially available fabrics with Ag NWs were conducted via dip and dry method in this thesis (Chapter 3). This method has several advantages over its alternatives. First, it does not require an expensive setup for small scale production. Moreover, preparing coating solution is relatively convenient since the coating solution can be directly used after purification of Ag NWs. However, dip and dry process has several shortcomings. Most importantly, patterning of the Ag NW coating is quite challenging via dip and drying. However, some electronic textile application may require patterned conductive paths. Moreover, successive dip and dry steps might be needed to obtain the desired conductivity, which slows down the overall coating process. The number of the dip and dry steps can be decreased with increasing the concentration of Ag NWs within the ethanolic solution. On the other hand, increasing Ag NW concentration without additional dispersants may cause inhomogeneous coatings. These problems can be solved by properly modifying the Ag NW surface. Screen printing of the Ag NWs onto fabrics stands out as an alternative and scalable solution method. It is necessary to develop an appropriate ink formulation for screen printing of Ag NWs onto fabrics. This will certainly enable deposition of patterned Ag NWs onto fabrics in a scalable and reproducible manner.

In this thesis, TPU and TPU matrix composites are used as the triboelectric layer without any post-treatment to fabricate wearable TENGs. Strategies to increase TENGs performance are mentioned in Chapter 4. Surface treatment of the

triboelectric layer is one of the important ways to increase TENGs performance. Therefore, chemical and physical post treatments can be applied to modify the fabricated TENGs electrodes. The effects of these post treatments should be investigated in detail using characterization techniques like kelvin probe force microscopy, Zeta potential analyzer and Fourier-transform infrared spectroscopy. The effect of molecular structures of TPU on contact electrification and TENG performance will be another interesting topic to investigate.

In this thesis, overcoating of Ag NW modified fabrics is proposed as an approach to increase the washing stability of functional fabrics (Chapter 5). According to the reported results, this approach has high potential. On the other hand, increasing interfacial interactions between Ag NWs and fabric surfaces are also worth investigating. Proper pretreatments of the fabrics might increase the interaction between Ag NWs and host fibers. For example, pretreatment with cellulose derivatives or chitosan has the potential to form more hydrogen bonds with PVP. (Lateral surfaces of the Ag NWs have a 10 nm thick PVP layer as a result of the synthesis method). Even if these hydrogen bonds alone would not increase the washing resistance to the targeted point, they will certainly allow a thinner overcoat layer. In the final part of the thesis (Chapter 6), core-shell wet spun fibers are utilized as the TENG electrodes. This study is very important as a proof of concept since it is the first report using co-wet spun fibers for the TENG electrodes. However, there are also plenty of steps to show the true potential of these electrodes. First of all, real case applications are needed to be demonstrated. Moreover, modifications of the shell layer can be investigated. For example, 2D nanostructures are often added to the composite shell matrix to increase the output of TENGs. In addition, the conductivity of the core layer can also be improved with the addition of conductive 2D nanostructures.

REFERENCES

1. Kittler, R., Kayser, M. & Stoneking, M. Erratum: Molecular evolution of pediculus humanus and the origin of clothing. *Current Biology* **14** 2309 (2004).

2. Toups, M. A., Kitchen, A., Light, J. E. & Reed, D. L. Origin of clothing lice indicates early clothing use by anatomically modern humans in Africa. *Mol Biol Evol* **28**, 29–32 (2011).

3. Wild John Peter. *The Cambridge History of Western Textiles*. (Cambridge University Press, 2003).

4. Thackeray, F. W., & Findling, J. E. (Eds.). *Events That Changed Great Britain Since 1689*. (Greenwood Press, 2002).

5. Britannica. rayon. *Encyclopedia Britannica*, (2016).

6. Rozek Thomas F., City Bay & Sommer Frederick J. Method for treating textile materials with a fluorocarbon resin. U.S. Patent No. 3,540,924 (1967).

7. Sun, G. *Antimicrobial Textiles*. (Woodhead Publishing, 2016).

8. Rachel Carson. *Silent Spring*. (Houghton Mifflin, 1962).

9. Carroll David W. Wearable Personal Computer System. U.S Patent No. 5,555,490 (1993).

10. Hughes-Riley, T., Dias, T. & Cork, C. A historical review of the development of electronic textiles. *Fibers* **6** (2018).

11. Hill I.G., Trotz S., Riddle G.H.N, Brookstein D.S. & Govindaraj M. Plural Layer Woven Electronic Textile, Article and Method. WO2003095729 (2006).

12. Jiang, S. Q., Kan, C. W., Yuen, C. W. M. & Wong, W. K. Electroless nickel plating of polyester fiber. *J Appl Polym Sci* **108**, 2630–2637 (2008).

13. Bourke Michael J. & Clothier Brain L. Inductively Heated Clothing. WO2008101203 (2008).

14. Kim, T. H. *et al.* Size-dependent cellular toxicity of silver nanoparticles. *J Biomed Mater Res A* **100 A**, 1033–1043 (2012).

15. Toybou, D., Celle, C., Aude-Garcia, C. & Rabilloud, T. A toxicology-informed, safer by design approach for the fabrication of transparent electrodes based on silver nanowires. *Environ Sci Nano* **6**, 684–694 (2019).

16. Doganay, D., Coskun, S., Genlik, S. P. & Unalan, H. E. Silver nanowire decorated heatable textiles. *Nanotechnology* **27**, (2016).

17. Uzun, S. *et al.* Knittable and Washable Multifunctional MXene-Coated Cellulose Yarns. *Adv Funct Mater* **29**, (2019).

18. Yuksel, R. & Unalan, H. E. Textile supercapacitors-based on MnO2/SWNT/conducting polymer ternary composites. *Int J Energy Res* **39**, 2042–2052 (2015).

19. Sahito, I. A., Sun, K. C., Arbab, A. A., Qadir, M. B. & Jeong, S. H. Graphene coated cotton fabric as textile structured counter electrode for DSSC. *Electrochim Acta* **173**, 164–171 (2015).

20. Chae, W. H., Sannicolo, T. & Grossman, J. C. Double-Sided Graphene Oxide Encapsulated Silver Nanowire Transparent Electrode with Improved Chemical and Electrical Stability. *ACS Appl Mater Interfaces* **12**, 17909–17920 (2020).

21. Bang, J. *et al.* Advances in protective layer-coating on metal nanowires with enhanced stability and their applications. *Appl Mater Today* **22** (2021).

22. Ren, W. & Cheng, H. M. The global growth of graphene. *Nature Nanotechnology* **9** 726–730 (2014).

23. Novoselov, K. S. *et al.* A roadmap for graphene. *Nature* **490** 192–200 (2012).

24. Hsu, P.-C. *et al.* Personal Thermal Management by Metallic Nanowire-Coated Textile. *Nano Lett* **15**, 365–371 (2015).

25. Murali, G. *et al.* A Review on MXene Synthesis, Stability, and Photocatalytic Applications. *ACS Nano* **16** 13370–13429 (2022).

26. Li, B., Ye, S., Stewart, I. E., Alvarez, S. & Wiley, B. J. Synthesis and Purification of Silver Nanowires to Make Conducting Films with a Transmittance of 99%. *Nano Lett* **15**, 6722–6726 (2015).

27. Fan, F. R., Tian, Z. Q. & Lin Wang, Z. Flexible triboelectric generator. *Nano Energy* **1**, 328–334 (2012).

28. Hollingsworth, T. D., Ferguson, N. M. & Anderson, R. M. Frequent Travelers and Rate of Spread of Epidemics. *Emerg Infect Dis* **13**, 1288–1294 (2007).

29. Soares, T. P. *et al.* Cytotoxicity and antibacterial efficacy of silver deposited onto titanium plates by low-energy ion implantation. *J Mater Res* **33**, 2545–2553 (2018).

30. Prasad S, S. *et al.* In vitro bioactivity and antibacterial properties of bismuth oxide modified bioactive glasses. *J Mater Res* **33**, 178–190 (2018).

31. Barbut, F. *et al.* Comparison of the antibacterial efficacy and acceptability of an alcohol-based hand rinse with two alcohol-based hand gels during routine patient care. *Journal of Hospital Infection* **66**, 167–173 (2007).

32. Li, Y., Leung, P., Yao, L., Song, Q. W. & Newton, E. Antimicrobial effect of surgical masks coated with nanoparticles. *Journal of Hospital Infection* **62**, 58–63 (2006).

33. Yuan Gao & Cranston, R. Recent Advances in Antimicrobial Treatments of Textiles. *Text Res J* **78**, 60–72 (2008).

34. Zanoaga, M. & Tanasa, F. Antimicrobial Reagents as Functional Finishing for Textiles Intended for Biomedical Applications. I. Synthetic Organic Compounds. *Chem J Mold* **9**, 14–32 (2014).

35. Hong, X., Wen, J., Xiong, X. & Hu, Y. Silver nanowire-carbon fiber cloth nanocomposites synthesized by UV curing adhesive for electrochemical point-of-use water disinfection. *Chemosphere* **154**, 537–545 (2016).

36. Antimicrobial Medical Textiles Market Analysis by Finishing Agent (Quaternary Ammonium, Triclosan, Metallic Salts), by Application (Implantable Goods, Non-implantable Goods, Healthcare & Hygiene Products) and Segment Forecasts to 2024. (2016). Available at: https://www.grandviewresearch.com/industry-analysis/antimicrobial-medical-textiles-market (accessed November 25, 2017).

37. Alexander, J. W. History of the Medical Use of Silver. *Surg Infect* **10**, 289–292 (2009).

38. Dubas, S. T., Kumlangdudsana, P. & Potiyaraj, P. Layer-by-layer deposition of antimicrobial silver nanoparticles on textile fibers. *Colloids Surf A Physicochem Eng Asp* **289**, 105–109 (2006).

39. Lee, H. J., Yeo, S. Y. & Jeomg S.H. Antibacterial effect of nanosized silver colloidal solution on textile fabrics. *J Mater Sci* **38**, 2199–2204 (2003).

40. Yeo, S. Y. & Jeong, S. H. Preparation and characterization of polypropylene/silver nanocomposite fibers. *Polym Int* **52**, 1053–1057 (2003).

41. Balantrapu, K. & Goia, D. v. Silver nanoparticles for printable electronics and biological applications. *J Mater Res* **24**, 2828–2836 (2009).

42. Feng, Q. L. *et al.* A mechanistic study of the antibacterial effect of silver ions on Escherichia coli and Staphylococcus aureus. *J Biomed Mater Res* **52**, 662–668 (2000).

43. Morones, J. R. *et al.* The bactericidal effect of silver nanoparticles. *Nanotechnology* **16**, 2346–2353 (2005).

44. Webster, T. J., Gorth, D. & Rand, D. Silver nanoparticle toxicity in Drosophila: size does matter. *Int J Nanomedicine* 343 (2011).

45. Charehsaz, M. *et al.* Genotoxicity study of high aspect ratio silver nanowires. *Toxicol Environ Chem* **99**, 837–847 (2017).

46. Lei, J. *et al.* High-Strength Konjac Glucomannan/Silver Nanowires Composite Films with Antibacterial Properties. *Materials* **10**, 524 (2017).

47. Zhao, C. *et al.* Large-area chemical vapor deposition-grown monolayer graphene-wrapped silver nanowires for broad-spectrum and robust antimicrobial coating. *Nano Res* **9**, 963–973 (2016).

48. Jiang, S. & Teng, C. P. Fabrication of silver nanowires-loaded polydimethylsiloxane film with antimicrobial activities and cell compatibility. *Mater Sci Eng. C* **70**, 1011–1017 (2017).

49. Satoungar, M. T., Fattahi, S., Azizi, H. & Khajeh Mehrizi, M. Electrospinning of Polylactic Acid/silver nanowire biocomposites: Antibacterial and electrical resistivity studies. *Polym Compos* **39**, E65–E72 (2018).

50. Cui, H.-W., Suganuma, K. & Uchida, H. Highly stretchable, electrically conductive textiles fabricated from silver nanowires and cupro fabrics using a simple dipping-drying method. *Nano Res* **8**, 1604–1614 (2015).

51. Coskun, S., Aksoy, B. & Unalan, H. E. Polyol Synthesis of Silver Nanowires: An Extensive Parametric Study. *Cryst Growth Des* **11**, 4963–4969 (2011).

52. Hebeish, A. *et al.* Highly effective antibacterial textiles containing green synthesized silver nanoparticles. *Carbohydr Polym* **86**, 936–940 (2011).

53. Messaoud, M. *et al.* Photocatalytic generation of silver nanoparticles and application to the antibacterial functionalization of textile fabrics. *J Photochem Photobiol A Chem* **215**, 147–156 (2010).

54. Xiu, Z., Zhang, Q., Puppala, H. L., Colvin, V. L. & Alvarez, P. J. J. Negligible Particle-Specific Antibacterial Activity of Silver Nanoparticles. *Nano Lett* **12**, 4271–4275 (2012).

55. Amro, N. A. *et al.* High-Resolution Atomic Force Microscopy Studies of the *Escherichia coli* Outer Membrane: Structural Basis for Permeability. *Langmuir* **16**, 2789–2796 (2000).

56. Rizzello, L. & Pompa, P. P. Nanosilver-based antibacterial drugs and devices: Mechanisms, methodological drawbacks, and guidelines. *Chem. Soc. Rev.* **43**, 1501–1518 (2014).

57. Stoppa, M. & Chiolerio, A. Wearable Electronics and Smart Textiles: A Critical Review. *Sensors* **14**, 11957–11992 (2014).

58. Coyle, S. *et al.* Smart Nanotextiles: A Review of Materials and Applications. *MRS Bull* **32**, 434–442 (2007).

59. Ates, E. S. & Unalan, H. E. Zinc oxide nanowire enhanced multifunctional coatings for cotton fabrics. *Thin Solid Films* **520**, 4658–4661 (2012).

60. Saini, P. & Choudhary, V. Conducting polymer coated textile based multilayered shields for suppression of microwave radiations in 8.2-12.4 GHz range. *J Appl Polym Sci* **129**, 2832–2839 (2013).

61. Yuehui Ouyang & Chappell, W. J. High Frequency Properties of Electro-Textiles for Wearable Antenna Applications. *IEEE Trans Antennas Propag* **56**, 381–389 (2008).

62. Hu, L. *et al.* Stretchable, Porous, and Conductive Energy Textiles. *Nano Lett* **10**, 708–714 (2010).

63. Pasta, M., la Mantia, F., Hu, L., Deshazer, H. D. & Cui, Y. Aqueous supercapacitors on conductive cotton. *Nano Res* **3**, 452–458 (2010).

64. Åkerfeldt, M., Strååt, M. & Walkenström, P. Electrically conductive textile coating with a PEDOT-PSS dispersion and a polyurethane binder. *Tex Res J* **83**, 618–627 (2013).

65. Bashir, T., Skrifvars, M. & Persson, N.-K. Production of highly conductive textile viscose yarns by chemical vapor deposition technique: a route to continuous process. *Polym Adv Technol* **22**, 2214–2221 (2011).

66. Anderson, E. B. *et al.* Synthesis and dry-spinning fibers of sulfinyl-based poly(p-phenylene vinylene) (ppv) for semi-conductive textile applications. *J Mater Chem* **22**, 11851 (2012).

67. Yang, K., Torah, R., Wei, Y., Beeby, S. & Tudor, J. Waterproof and durable screen printed silver conductive tracks on textiles. *Tex Res J* **83**, 2023–2031 (2013).

68. Maity, S., Chatterjee, A., Singh, B. & Pal Singh, A. Polypyrrole based electro-conductive textiles for heat generation. *J Textile Inst* **105**, 887–893 (2014).

69. Lim, Z. H., Chia, Z. X., Kevin, M., Wong, A. S. W. & Ho, G. W. A facile approach towards ZnO nanorods conductive textile for room temperature multifunctional sensors. *Sens Actuators B Chem* **151**, 121–126 (2010).

70. Perumalraj, R. *et al.* Silver-filled electrically conductive epoxy and silver nitrate-plated textile composite materials for EMC. *J Reinf Plast Compos* **30**, 203–215 (2011).

71. Nilsson, E., Oxfall, H., Wandelt, W., Rychwalski, R. & Hagström, B. Melt spinning of conductive textile fibers with hybridized graphite nanoplatelets and carbon black filler. *J Appl Polym Sci* **130**, 2579–2587 (2013).

72. Ilanchezhiyan, P. *et al.* Highly efficient CNT functionalized cotton fabrics for flexible/wearable heating applications. *RSC Adv* **5**, 10697–10702 (2015).

73. Rahman, M. J. & Mieno, T. Conductive Cotton Textile from Safely Functionalized Carbon Nanotubes. *J Nanomater* **2015**, 1–10 (2015).

74. Buldum, A. & Lu, J. P. Contact resistance between carbon nanotubes. *Phys Rev B* **63**, 161403 (2001).

75. Han, J.-W. & Meyyappan, M. Copper oxide resistive switching memory for e-textile. *AIP Adv* **1**, 032162 (2011).

76. Han, J.-W., Kim, B., Li, J. & Meyyappan, M. A carbon nanotube-based ammonia sensor on cotton textile. *Appl Phys Lett* **102**, 193104 (2013).

77. Coskun, S., Selen Ates, E. & Emrah Unalan, H. Optimization of silver nanowire networks for polymer light emitting diode electrodes. *Nanotechnology* **24**, 125202 (2013).

78. Leem, D.-S. *et al.* Efficient Organic Solar Cells with Solution-Processed Silver Nanowire Electrodes. *Adv Mater* **23**, 4371–4375 (2011).

79. Afal, A., Coskun, S. & Emrah Unalan, H. All solution processed, nanowire enhanced ultraviolet photodetectors. *Appl Phys Lett* **102**, 043503 (2013).

80. Celle, C. *et al.* Highly flexible transparent film heaters based on random networks of silver nanowires. *Nano Res* **5**, 427–433 (2012).

81. Hong, S. *et al.* Highly Stretchable and Transparent Metal Nanowire Heater for Wearable Electronics Applications. *Adv Mater* **27**, 4744–4751 (2015).

82. Kim, A.-Y. *et al.* Oxidation-resistant hybrid metal oxides/metal nanodots/silver nanowires for high performance flexible transparent heaters. *Nanoscale* **8**, 3307–3313 (2016).

83. Nateghi, M. R. & Shateri-Khalilabad, M. Silver nanowire-functionalized cotton fabric. *Carbohydr Polym* **117**, 160–168 (2015).

84. Atwa, Y., Maheshwari, N. & Goldthorpe, I. A. Silver nanowire coated threads for electrically conductive textiles. *J Mater Chem C Mater* **3**, 3908–3912 (2015).

85. Maize, K. *et al.* Super-Joule heating in graphene and silver nanowire network. *Appl Phys Lett* **106**, 143104 (2015).

86. Marzbanrad, E., Rivers, G., Peng, P., Zhao, B. & Zhou, N. Y. How morphology and surface crystal texture affect thermal stability of a metallic nanoparticle: the case of silver nanobelts and pentagonal silver nanowires. *Phys Chem Chem Phys* **17**, 315–324 (2015).

87. Loraine, G. A. Oxidation of Polyvinylpyrrolidone and an Ethoxylate Surfactant in Phase-Inversion Wastewater. *Wat Environ Res* **80**, 373–379 (2008).

88. Lowell, J. & Rose-Innes, A. C. Contact electrification. *Adv Phys* **29**, 947–1023 (1980).

89. Xu, R., Ye, S. & Xu, K. Theory of contact electrification. *Br J Appl Phys* **4** (1953).

90. Wu, J. *et al.* Insights into the mechanism of metal-polymer contact electrification for triboelectric nanogenerator via first-principles investigations. *Nano Energy* **48**, 607–616 (2018).

91. Wu, J., Wang, X., Li, H., Wang, F. & Hu, Y. First-principles investigations on the contact electrification mechanism between metal and amorphous polymers for triboelectric nanogenerators. *Nano Energy* **63**, (2019).

92. Terris, B. D., Stern, J. E., Rugar, ' D & Mamin, H. J. Contact Electrification Using Force Microscopy. *Phys Rev Lett* **63,** 2669, (1989).

93. McCarty, L. S. & Whitesides, G. M. Electrostatic charging due to separation of ions at interfaces: Contact electrification of ionic electrets. *Angew Chem Inte* **47** 2188–2207 (2008).

94. Liu, C. & Bard, A. J. Electrostatic electrochemistry at insulators. *Nat Mater* **7**, 505–509 (2008).

95. Liu, C. Y. & Bard, A. J. Chemical redox reactions induced by cryptoelectrons on a PMMA surface. *J Am Chem Soc* **131**, 6397–6401 (2009).

96. Liu, C. yang & Bard, A. J. Electrostatic electrochemistry: Nylon and polyethylene systems. *Chem Phys Lett* **485**, 231–234 (2010).

97. Baytekin, B., Baytekin, H. T. & Grzybowski, B. A. What really drives chemical reactions on contact charged surfaces? *J Am Chem Soc* **134**, 7223–7226 (2012).

98. Wang, Z. L. & Wang, A. C. On the origin of contact-electrification. *Mater Today* **30** 34–51 (2019).

99. Lin, S. *et al.* Electron Transfer in Nanoscale Contact Electrification: Effect of Temperature in the Metal–Dielectric Case. *Adv Mater* **31**, (2019).

100. Lin, S., Xu, L., Zhu, L., Chen, X. & Wang, Z. L. Electron Transfer in Nanoscale Contact Electrification: Photon Excitation Effect. *Adv Mater* **31**, (2019).

101. Luo, J. & Wang, Z. L. Recent progress of triboelectric nanogenerators: From fundamental theory to practical applications. *EcoMat* **2**, (2020).

102. Mendley J.A. Frictional Electrification of Polar Polymers. *Nature* **171**, 1077 (1953).

103. Diaz, A. F. Contact Electrification of Materials: The Chemistry of Ions on Polymer Surfaces. *J Adhes* **67**, 111–122 (1998).

104. Diaz A.F, W. D. , D. D. Contact Electrification: Ion Transfer to Metals and Polymers. *Chem Mater* **3**, 997 (1991).

105. Wiles, J. A., Fialkowski, M., Radowski, M. R., Whitesides, G. M. & Grzybowski, B. A. Effects of surface modification and moisture on the rates

of charge transfer between metals and organic materials. *J Phys Chem B* **108**, 20296–20302 (2004).

106. Lacks, D. J. & Shinbrot, T. Long-standing and unresolved issues in triboelectric charging. *Nature Reviews Chemistry* **3** 465–476 (2019).

107. Pence, S., Novotny, V. J. & Diaz, A. F. Effect of surface moisture on contact charge of polymers containing ions. *Langmuir* **10** (1994).

108. Homewood, K. P. Do 'dirty' surfaces matter in contact electrification experiments. J Electrostat **10** (1981).

109. Baytekin, H. T., Baytekin, B., Soh, S. & Grzybowski, B. A. Is Water Necessary for Contact Electrification? *Angew Chem* **123**, 6898–6902 (2011).

110. John Henniker. Triboelectricity in Polymers. *Nature* **196**, 474 (1962).

111. Salaneck, W. R., Paton, A. & Clark, D. T. Double mass transfer during polymer-polymer contacts. *J Appl Phys* **47**, 144–147 (1976).

112. Sakaguchi, M., Shigetaka, S. & Hisatsugu Kashiwabara. Mechanoions produced by mechanical fracture of solid polymer. 6. A generation mechanism of triboelectricity due to the reaction of mechanoradicals with mechanoanions on the Friction Surface. *Macromolecules*, **23,** 5038-5040, (1990).

113. Baytekin, H. T. *et al.* The mosaic of surface charge in contact electrification *Science* **333,** 308-312, (2011).

114. Yun, C. *et al.* Can Static Electricity on a Conductor Drive a Redox Reaction: Contact Electrification of Au by Polydimethylsiloxane, Charge Inversion in Water, and Redox Reaction. *J Am Chem Soc* **140**, 14687–14695 (2018).

115. Baytekin, H. T., Baytekin, B., Incorvati, J. T. & Grzybowski, B. A. Material transfer and polarity reversal in contact charging. *Angew Chem Int* **51**, 4843–4847 (2012).

116. Pandey, R. K., Kakehashi, H., Nakanishi, H. & Soh, S. Correlating Material Transfer and Charge Transfer in Contact Electrification. *J Phys Chem C* **122**, 16154–16160 (2018).

117. Shao, J., Willatzen, M. & Wang, Z. L. Theoretical modeling of triboelectric nanogenerators (TENGs). *J Appl Phys* **128**, (2020).

118. Niu, S. & Wang, Z. L. Theoretical systems of triboelectric nanogenerators. *Nano Energy* **14**, 161–192 (2014).

119. Niu, S. *et al.* Theoretical study of contact-mode triboelectric nanogenerators as an effective power source. *Energy Environ Sci* **6**, 3576–3583 (2013).

120. Dharmasena, R. D. I. G., Deane, J. H. B. & Silva, S. R. P. Nature of Power Generation and Output Optimization Criteria for Triboelectric Nanogenerators. *Adv Energy Mater* **8**, (2018).

121. Wang, Z. L. On the first principle theory of nanogenerators from Maxwell's equations. *Nano Energy* **68**, (2020).

122. Dharmasena, R. D. I. G. *et al.* Triboelectric nanogenerators: Providing a fundamental framework. *Energy Environ Sci* **10**, 1801–1811 (2017).

123. Dharmasena, R. D. I. G., Jayawardena, K. D. G. I., Mills, C. A., Dorey, R. A. & Silva, S. R. P. A unified theoretical model for Triboelectric Nanogenerators. *Nano Energy* **48**, 391–400 (2018).

124. Shao, J., Willatzen, M., Shi, Y. & Wang, Z. L. 3D mathematical model of contact-separation and single-electrode mode triboelectric nanogenerators. *Nano Energy* **60**, 630–640 (2019).

125. Shao, J. J., Jiang, T. & Wang, Z. L. Theoretical foundations of triboelectric nanogenerators (TENGs). *Sci China Technol Sci* **63** 1087–1109 (2020).

126. Doganay, D. *et al.* Fabric based wearable triboelectric nanogenerators for human machine interface. *Nano Energy* **89**, (2021).

127. Xia, K., Wu, D., Fu, J. & Xu, Z. A pulse controllable voltage source based on triboelectric nanogenerator. *Nano Energy* **77**, (2020).

128. Salauddin, M. *et al.* A Novel MXene/Ecoflex Nanocomposite-Coated Fabric as a Highly Negative and Stable Friction Layer for High-Output Triboelectric Nanogenerators. *Adv Energy Mater* **11**, (2021).

129. Xiao, T. X. *et al.* Silicone-Based Triboelectric Nanogenerator for Water Wave Energy Harvesting. *ACS Appl Mater Interfaces* **10**, 3616–3623 (2018).

130. Harper, W. R. *Contact and Frictional Electrification*. (Oxford, 1967).

131. Zou, H. *et al.* Quantifying the triboelectric series. *Nat Commun* **10**, (2019).

132. Zou, H. *et al.* Quantifying and understanding the triboelectric series of inorganic non-metallic materials. *Nat Commun* **11**, (2020).

133. Zou, Y., Xu, J., Chen, K. & Chen, J. Advances in Nanostructures for High-Performance Triboelectric Nanogenerators. *Adv Mater Technol* **6** (2021).

134. Sriphan, S. & Vittayakorn, N. Facile roughness fabrications and their roughness effects on electrical outputs of the triboelectric nanogenerator. *Smart Mater Struct* **27**, (2018).

135. Wang, S. *et al.* Maximum surface charge density for triboelectric nanogenerators achieved by ionized-air injection: Methodology and theoretical understanding. *Adv Mater* **26**, 6720–6728 (2014).

136. Yang, J. R., Lee, C. J. & Chang, C. Y. An electrostatically self-assembled fluorinated molecule as a surface modification layer for a high-performance and stable triboelectric nanogenerator. *J Mater Chem A Mater* **9**, 4230–4239 (2021).

137. Li, H. Y. *et al.* Significant Enhancement of Triboelectric Charge Density by Fluorinated Surface Modification in Nanoscale for Converting Mechanical Energy. *Adv Funct Mater* **25**, 5691–5697 (2015).

138. Majumder, S., Mondal, T. & Deen, M. J. Wearable sensors for remote health monitoring. *Sensors (Switzerland)* **17**, (2017).

139. Liu, M. *et al.* Large-Area All-Textile Pressure Sensors for Monitoring Human Motion and Physiological Signals. *Adv Mater* **29**, 1–9 (2017).

140. Lin, Z. *et al.* Triboelectric Nanogenerator Enabled Body Sensor Network for Self-Powered Human Heart-Rate Monitoring. *ACS Nano* **11**, 8830–8837 (2017).

141. Kim, K. K. *et al.* A deep-learned skin sensor decoding the epicentral human motions. *Nat Commun* **11**, 1–8 (2020).

142. Kim, J. *et al.* Ultrathin Quantum Dot Display Integrated with Wearable Electronics. *Adv Mater* **29**, 1–6 (2017).

143. Cicek, M. O., Doganay, D., Durukan, M. B., Gorur, M. C. & Unalan, H. E. Seamless Monolithic Design for Foam Based, Flexible, Parallel Plate Capacitive Sensors. *Adv Mater Technol* **2001168**, 1–11 (2021).

144. Fan, F. R., Tian, Z. Q. & Lin Wang, Z. Flexible triboelectric generator. *Nano Energy* **1**, 328–334 (2012).

145. Yu, Y., Li, Z., Wang, Y., Gong, S. & Wang, X. Sequential Infiltration Synthesis of Doped Polymer Films with Tunable Electrical Properties for Efficient Triboelectric Nanogenerator Development. *Adv Mater* **27**, 4938–4944 (2015).

146. Sun, J., Li, W., Liu, G., Li, W. & Chen, M. Triboelectric nanogenerator based on biocompatible polymer materials. *J Phys Chem C* **119**, 9061–9068 (2015).

147. Zhang, M. *et al.* Robust design of unearthed single-electrode TENG from three-dimensionally hybridized copper/polydimethylsiloxane film. *Nano Energy* **30**, 155–161 (2016).

148. He, X. *et al.* A Highly Stretchable Fiber-Based Triboelectric Nanogenerator for Self-Powered Wearable Electronics. *Adv Funct Mater* **27**, 1–8 (2017).

149. Yang, Y. *et al.* Coaxial Triboelectric Nanogenerator and Supercapacitor Fiber-Based Self-Charging Power Fabric. *ACS Appl Mater Interfaces* **10**, 42356–42362 (2018).

150. Xie, L. *et al.* Spiral Steel Wire Based Fiber-Shaped Stretchable and Tailorable Triboelectric Nanogenerator for Wearable Power Source and Active Gesture Sensor. *Nanomicro Lett* **11**, 1–10 (2019).

151. Han, J. *et al.* Multifunctional Coaxial Energy Fiber toward Energy Harvesting, Storage, and Utilization. *ACS Nano* **15**, 1597–1607 (2021).

152. He, X. *et al.* A Highly Stretchable Fiber-Based Triboelectric Nanogenerator for Self-Powered Wearable Electronics. *Adv Funct Mater* **27**, 1–8 (2017).

153. Yang, Y. *et al.* Coaxial Triboelectric Nanogenerator and Supercapacitor Fiber-Based Self-Charging Power Fabric. *ACS Appl Mater Interfaces* **10**, 42356–42362 (2018).

154. Peng, F. *et al.* Facile fabrication of triboelectric nanogenerator based on low-cost thermoplastic polymeric fabrics for large-area energy harvesting and self-powered sensing. *Nano Energy* **65**, 104068 (2019).

155. Feng, P. *et al.* Enhancing the performance of fabric-based triboelectric nanogenerators by structural and chemical modification. *ACS Appl Mater Interfaces*, **13,** 16916-16927 (2021).

156. Zhu, M. *et al.* 3D spacer fabric based multifunctional triboelectric nanogenerator with great feasibility for mechanized large-scale production. *Nano Energy* **27**, 439–446 (2016).

157. He, W., Sohn, M., Ma, R. & Kang, D. J. Flexible single-electrode triboelectric nanogenerators with MXene/PDMS composite film for biomechanical motion sensors. *Nano Energy* **78**, 105383 (2020).

158. Jiang, C., Li, X., Ying, Y. & Ping, J. A multifunctional TENG yarn integrated into agrotextile for building intelligent agriculture. *Nano Energy* **74**, 104863 (2020).

159. Mule, A. R., Dudem, B., Patnam, H., Graham, S. A. & Yu, J. S. Wearable Single-Electrode-Mode Triboelectric Nanogenerator via Conductive Polymer-Coated Textiles for Self-Power Electronics. *ACS Sustain Chem Eng* **7**, 16450–16458 (2019).

160. Jiang, C. *et al.* All-electrospun flexible triboelectric nanogenerator based on metallic MXene nanosheets. *Nano Energy* **59**, 268–276 (2019).

161. Ho, D. H. *et al.* β-Phase-Preferential blow-spun fabrics for wearable triboelectric nanogenerators and textile interactive interface. *Nano Energy* **77**, (2020).

162. Ye, Q. *et al.* Effects of liquid metal particles on performance of triboelectric nanogenerator with electrospun polyacrylonitrile fiber films. *Nano Energy* **61**, 381–388 (2019).

163. Doganay, D., Kanicioglu, A., Coskun, S., Akca, G. & Unalan, H. E. Silver-nanowire-modified fabrics for wide-spectrum antimicrobial applications. *J Mater Res* **34**, 500–509 (2019).

164. Doganay, D., Coskun, S., Kaynak, C. & Unalan, H. E. Electrical, mechanical and thermal properties of aligned silver nanowire/polylactide nanocomposite films. *Compos B Eng* **99**, 288–296 (2016).

165. Doğanay, D. Production and characterization of polylactide/silver nanowire nanocomposite films. (Middle East Technical University, 2016).

166. Nandiyanto, A. B. D., Oktiani, R. & Ragadhita, R. How to read and interpret ftir spectroscope of organic material. *Indones J Sci Technol* **4**, 97–118 (2019).

167. Jiao, L., Xiao, H., Wang, Q. & Sun, J. Thermal degradation characteristics of rigid polyurethane foam and the volatile products analysis with TG-FTIR-MS. *Polym Degrad Stab* **98**, 2687–2696 (2013).

168. Wang, J. *et al.* Construction of multifunctional MoSe2 hybrid towards the simultaneous improvements in fire safety and mechanical property of polymer. *J Hazard Mater* **352**, 36–46 (2018).

169. Tabuani, D., Bellucci, F., Terenzi, A. & Camino, G. Flame retarded Thermoplastic Polyurethane (TPU) for cable jacketing application. *Polym Degrad Stab* **97**, 2594–2601 (2012).

170. Saiani, A. *et al.* Origin of multiple melting endotherms in a high hard block content polyurethane: Effect of annealing temperature. *Macromolecules* **40**, 7252–7262 (2007).

171. Tian, Z. *et al.* Wearable and Washable Regulated Light/thermal Emitting Textiles. *Nanoscale Adv* **3,** 2475-2480 (2021)

172. Khan, M. R. *et al.* Tunable Color Coating of E-Textiles by Atomic Layer Deposition of Multilayer TiO2/Al2O3 Films. *Langmuir* **36**, 2794–2801 (2020).

173. Xiong, J. *et al.* Skin-touch-actuated textile-based triboelectric nanogenerator with black phosphorus for durable biomechanical energy harvesting. *Nat Commun* **9**, 1–9 (2018).

174. Zou, H. *et al.* Quantifying the triboelectric series. *Nat Commun* **10**, 1–9 (2019).

175. Ross Robert. *Clothing: A GlobalHhistory*. (Polity, 2008).

176. Sun, Z. *et al.* Artificial Intelligence of Things (AIoT) Enabled Virtual Shop Applications Using Self-Powered Sensor Enhanced Soft Robotic Manipulator. *Adv Sci* **8**, (2021).

177. Dong, K., Peng, X. & Wang, Z. L. Fiber/Fabric-Based Piezoelectric and Triboelectric Nanogenerators for Flexible/Stretchable and Wearable Electronics and Artificial Intelligence. *Adv Mater* **32** (2020).

178. Maharjan, P. *et al.* A Fully Functional Universal Self-Chargeable Power Module for Portable/Wearable Electronics and Self-Powered IoT Applications. *Adv Energy Mater* **10**, (2020).

179. Yang, Z., Zhou, Q., Lei, L., Zheng, K. & Xiang, W. An IoT-cloud Based Wearable ECG Monitoring System for Smart Healthcare. *J Med Syst* **40**, (2016).

180. Majumder, S., Mondal, T. & Deen, M. J. Wearable sensors for remote health monitoring. *Sensors (Switzerland)* **17** (2017).

181. Kumar, S. *et al.* Mobile health technology evaluation: The mHealth evidence workshop. *Am J Prev Med* **45**, 228–236 (2013).

182. Lee, J. *et al.* Stretchable Skin-Like Cooling/Heating Device for Reconstruction of Artificial Thermal Sensation in Virtual Reality. *Adv Funct Mater* **30**, (2020).

183. Pyun, K. R., Rogers, J. A. & Ko, S. H. Materials and devices for immersive virtual reality. *Nat Rev Mater* **1** (2022)

184. Liu, Z. *et al.* Wearable and Implantable Triboelectric Nanogenerators. *Adv Funct Mater* **29** (2019).

185. Wang, J. *et al.* Sustainably powering wearable electronics solely by biomechanical energy. *Nat Commun* **7**, (2016).

186. Chen, C. *et al.* Direct Current Fabric Triboelectric Nanogenerator for Biomotion Energy Harvesting. *ACS Nano* **14**, 4585–4594 (2020).

187. Kwak, S. S., Yoon, H. J. & Kim, S. W. Textile-Based Triboelectric Nanogenerators for Self-Powered Wearable Electronics. *Adv Funct Mater* **29** (2019).

188. Dong, S. *et al.* Seamlessly knitted stretchable comfortable textile triboelectric nanogenerators for E-textile power sources. *Nano Energy* **78**, (2020).

189. Dong, K. *et al.* Versatile Core–Sheath Yarn for Sustainable Biomechanical Energy Harvesting and Real-Time Human-Interactive Sensing. *Adv Energy Mater* **8**, (2018).

190. Yang, Y. *et al.* Coaxial Triboelectric Nanogenerator and Supercapacitor Fiber-Based Self-Charging Power Fabric. *ACS Appl Mater Interfaces* **10**, 42356–42362 (2018).

191. Xie, L. *et al.* Spiral Steel Wire Based Fiber-Shaped Stretchable and Tailorable Triboelectric Nanogenerator for Wearable Power Source and Active Gesture Sensor. *Nanomicro Lett* **11** (2019).

192. Wang, W. *et al.* Large-scale fabrication of robust textile triboelectric nanogenerators. *Nano Energy* **71**, (2020).

193. He, M. *et al.* Flexible and stretchable triboelectric nanogenerator fabric for biomechanical energy harvesting and self-powered dual-mode human motion monitoring. *Nano Energy* **86**, (2021).

194. Dong, K. *et al.* Shape adaptable and highly resilient 3D braided triboelectric nanogenerators as e-textiles for power and sensing. *Nat Commun* **11**, (2020).

195. Liu, J. *et al.* Coaxial double helix structured fiber-based triboelectric nanogenerator for effectively harvesting mechanical energy. *Nanoscale Adv* **2**, 4482–4490 (2020).

196. Ma, L. *et al.* A Machine-Fabricated 3D Honeycomb-Structured Flame-Retardant Triboelectric Fabric for Fire Escape and Rescue. *Adv Mater* **32**, (2020).

197. Ma, L. *et al.* Continuous and Scalable Manufacture of Hybridized Nano-Micro Triboelectric Yarns for Energy Harvesting and Signal Sensing. *ACS Nano* **14**, 4716–4726 (2020).

198. Dong, S. *et al.* Seamlessly knitted stretchable comfortable textile triboelectric nanogenerators for E-textile power sources. *Nano Energy* **78**, (2020).

199. Chen, L. *et al.* Stretchable negative Poisson's ratio yarn for triboelectric nanogenerator for environmental energy harvesting and self-powered sensor. *Energy Environ Sci* **14**, 955–964 (2021).

200. Yang, Y., Xu, B., Gao, Y. & Li, M. Conductive Composite Fiber with Customizable Functionalities for Energy Harvesting and Electronic Textiles. *ACS Appl Mater Interfaces* **13**, 49927–49935 (2021).

201. Lu, Y. *et al.* High-Performance Stretchable Conductive Composite Fibers from Surface-Modified Silver Nanowires and Thermoplastic Polyurethane by Wet Spinning. *ACS Appl Mater Interfaces* **10**, 2093–2104 (2018).

202. Lee, S. *et al.* Ag nanowire reinforced highly stretchable conductive fibers for wearable electronics. *Adv Funct Mater* **25**, 3114–3121 (2015).

203. Cui, N. *et al.* Dynamic Behavior of the Triboelectric Charges and Structural Optimization of the Friction Layer for a Triboelectric Nanogenerator. *ACS Nano* **10**, 6131–6138 (2016).

APPENDICES

A. Permission Licenses

SPRINGER NATURE LICENSE
TERMS AND CONDITIONS

Nov 07, 2022

This Agreement between Doga Doganay ("You") and Springer Nature ("Springer Nature") consists of your license details and the terms and conditions provided by Springer Nature and Copyright Clearance Center.

License Number	5423690332638
License date	Nov 07, 2022
Licensed Content Publisher	Springer Nature
Licensed Content Publication	Journal of Materials Research
Licensed Content Title	Silver-nanowire-modified fabrics for wide-spectrum antimicrobial applications
Licensed Content Author	Doga Doganay et al
Licensed Content Date	Feb 1, 2019
Type of Use	Thesis/Dissertation
Requestor type	academic/university or research institute
Format	print and electronic
Portion	full article/chapter
Will you be translating?	no
Circulation/distribution	1 - 29
Author of this Springer Nature content	yes

Title	Silver-nanowire-modified fabrics for wide-spectrum antimicrobial applications
Institution name	Middle East Technical University
Expected presentation date	Nov 2022
Requestor Location	Doga Doganay Middle East Technical University Metallurgical and Materials Engineering Ankara, 06800 Turkey Attn: Doga Doganay
Total	0.00 USD

Terms and Conditions

Springer Nature Customer Service Centre GmbH
Terms and Conditions

This agreement sets out the terms and conditions of the licence (the **Licence**) between you and **Springer Nature Customer Service Centre GmbH** (the **Licensor**). By clicking 'accept' and completing the transaction for the material (**Licensed Material**), you also confirm your acceptance of these terms and conditions.

1. Grant of License

1. 1. The Licensor grants you a personal, non-exclusive, non-transferable, world-wide licence to reproduce the Licensed Material for the purpose specified in your order only. Licences are granted for the specific use requested in the order and for no other use, subject to the conditions below.

1. 2. The Licensor warrants that it has, to the best of its knowledge, the rights to license reuse of the Licensed Material. However, you should ensure that the material you are requesting is original to the Licensor and does not carry the copyright of another entity (as credited in the published version).

1. 3. If the credit line on any part of the material you have requested indicates that it was reprinted or adapted with permission from another source, then you should also seek permission from that source to reuse the material.

2. Scope of Licence

2. 1. You may only use the Licensed Content in the manner and to the extent permitted by these Ts&Cs and any applicable laws.

2. 2. A separate licence may be required for any additional use of the Licensed Material, e.g. where a licence has been purchased for print only use, separate

permission must be obtained for electronic re-use. Similarly, a licence is only valid in the language selected and does not apply for editions in other languages unless additional translation rights have been granted separately in the licence. Any content owned by third parties are expressly excluded from the licence.

2. 3. Similarly, rights for additional components such as custom editions and derivatives require additional permission and may be subject to an additional fee. Please apply to Journalpermissions@springernature.com/bookpermissions@springernature.com for these rights.

2. 4. Where permission has been granted **free of charge** for material in print, permission may also be granted for any electronic version of that work, provided that the material is incidental to your work as a whole and that the electronic version is essentially equivalent to, or substitutes for, the print version.

2. 5. An alternative scope of licence may apply to signatories of the STM Permissions Guidelines, as amended from time to time.

3. Duration of Licence

3. 1. A licence for is valid from the date of purchase ('Licence Date') at the end of the relevant period in the below table:

Scope of Licence	Duration of Licence
Post on a website	12 months
Presentations	12 months
Books and journals	Lifetime of the edition in the language purchased

4. Acknowledgement

4. 1. The Licensor's permission must be acknowledged next to the Licenced Material in print. In electronic form, this acknowledgement must be visible at the same time as the figures/tables/illustrations or abstract, and must be hyperlinked to the journal/book's homepage. Our required acknowledgement format is in the Appendix below.

5. Restrictions on use

5. 1. Use of the Licensed Material may be permitted for incidental promotional use and minor editing privileges e.g. minor adaptations of single figures, changes of format, colour and/or style where the adaptation is credited as set out in Appendix 1 below. Any other changes including but not limited to, cropping, adapting, omitting material that affect the meaning, intention or moral rights of the author are strictly prohibited.

5. 2. You must not use any Licensed Material as part of any design or trademark.

5. 3. Licensed Material may be used in Open Access Publications (OAP) before publication by Springer Nature, but any Licensed Material must be removed from OAP sites prior to final publication.

6. Ownership of Rights

6. 1. Licensed Material remains the property of either Licensor or the relevant third party and any rights not explicitly granted herein are expressly reserved.

7. Warranty

IN NO EVENT SHALL LICENSOR BE LIABLE TO YOU OR ANY OTHER PARTY OR ANY OTHER PERSON OR FOR ANY SPECIAL, CONSEQUENTIAL, INCIDENTAL OR INDIRECT DAMAGES, HOWEVER CAUSED, ARISING OUT OF OR IN CONNECTION WITH THE DOWNLOADING, VIEWING OR USE OF THE MATERIALS REGARDLESS OF THE FORM OF ACTION, WHETHER FOR BREACH OF CONTRACT, BREACH OF WARRANTY, TORT, NEGLIGENCE, INFRINGEMENT OR OTHERWISE (INCLUDING, WITHOUT LIMITATION, DAMAGES BASED ON LOSS OF PROFITS, DATA, FILES, USE, BUSINESS OPPORTUNITY OR CLAIMS OF THIRD PARTIES), AND
WHETHER OR NOT THE PARTY HAS BEEN ADVISED OF THE POSSIBILITY OF SUCH DAMAGES. THIS LIMITATION SHALL APPLY NOTWITHSTANDING ANY FAILURE OF ESSENTIAL PURPOSE OF ANY LIMITED REMEDY PROVIDED HEREIN.

8. Limitations

8. 1. ***BOOKS ONLY:*** Where **'reuse in a dissertation/thesis'** has been selected the following terms apply: Print rights of the final author's accepted manuscript (for clarity, NOT the published version) for up to 100 copies, electronic rights for use only on a personal website or institutional repository as defined by the Sherpa guideline (www.sherpa.ac.uk/romeo/).

8. 2. For content reuse requests that qualify for permission under the STM Permissions Guidelines, which may be updated from time to time, the STM Permissions Guidelines supersede the terms and conditions contained in this licence.

9. Termination and Cancellation

9. 1. Licences will expire after the period shown in Clause 3 (above).

9. 2. Licensee reserves the right to terminate the Licence in the event that payment is not received in full or if there has been a breach of this agreement by you.

Appendix 1 — Acknowledgements:

For Journal Content:
Reprinted by permission from [**the Licensor**]: [**Journal Publisher** (e.g. Nature/Springer/Palgrave)] [**JOURNAL NAME**] [**REFERENCE CITATION** (Article name, Author(s) Name), [**COPYRIGHT**] (year of publication)

For **Advance Online Publication papers:**
Reprinted by permission from [**the Licensor**]: [**Journal Publisher** (e.g.

Nature/Springer/Palgrave)] [**JOURNAL NAME**] [**REFERENCE CITATION** (Article name, Author(s) Name), [**COPYRIGHT**] (year of publication), advance online publication, day month year (doi: 10.1038/sj.[JOURNAL ACRONYM].)

For Adaptations/Translations:
Adapted/Translated by permission from [**the Licensor**]: [**Journal Publisher** (e.g. Nature/Springer/Palgrave)] [**JOURNAL NAME**] [**REFERENCE CITATION** (Article name, Author(s) Name), [**COPYRIGHT**] (year of publication)

Note: For any republication from the British Journal of Cancer, the following credit line style applies:

Reprinted/adapted/translated by permission from [**the Licensor**]: on behalf of Cancer Research UK: : [**Journal Publisher** (e.g. Nature/Springer/Palgrave)] [**JOURNAL NAME**] [**REFERENCE CITATION** (Article name, Author(s) Name), [**COPYRIGHT**] (year of publication)

For **Advance Online Publication** papers:
Reprinted by permission from The [**the Licensor**]: on behalf of Cancer Research UK: [**Journal Publisher** (e.g. Nature/Springer/Palgrave)] [**JOURNAL NAME**] [**REFERENCE CITATION** (Article name, Author(s) Name), [**COPYRIGHT**] (year of publication), advance online publication, day month year (doi: 10.1038/sj.[JOURNAL ACRONYM])

For Book content:
Reprinted/adapted by permission from [**the Licensor**]: [**Book Publisher** (e.g. Palgrave Macmillan, Springer etc) [**Book Title**] by [**Book author**(s)] [**COPYRIGHT**] (year of publication)

Other Conditions:

Version 1.3

Questions? customercare@copyright.com or +1-855-239-3415 (toll free in the US) or +1-978-646-2777.

CCC Marketplace

This is a License Agreement between Doga Doganay ("User") and Copyright Clearance Center, Inc. ("CCC") on behalf of the Rightsholder identified in the order details below. The license consists of the order details, the Marketplace Order General Terms and Conditions below, and any Rightsholder Terms and Conditions which are included below.

All payments must be made in full to CCC in accordance with the Marketplace Order General Terms and Conditions below.

Order Date	28-Nov-2022	Type of Use	Republish in a thesis/dissertation
Order License ID	1294522-1		
ISSN	0957-4484	Publisher	IOP Publishing
		Portion	Chapter/article

LICENSED CONTENT

Publication Title	Nanotechnology	Country	United Kingdom of Great Britain and Northern Ireland
Author/Editor	Institute of Physics (Great Britain)		
Date	01/01/1990	Rightsholder	IOP Publishing, Ltd
Language	English	Publication Type	Journal

REQUEST DETAILS

Portion Type	Chapter/article	Rights Requested	Main product
Page Range(s)	435201	Distribution	Worldwide
Total Number of Pages	8	Translation	Original language of publication
Format (select all that apply)	Print, Electronic	Copies for the Disabled?	No
Who Will Republish the Content?	Author of requested content	Minor Editing Privileges?	No
Duration of Use	Life of current and all future editions	Incidental Promotional Use?	No
Lifetime Unit Quantity	Up to 999	Currency	USD

NEW WORK DETAILS

Title	Doga Doganay	Institution Name	Middle East Technical University
Instructor Name	Middle East Technical University	Expected Presentation Date	2022-11-23

ADDITIONAL DETAILS

Order Reference Number	N/A	The Requesting Person/Organization to Appear on the License	Doga Doganay

REUSE CONTENT DETAILS

Title, Description or Numeric Reference of the Portion(s)	Thesis	Title of the Article/Chapter the Portion Is From	Silver nanowire decorated heatable textiles
Editor of Portion(s)	NA	Author of Portion(s)	Doğa Doğanay

Volume of Serial or Monograph	NA	Issue, if Republishing an Article From a Serial	N/A
Page or Page Range of Portion	NA	Publication Date of Portion	1990-01-23

RIGHTSHOLDER TERMS AND CONDITIONS

These special terms and conditions are in addition to the standard terms and conditions for CCC's Republication Service and, together with those standard terms and conditions, govern the use of the Works. As the User you will make all reasonable efforts to contact the author(s) of the article which the Work is to be reused from, to seek consent for your intended use. Contacting one author who is acting expressly as authorised agent for their co-author(s) is acceptable. User will reproduce the following wording prominently alongside the Work: the source of the Work, including author, article title, title of journal, volume number, issue number (if relevant), page range (or first page if this is the only information available) and date of first publication; and a link back to the article (via DOI); and if practicable, and IN ALL CASES for new works published under any of the Creative Commons licences, the words "© IOP Publishing. Reproduced with permission. All rights reserved" Without the express permission of the author(s) and the Rightsholder of the article from which the Work is to be reused, User shall not use it in any way which, in the opinion of the Rightsholder, could: (i) distort or alter the author(s)' original intention(s) and meaning; (ii) be prejudicial to the honour or reputation of the author(s); and/or (iii) imply endorsement by the author(s) and/or the Rightsholder. This licence does not apply to any article which is credited to another source and which does not have the copyright line '© IOP Publishing Ltd'. User must check the copyright line of the article from which the Work is to be reused to check that IOP Publishing Ltd has all the necessary rights to be able to grant permission. User is solely responsible for identifying and obtaining separate licences and permissions from the copyright owner for reuse of any such third party material/figures which the Rightsholder is not the copyright owner of. The Rightsholder shall not reimburse any fees which User pays for a republication license for such third party content. This licence does not apply to any material/figure which is credited to another source in the Rightsholder's publication or has been obtained from a third party. User must check the Version of Record of the article from which the Work is to be reused, to check whether any of the material in the Work is third party material. Third party citations and/or copyright notices and/or permissions statements may not be included in any other version of the article from which the Work is to be reused and so cannot be relied upon by the User. User is solely responsible for identifying and obtaining separate licences and permissions from the copyright owner for reuse of any such third party material/figures where the Rightsholder is not the copyright owner. The Rightsholder shall not reimburse any fees which User pays for a republication license for such third party content. User and CCC acknowledge that the Rightsholder may, from time to time, make changes or additions to these special terms and conditions without express notification, provided that these shall not apply to permissions already secured and paid for by User prior to such change or addition. User acknowledges that the Rightsholder (which includes companies within its group and third parties for whom it publishes its titles) may make use of personal data collected through the service in the course of their business. If User is the author of the Work, User may automatically have the right to reuse it under the rights granted back when User transferred the copyright in the article to the Rightsholder. User should check the copyright form and the relevant author rights policy to check whether permission is required. If User is the author of the Work and does require permission for proposed reuse of the Work, User should select 'Author of requested content' as the Requestor Type. The Rightsholder shall not reimburse any fees which User pays for a republication license. If User is the author of the article which User wishes to reuse in User's thesis or dissertation, the republication licence covers the right to include the Version of Record of the article, provided it is not then shared or deposited online. User must include citation details. Where User wishes to share their thesis or dissertation online, they should remove the Version of Record before uploading it. User may include a Preprint or the Accepted Manuscript (after the embargo period) in the online version of the thesis or dissertation, provided they do so in accordance with the Rightsholder's policies on sharing Preprints or Accepted Manuscripts. User may need to obtain separate permission for any third party content included within the article. User must check this with the copyright owner of such third party content. Any online or commercial use of User's thesis or dissertation containing the article, including publication via ProQuest, would need to be expressly notified in writing to the Rightsholder at the time of request and would require separate written permission from the Rightsholder. As well as CCC, the Rightsholder shall have the right to bring any legal action that it deems necessary to enforce its rights should it consider that the Work infringes those rights in any way. For content reuse requests that qualify for permission under the STM Permissions Guidelines, which may be updated from time to time, the STM Permissions Guidelines supplement the terms and conditions contained in this license.

SPECIAL RIGHTSHOLDER TERMS AND CONDITIONS

When you transferred the copyright in your article to IOP, we granted back to you certain rights, including the right to include all or part of the Final Published Version of the article within any thesis or dissertation. Please note you may need to obtain separate permission for any third party content you included within your article. Please include citation details, "© IOP Publishing. Reproduced with permission. All rights reserved" and for online use, a link to the Version of Record. The only restriction is that if, at a later date, you wanted your thesis/dissertation to be published commercially, further permission would be required.

The following terms and conditions ("General Terms"), together with any applicable Publisher Terms and Conditions, govern User's use of Works pursuant to the Licenses granted by Copyright Clearance Center, Inc. ("CCC") on behalf of the applicable Rightsholders of such Works through CCC's applicable Marketplace transactional licensing services (each, a "Service").

1) **Definitions.** For purposes of these General Terms, the following definitions apply:

"License" is the licensed use the User obtains via the Marketplace platform in a particular licensing transaction, as set forth in the Order Confirmation.

"Order Confirmation" is the confirmation CCC provides to the User at the conclusion of each Marketplace transaction. "Order Confirmation Terms" are additional terms set forth on specific Order Confirmations not set forth in the General Terms that can include terms applicable to a particular CCC transactional licensing service and/or any Rightsholder-specific terms.

"Rightsholder(s)" are the holders of copyright rights in the Works for which a User obtains licenses via the Marketplace platform, which are displayed on specific Order Confirmations.

"Terms" means the terms and conditions set forth in these General Terms and any additional Order Confirmation Terms collectively.

"User" or "you" is the person or entity making the use granted under the relevant License. Where the person accepting the Terms on behalf of a User is a freelancer or other third party who the User authorized to accept the General Terms on the User's behalf, such person shall be deemed jointly a User for purposes of such Terms.

"Work(s)" are the copyright protected works described in relevant Order Confirmations.

2) **Description of Service.** CCC's Marketplace enables Users to obtain Licenses to use one or more Works in accordance with all relevant Terms. CCC grants Licenses as an agent on behalf of the copyright rightsholder identified in the relevant Order Confirmation.

3) **Applicability of Terms.** The Terms govern User's use of Works in connection with the relevant License. In the event of any conflict between General Terms and Order Confirmation Terms, the latter shall govern. User acknowledges that Rightsholders have complete discretion whether to grant any permission, and whether to place any limitations on any grant, and that CCC has no right to supersede or to modify any such discretionary act by a Rightsholder.

4) **Representations; Acceptance.** By using the Service, User represents and warrants that User has been duly authorized by the User to accept, and hereby does accept, all Terms.

5) **Scope of License; Limitations and Obligations.** All Works and all rights therein, including copyright rights, remain the sole and exclusive property of the Rightsholder. The License provides only those rights expressly set forth in the terms and conveys no other rights in any Works

6) **General Payment Terms.** User may pay at time of checkout by credit card or choose to be invoiced. If the User chooses to be invoiced, the User shall: (i) remit payments in the manner identified on specific invoices, (ii) unless otherwise specifically stated in an Order Confirmation or separate written agreement, Users shall remit payments upon receipt of the relevant invoice from CCC, either by delivery or notification of availability of the invoice via the Marketplace platform, and (iii) if the User does not pay the invoice within 30 days of receipt, the User may incur a service charge of 1.5% per month or the maximum rate allowed by applicable law, whichever is less. While User may exercise the rights in the License immediately upon receiving the Order Confirmation, the License is automatically revoked and is null and void, as if it had never been issued, if CCC does not receive complete payment on a timely basis.

7) **General Limits on Use.** Unless otherwise provided in the Order Confirmation, any grant of rights to User (i) involves only the rights set forth in the Terms and does not include subsequent or additional uses, (ii) is non-exclusive and non-transferable, and (iii) is subject to any and all limitations and restrictions (such as, but not limited to, limitations on duration of use or circulation) included in the Terms. Upon completion of the licensed use as set forth in the Order Confirmation, User shall either secure a new permission for further use of the Work(s) or immediately cease any new use of the Work(s) and shall render inaccessible (such as by deleting or by removing or severing links or other locators) any further copies of the Work. User may only make alterations to the Work if and as expressly set forth in the Order Confirmation. No Work may be used in any way that is defamatory, violates the rights of third parties (including such third parties' rights of copyright, privacy, publicity, or other tangible or intangible property), or is otherwise illegal, sexually explicit, or obscene. In addition, User may not conjoin a Work with any other material that may result in damage to the reputation of the Rightsholder. User agrees to inform CCC if it becomes aware of any infringement of any rights in a Work and to cooperate with any reasonable request of CCC or the Rightsholder in connection therewith.

8) **Third Party Materials.** In the event that the material for which a License is sought includes third party materials (such as photographs, illustrations, graphs, inserts and similar materials) that are identified in such material as having been

used by permission (or a similar indicator), User is responsible for identifying, and seeking separate licenses (under this Service, if available, or otherwise) for any of such third party materials; without a separate license, User may not use such third party materials via the License.

9) **Copyright Notice.** Use of proper copyright notice for a Work is required as a condition of any License granted under the Service. Unless otherwise provided in the Order Confirmation, a proper copyright notice will read substantially as follows: "Used with permission of [Rightsholder's name], from [Work's title, author, volume, edition number and year of copyright]; permission conveyed through Copyright Clearance Center, Inc." Such notice must be provided in a reasonably legible font size and must be placed either on a cover page or in another location that any person, upon gaining access to the material which is the subject of a permission, shall see, or in the case of republication Licenses, immediately adjacent to the Work as used (for example, as part of a by-line or footnote) or in the place where substantially all other credits or notices for the new work containing the republished Work are located. Failure to include the required notice results in loss to the Rightsholder and CCC, and the User shall be liable to pay liquidated damages for each such failure equal to twice the use fee specified in the Order Confirmation, in addition to the use fee itself and any other fees and charges specified.

10) **Indemnity.** User hereby indemnifies and agrees to defend the Rightsholder and CCC, and their respective employees and directors, against all claims, liability, damages, costs, and expenses, including legal fees and expenses, arising out of any use of a Work beyond the scope of the rights granted herein and in the Order Confirmation, or any use of a Work which has been altered in any unauthorized way by User, including claims of defamation or infringement of rights of copyright, publicity, privacy, or other tangible or intangible property.

11) **Limitation of Liability.** UNDER NO CIRCUMSTANCES WILL CCC OR THE RIGHTSHOLDER BE LIABLE FOR ANY DIRECT, INDIRECT, CONSEQUENTIAL, OR INCIDENTAL DAMAGES (INCLUDING WITHOUT LIMITATION DAMAGES FOR LOSS OF BUSINESS PROFITS OR INFORMATION, OR FOR BUSINESS INTERRUPTION) ARISING OUT OF THE USE OR INABILITY TO USE A WORK, EVEN IF ONE OR BOTH OF THEM HAS BEEN ADVISED OF THE POSSIBILITY OF SUCH DAMAGES. In any event, the total liability of the Rightsholder and CCC (including their respective employees and directors) shall not exceed the total amount actually paid by User for the relevant License. User assumes full liability for the actions and omissions of its principals, employees, agents, affiliates, successors, and assigns.

12) **Limited Warranties.** THE WORK(S) AND RIGHT(S) ARE PROVIDED "AS IS." CCC HAS THE RIGHT TO GRANT TO USER THE RIGHTS GRANTED IN THE ORDER CONFIRMATION DOCUMENT. CCC AND THE RIGHTSHOLDER DISCLAIM ALL OTHER WARRANTIES RELATING TO THE WORK(S) AND RIGHT(S), EITHER EXPRESS OR IMPLIED, INCLUDING WITHOUT LIMITATION IMPLIED WARRANTIES OF MERCHANTABILITY OR FITNESS FOR A PARTICULAR PURPOSE. ADDITIONAL RIGHTS MAY BE REQUIRED TO USE ILLUSTRATIONS, GRAPHS, PHOTOGRAPHS, ABSTRACTS, INSERTS, OR OTHER PORTIONS OF THE WORK (AS OPPOSED TO THE ENTIRE WORK) IN A MANNER CONTEMPLATED BY USER; USER UNDERSTANDS AND AGREES THAT NEITHER CCC NOR THE RIGHTSHOLDER MAY HAVE SUCH ADDITIONAL RIGHTS TO GRANT.

13) **Effect of Breach.** Any failure by User to pay any amount when due, or any use by User of a Work beyond the scope of the License set forth in the Order Confirmation and/or the Terms, shall be a material breach of such License. Any breach not cured within 10 days of written notice thereof shall result in immediate termination of such License without further notice. Any unauthorized (but licensable) use of a Work that is terminated immediately upon notice thereof may be liquidated by payment of the Rightsholder's ordinary license price therefor; any unauthorized (and unlicensable) use that is not terminated immediately for any reason (including, for example, because materials containing the Work cannot reasonably be recalled) will be subject to all remedies available at law or in equity, but in no event to a payment of less than three times the Rightsholder's ordinary license price for the most closely analogous licensable use plus Rightsholder's and/or CCC's costs and expenses incurred in collecting such payment.

14) **Additional Terms for Specific Products and Services.** If a User is making one of the uses described in this Section 14, the additional terms and conditions apply:

a) ***Print Uses of Academic Course Content and Materials (photocopies for academic coursepacks or classroom handouts).*** For photocopies for academic coursepacks or classroom handouts the following additional terms apply:

i) The copies and anthologies created under this License may be made and assembled by faculty members individually or at their request by on-campus bookstores or copy centers, or by off-campus copy shops and other similar entities.

ii) No License granted shall in any way: (i) include any right by User to create a substantively non-identical copy of the Work or to edit or in any other way modify the Work (except by means of deleting material immediately preceding or following the entire portion of the Work copied) (ii) permit "publishing ventures" where any particular anthology would be systematically marketed at multiple institutions.

iii) Subject to any Publisher Terms (and notwithstanding any apparent contradiction in the Order Confirmation arising from data provided by User), any use authorized under the academic pay-per-use service is limited as follows:

A) any License granted shall apply to only one class (bearing a unique identifier as assigned by the institution, and thereby including all sections or other subparts of the class) at one institution;

B) use is limited to not more than 25% of the text of a book or of the items in a published collection of essays, poems or articles;

C) use is limited to no more than the greater of (a) 25% of the text of an issue of a journal or other periodical or (b) two articles from such an issue;

D) no User may sell or distribute any particular anthology, whether photocopied or electronic, at more than one institution of learning;

E) in the case of a photocopy permission, no materials may be entered into electronic memory by User except in order to produce an identical copy of a Work before or during the academic term (or analogous period) as to which any particular permission is granted. In the event that User shall choose to retain materials that are the subject of a photocopy permission in electronic memory for purposes of producing identical copies more than one day after such retention (but still within the scope of any permission granted), User must notify CCC of such fact in the applicable permission request and such retention shall constitute one copy actually sold for purposes of calculating permission fees due; and

F) any permission granted shall expire at the end of the class. No permission granted shall in any way include any right by User to create a substantively non-identical copy of the Work or to edit or in any other way modify the Work (except by means of deleting material immediately preceding or following the entire portion of the Work copied).

iv) Books and Records; Right to Audit. As to each permission granted under the academic pay-per-use Service, User shall maintain for at least four full calendar years books and records sufficient for CCC to determine the numbers of copies made by User under such permission. CCC and any representatives it may designate shall have the right to audit such books and records at any time during User's ordinary business hours, upon two days' prior notice. If any such audit shall determine that User shall have underpaid for, or underreported, any photocopies sold or by three percent (3%) or more, then User shall bear all the costs of any such audit; otherwise, CCC shall bear the costs of any such audit. Any amount determined by such audit to have been underpaid by User shall immediately be paid to CCC by User, together with interest thereon at the rate of 10% per annum from the date such amount was originally due. The provisions of this paragraph shall survive the termination of this License for any reason.

b) *Digital Pay-Per-Uses of Academic Course Content and Materials (e-coursepacks, electronic reserves, learning management systems, academic institution intranets).* For uses in e-coursepacks, posts in electronic reserves, posts in learning management systems, or posts on academic institution intranets, the following additional terms apply:

i) The pay-per-uses subject to this Section 14(b) include:

A) **Posting e-reserves, course management systems, e-coursepacks for text-based content,** which grants authorizations to import requested material in electronic format, and allows electronic access to this material to members of a designated college or university class, under the direction of an instructor designated by the college or university, accessible only under appropriate electronic controls (e.g., password);

B) **Posting e-reserves, course management systems, e-coursepacks for material consisting of photographs or other still images not embedded in text,** which grants not only the authorizations described in Section 14(b)(i)(A) above, but also the following authorization: to include the requested material in course materials for use consistent with Section 14(b)(i)(A) above, including any necessary resizing, reformatting or modification of the resolution of such requested material (provided that such modification does not alter the underlying editorial content or meaning of the requested material, and provided that the resulting modified content is used solely within the scope of, and in a manner consistent with, the particular authorization described in the Order Confirmation and the Terms), but not including any other form of manipulation, alteration or editing of the requested material;

C) **Posting e-reserves, course management systems, e-coursepacks or other academic distribution for audiovisual content,** which grants not only the authorizations described in Section 14(b)(i)(A) above, but also the following authorizations: (i) to include the requested material in course materials for use consistent with Section 14(b)(i)(A) above; (ii) to display and perform the requested material to such members of such class in the physical classroom or remotely by means of streaming media or other video formats; and (iii) to "clip" or reformat the requested material for purposes of time or content management or ease of delivery, provided that such "clipping" or reformatting does not alter the underlying editorial content or meaning of the requested material and that the resulting material is used solely within the scope of, and in a manner consistent with, the particular authorization described in the Order Confirmation and the Terms. Unless

expressly set forth in the relevant Order Conformation, the License does not authorize any other form of manipulation, alteration or editing of the requested material.

ii) Unless expressly set forth in the relevant Order Confirmation, no License granted shall in any way: (i) include any right by User to create a substantively non-identical copy of the Work or to edit or in any other way modify the Work (except by means of deleting material immediately preceding or following the entire portion of the Work copied or, in the case of Works subject to Sections 14(b)(1)(B) or (C) above, as described in such Sections) (ii) permit "publishing ventures" where any particular course materials would be systematically marketed at multiple institutions.

iii) Subject to any further limitations determined in the Rightsholder Terms (and notwithstanding any apparent contradiction in the Order Confirmation arising from data provided by User), any use authorized under the electronic course content pay-per-use service is limited as follows:

A) any License granted shall apply to only one class (bearing a unique identifier as assigned by the institution, and thereby including all sections or other subparts of the class) at one institution;

B) use is limited to not more than 25% of the text of a book or of the items in a published collection of essays, poems or articles;

C) use is limited to not more than the greater of (a) 25% of the text of an issue of a journal or other periodical or (b) two articles from such an issue;

D) no User may sell or distribute any particular materials, whether photocopied or electronic, at more than one institution of learning;

E) electronic access to material which is the subject of an electronic-use permission must be limited by means of electronic password, student identification or other control permitting access solely to students and instructors in the class;

F) User must ensure (through use of an electronic cover page or other appropriate means) that any person, upon gaining electronic access to the material, which is the subject of a permission, shall see:

- a proper copyright notice, identifying the Rightsholder in whose name CCC has granted permission,
- a statement to the effect that such copy was made pursuant to permission,
- a statement identifying the class to which the material applies and notifying the reader that the material has been made available electronically solely for use in the class, and
- a statement to the effect that the material may not be further distributed to any person outside the class, whether by copying or by transmission and whether electronically or in paper form, and User must also ensure that such cover page or other means will print out in the event that the person accessing the material chooses to print out the material or any part thereof.

G) any permission granted shall expire at the end of the class and, absent some other form of authorization, User is thereupon required to delete the applicable material from any electronic storage or to block electronic access to the applicable material.

iv) Uses of separate portions of a Work, even if they are to be included in the same course material or the same university or college class, require separate permissions under the electronic course content pay-per-use Service. Unless otherwise provided in the Order Confirmation, any grant of rights to User is limited to use completed no later than the end of the academic term (or analogous period) as to which any particular permission is granted.

v) Books and Records; Right to Audit. As to each permission granted under the electronic course content Service, User shall maintain for at least four full calendar years books and records sufficient for CCC to determine the numbers of copies made by User under such permission. CCC and any representatives it may designate shall have the right to audit such books and records at any time during User's ordinary business hours, upon two days' prior notice. If any such audit shall determine that User shall have underpaid for, or underreported, any electronic copies used by three percent (3%) or more, then User shall bear all the costs of any such audit; otherwise, CCC shall bear the costs of any such audit. Any amount determined by such audit to have been underpaid by User shall immediately be paid to CCC by User, together with interest thereon at the rate of 10% per annum from the date such amount was originally due. The provisions of this paragraph shall survive the termination of this license for any reason.

c) ***Pay-Per-Use Permissions for Certain Reproductions (Academic photocopies for library reserves and interlibrary loan reporting) (Non-academic internal/external business uses and commercial document delivery).*** The License

expressly excludes the uses listed in Section (c)(i)-(v) below (which must be subject to separate license from the applicable Rightsholder) for: academic photocopies for library reserves and interlibrary loan reporting; and non-academic internal/external business uses and commercial document delivery.

i) electronic storage of any reproduction (whether in plain-text, PDF, or any other format) other than on a transitory basis;

ii) the input of Works or reproductions thereof into any computerized database;

iii) reproduction of an entire Work (cover-to-cover copying) except where the Work is a single article;

iv) reproduction for resale to anyone other than a specific customer of User;

v) republication in any different form. Please obtain authorizations for these uses through other CCC services or directly from the rightsholder.

Any license granted is further limited as set forth in any restrictions included in the Order Confirmation and/or in these Terms.

d) ***Electronic Reproductions in Online Environments (Non-Academic-email, intranet, internet and extranet).*** For "electronic reproductions", which generally includes e-mail use (including instant messaging or other electronic transmission to a defined group of recipients) or posting on an intranet, extranet or Intranet site (including any display or performance incidental thereto), the following additional terms apply:

i) Unless otherwise set forth in the Order Confirmation, the License is limited to use completed within 30 days for any use on the Internet, 60 days for any use on an intranet or extranet and one year for any other use, all as measured from the "republication date" as identified in the Order Confirmation, if any, and otherwise from the date of the Order Confirmation.

ii) User may not make or permit any alterations to the Work, unless expressly set forth in the Order Confirmation (after request by User and approval by Rightsholder); provided, however, that a Work consisting of photographs or other still images not embedded in text may, if necessary, be resized, reformatted or have its resolution modified without additional express permission, and a Work consisting of audiovisual content may, if necessary, be "clipped" or reformatted for purposes of time or content management or ease of delivery (provided that any such resizing, reformatting, resolution modification or "clipping" does not alter the underlying editorial content or meaning of the Work used, and that the resulting material is used solely within the scope of, and in a manner consistent with, the particular License described in the Order Confirmation and the Terms.

15) **Miscellaneous.**

a) User acknowledges that CCC may, from time to time, make changes or additions to the Service or to the Terms, and that Rightsholder may make changes or additions to the Rightsholder Terms. Such updated Terms will replace the prior terms and conditions in the order workflow and shall be effective as to any subsequent Licenses but shall not apply to Licenses already granted and paid for under a prior set of terms.

b) Use of User-related information collected through the Service is governed by CCC's privacy policy, available online at www.copyright.com/about/privacy-policy/.

c) The License is personal to User. Therefore, User may not assign or transfer to any other person (whether a natural person or an organization of any kind) the License or any rights granted thereunder; provided, however, that, where applicable, User may assign such License in its entirety on written notice to CCC in the event of a transfer of all or substantially all of User's rights in any new material which includes the Work(s) licensed under this Service.

d) No amendment or waiver of any Terms is binding unless set forth in writing and signed by the appropriate parties, including, where applicable, the Rightsholder. The Rightsholder and CCC hereby object to any terms contained in any writing prepared by or on behalf of the User or its principals, employees, agents or affiliates and purporting to govern or otherwise relate to the License described in the Order Confirmation, which terms are in any way inconsistent with any Terms set forth in the Order Confirmation, and/or in CCC's standard operating procedures, whether such writing is prepared prior to, simultaneously with or subsequent to the Order Confirmation, and whether such writing appears on a copy of the Order Confirmation or in a separate instrument.

e) The License described in the Order Confirmation shall be governed by and construed under the law of the State of New York, USA, without regard to the principles thereof of conflicts of law. Any case, controversy, suit, action, or proceeding arising out of, in connection with, or related to such License shall be brought, at CCC's sole discretion, in any federal or state court located in the County of New York, State of New York, USA, or in any federal or state court whose geographical jurisdiction covers the location of the Rightsholder set forth in the Order Confirmation. The parties expressly submit to the personal jurisdiction and venue of each such federal or state court.

CURRICULUM VITAE

Doğa Doğanay

Research Assistant
Department of Metallurgical and Materials Engineering
Middle East Technical University (METU)
06800, Ankara, TURKEY.
e-mail: ddoganay00@gmail.com
doganay@nanovatif.com

FORMAL EDUCATION

- ***Doctor of Philosophy***, Department of Metallurgical and Materials Engineering, (Ongoing)
  Middle East Technical University, Ankara TURKEY.
  Dissertation Title: "Silver Nanowire Based Multifunctional Fibers and Fabrics"

- ***Master of Science***, Department of Metallurgical and Materials Engineering, (2016)
  Middle East Technical University, Ankara, TURKEY.
  Dissertation Title: "Production and Characterization of Polylactide/Silver Nanowire Nanocomposite Films"

- ***Bachelor of Science***, Department of Metallurgical and Materials Engineering, (2013)
  Middle East Technical University, Ankara, TURKEY.

AWARDS AND ACHIEVEMENTS

- Nature Spinoff Price, Nature Research Award, 2020.
- Mercedes Benz StartUP Finalist, Mercedes Benz Turkey, 2017
- Thesis of the Year Award, METU Parlar Foundation, 2016.
- Young Researcher Award, 18th International Metallurgy & Materials Congress (IMMC) 2016.
- Winner Award, New Ideas & New Business 2016 (YFYİ), METU TEKNOKENT 2016.

ACADEMIC RESEARCH EXPERIENCE

- Research Assistant (2013 - Ongoing)
  Nanomaterials and Devices Laboratory, Metallurgical and Materials Engineering, Middle East Technical University.

JOB EXPERIENCE

- Co-Founder and Chief Technical Officer of Nanovatif Materials Technologies, METU Teknokent, Ankara, Turkey (2017-Ongoing).

RESEARCH INTERESTS

Synthesis of 1-D nanomaterials (nanowires), functional textiles, triboelectric nanogenerators, soft electronics.

PATENTS (4)

- TPE: Metal Nanotel Kaplamalı Isıtılabilir Kumaş (2015/10587)
- US: Metal Nanowire Decorated Heatable Fabrics (US10271385B2)
- EPO: Metal Nanowire Decorated Heatable Fabrics (EP3342252A1)
- EAO: Metal Nanowire Decorated Heatable Fabrics (EA035310B1)

PUBLICATIONS (13) (Total Citations:318, h-index:10 as 15.12.2022)

1. Cicek, M. O., Durukan, M.B., Yıldız, B., Keskin, D., **Doganay, D.,** Cınar, S., Cakır, M.P., Unalan, H.E. (2022) Ultra-Sensitive Bio-Polymer Iontronic Sensor for Object Recognition from Tactile Feedback. Submitted to: Nature Communications.
2. Durukan, M. B., Cicek, M. O., **Doganay, D.,** Gorur, M. C., Çınar, S., & Unalan, H. E. (2022). Multifunctional and Physically Transient Supercapacitors, Triboelectric Nanogenerators, and Capacitive Sensors. Advanced Functional Materials, 32 (1) 2106066.
3. Basturkmen, B., Ergene, E., **Doganay, D**., Huri, P., Y., Unalan, H., E., Aksoy, E., A. (2021) Silver Nanowire Loaded Poly(ε-caprolactone)

Nanocomposite Fibers as Electroactive Scaffolds for Skeletal Muscle Regeneration. Material Science & Engineering C. 112567.

4. **Doganay, D**., Cicek, M. O., Durukan, M. B., Altuntas, B., Agbahca, E., Coskun, S., & Unalan, H. E. (2021). Fabric based wearable triboelectric nanogenerators for human machine interface. Nano Energy, 89, 106412.
5. Cicek, M. O., **Doganay, D**., Durukan, M. B., Gorur, M. C., & Unalan, H. E. (2021). Seamless Monolithic Design for Foam Based, Flexible, Parallel Plate Capacitive Sensors. Advanced Materials Technologies, 6(6), 2001168.
6. Bang, J., Coskun, S., Pyun, K. R., **Doganay, D**., Tunca, S., Koylan, S., ... & Ko, S. H. (2021). Advances in protective layer-coating on metal nanowires with enhanced stability and their applications. Applied Materials Today, 22, 100909.
7. Birant, G., Ozturk, I. M., **Doganay, D**., Unalan, H. E., & Bek, A. (2020). Plasmonic light-management interfaces by polyol-synthesized silver nanoparticles for industrial scale silicon solar cells. ACS Applied Nano Materials, 3(12), 12231-12239.
8. Bahcelioglu, E., **Doganay, D**., Coskun, S., Unalan, H. E., & Erguder, T. H. (2020). A Point-of-Use (POU) Water Disinfection: Silver Nanowire Decorated Glass Fiber Filters. Journal of Water Process Engineering, 38, 101616.
9. Demirtaş, Ö., **Doganay, D**., Öztürk, İ. M., Ünalan, H. E., & Bek, A. (2020). Facile preparation of nanoparticle-based SERS substrates for trace molecule detection. Physical Chemistry Chemical Physics, 22(37), 21139-21146.
10. Bayraktar, I., **Doganay, D**., Coskun, S., Kaynak, C., Akca, G., & Unalan, H. E. (2019). 3D printed antibacterial silver nanowire/polylactide nanocomposites. Composites Part B: Engineering, 172, 671-678.
11. **Doganay, D**., Kanicioglu, A., Coskun, S., Akca, G., & Unalan, H. E. (2019). Silver-nanowire-modified fabrics for wide-spectrum antimicrobial applications. Journal of Materials Research, 34(4), 500-509.

12. Aurang, P., **Doganay, D**., Bek, A., Turan, R., & Unalan, H. E. (2017). Silver nanowire networks as transparent top electrodes for silicon solar cells. Solar Energy, 141, 110-117.
13. **Doganay, D**., Coskun, S., Genlik, S. P., & Unalan, H. E. (2016). Silver nanowire decorated heatable textiles. Nanotechnology, 27(43), 435201.
14. **Doganay, D**., Coskun, S., Kaynak, C., & Unalan, H. E. (2016). Electrical, mechanical and thermal properties of aligned silver nanowire/polylactide nanocomposite films. Composites Part B: Engineering, 99, 288-296.

PROJECTS (10)

1. Wearable TENGs with Wet-Spun Thermoplastic Polyurethane Fibers, Unalan, H.E., **Doganay, D.,** (2021-) (Research)
2. Metal Paste Development of k-Si Solar Cells, **Doganay, D.,** Coskun, S., Unalan, H.E., (2021-). (Industry)
3. Development of High Thermal Conductivity Thermal Interface Material with Vertically Aligned Carbon Nanotube Arrays, **Doganay, D.,** Coskun, S., Unalan, H.E., (2021-). (Industry)
4. Development of Ag NW Based Transparent Heaters, **Doganay, D.,** Coskun, S., Unalan, H.E., (2019-2020). (Industry)
5. A New Approach for Anti Icing Systems, **Doganay, D.,** Coskun, S., Unalan, H.E., (2019-2020). (Industry)
6. Investigation of *E.Coli* Removal from Water with Ag NWs, **Doganay, D.,** Bayramoglu T. H., Unalan., H.E., (2018-2020) (Research)
7. Development of Ag NW Based Flexible OLED Electrodes, **Doganay, D.,** Unalan, H.E., Coskun., S., (2018-2020) (Industry)
8. Development of Highly Conductive Fibers, **Doganay, D.,** Coskun, S., Unalan, H.E., (2018-2019) (Industry)
9. Metal Nanowire Modified Wearable Heaters, **Doganay, D.,** Coskun, S., Unalan, H.E., (2017-2019). (Industry)

10. 3D Printing of Ag NW/PLA Nanocomposites, Unalan, H.E., **Doganay, D.,** Cırpan, A. (2015-2016). (Research)

PRESENTATIONS (17)

1. Comparison of ALD grown AZO and ZnO Thin Film Heater Performances, Turgul D., **Doganay D.**, Unalan H.E., Imer M.B., MRS Fall'2021 USA.
2. Wearable Triboelectric Nanogenerators with Thermoplastic Polyurethane/Silver Nanowire Textiles for Human Machine Interface, **Doganay, D.,** Cicek, M.Ö., Durukan, M.B., Altuntas, B., Agbahca, E., Coskun, S., Unalan, H.E., MRS Fall'2021 USA.
3. Silver Nanowire–Cobalt Hydroxide Textile Electrodes for Flexible and Wearable Energy Storage Applications, Durukan, M.B., Hekmat, F., **Doganay**, **D.,** Unalan, H.E., MRS Fall' 2019 USA.
4. Silver Nanowire Modified Fabrics for Wearable Triboelectric Nanogenerators, **Doganay, D.,** Durukan, M. B., Cicek, M.Ö., Guven, M.N., Unalan, H.E., MRS Fall' 2019 USA.
5. Silver Nanowire/Chitosan Nanocomposites Scaffolds for Tissue Engineering with Enhanced Durability, Unalan, H.E., Aydın, D., Aksoy, E.A., Senel, S., **Doganay, D.,** MRS Fall 2018 USA.
6. Silver Nanowire Based Transparent Electrodes and Heaters, Coskun, S., **Doganay, D.**, Unalan, H.E., ISASE 2018, Erzurum, Turkey.
7. Nanowire Modified Antibacterial Fabrics, **Doğanay, D.,** Kanıcıoğlu, A., Coskun, S., Akça, G., Unalan, H.E., IMMC' 2018 İstanbul, Turkey.
8. Silver Nanowire Decorated Antibacterial Fabrics, **Doganay, D.,** Kanicioglu, A., Coskun, S., Akca, G., Unalan, H.E., MRS Fall' 2017 USA.
9. 3D Printed Antibacterial Ag NW/PLA Nanocomposites, Bayraktar, I., **Doganay, D.,** Coskun, S., Kanicioglu, A., Akca, G., Unalan, H.E., MRS Fall' 2017 USA.

10. Antibacterial Silver Nanowire-Chitosan Nanocomposite Films, **Doganay, D.**, Somek, S.K., Aydin, D., Kanicioglu, A., Coskun, S., Senel, S., Akca, A., Unalan, H.E., MRS Fall' 2017 USA.
11. Heatable Textiles with Silver Nanowires, **Doganay, D.**, Coskun, S., Polat, S., Unalan, H.E, EMRS Spring' 2017 France.
12. Silver Nanowire Heaters on Glass and Textiles, Coskun, S., Ergun, O., **Doganay, D.,** Polat, S., Yusufoglu, Y., Unalan, H.E., TMS Meeting' 2017 USA.
13. Solar Cells with Silver Nanowire Top Electrodes, Aurang, P., **Doganay, D.,** Es, F., Bek, A., Turan, R., Unalan, H.E., MRS Fall'2016
14. Characterization of Silver Nanowire Modified Textile Heaters, **Doganay, D.,** Coskun, C., Genlik, S.P., Unalan, H.E., IMMC 2016, Turkey.
15. Silver Nanowire Networks as Transparent Top Electrodes for Single Crystalline Silicon Solar Cells, Aurang, P. **Doganay, D.**, Coskun, S., Es, F., Turan, R., Unalan, H.E., EMRS Spring' 2016 France.
16. Silver nanowire/polylactide Nanocomposite conducting films, **Doğanay, D.**, Coskun, S., Kaynak, C., Unalan, H.E., TMS Meeting' 2016 USA.
17. Electrical Properties of Silver Nanowire/Polylactide Nanocomposite Films, **Doganay, D.,** Coskun, S., Kaynak, C., Unalan, H.E., MRS Fall' 2015 USA.
18. Effects of Silver Nanowires on the Behavior of Polylactide Nanocomposite Films, Doganay, D., Coskun, S., Unalan, H.E., Kaynak, C., TMS Meeting' 2015 USA.